# Transfer Matrices and Partition-Function Zeros for Antiferromagnetic Potts Models

## III. Triangular-lattice chromatic polynomial

Jesper Lykke Jacobsen
*Laboratoire de Physique Théorique et Modèles Statistiques*
*Université Paris-Sud*
*Bâtiment 100*
*F-91405 Orsay, FRANCE*
JACOBSEN@IPNO.IN2P3.FR


Jesús Salas
*Departamento de Física Teórica*
*Facultad de Ciencias, Universidad de Zaragoza*
*Zaragoza 50009, SPAIN*
JESUS@MELKWEG.UNIZAR.ES


Alan D. Sokal
*Department of Physics*
*New York University*
*4 Washington Place*
*New York, NY 10003 USA*
SOKAL@NYU.EDU

April 26, 2002
revised March 21, 2003

## Abstract

We study the chromatic polynomial $P_G(q)$ for $m \times n$ triangular-lattice strips of widths $m \leq 12_{\rm P}, 9_{\rm F}$ (with periodic or free transverse boundary conditions, respectively) and arbitrary lengths $n$ (with free longitudinal boundary conditions). The chromatic polynomial gives the zero-temperature limit of the partition function for the $q$-state Potts antiferromagnet. We compute the transfer matrix for such strips in the Fortuin–Kasteleyn representation and obtain the corresponding accumulation sets of chromatic zeros in the complex $q$-plane in the limit $n \to \infty$. We recompute the limiting curve obtained by Baxter in the thermodynamic limit $m, n \to \infty$ and find new interesting features with possible physical consequences. Finally, we analyze the isolated limiting points and their relation with the Beraha numbers.

**Key Words:** Chromatic polynomial; chromatic root; antiferromagnetic Potts model; triangular lattice; transfer matrix; Fortuin–Kasteleyn representation; Beraha–Kahane–Weiss theorem; Beraha numbers.

# 1  Introduction

The antiferromagnetic $q$-state Potts model [1, 2, 3, 4, 5, 6, 7, 8, 9, 10, 11, 12, 13, 14] exhibits unusual behavior not found in ferromagnets. Indeed, its phase diagram and critical behavior depend crucially on the lattice structure, unlike the ferromagnetic case where the concept of universality applies. Specifically, for each lattice $\mathcal{L}$ there exists a number $q_c(\mathcal{L})$ such that for all $q > q_c$ the model is disordered at any temperature, including zero temperature [11]. Exactly at $q = q_c(\mathcal{L})$ the system is disordered at all positive temperatures and has a zero-temperature critical point. The zero-temperature limit of the antiferromagnetic Potts model is particularly interesting because its partition function on a finite graph $G$ coincides with the chromatic polynomial $P_G(q)$, which counts the number of ways of coloring the vertices of $G$ using $q$ colors subject to the constraint that adjacent vertices always receive different colors [15].

In Refs. [16, 17] we undertook a study of the zeros of the chromatic polynomial when the parameter $q$ is allowed to take complex values (see [16] for detailed references to the previous literature). In those papers we studied strips of the square lattice; here we extend that work to the triangular lattice. The triangular-lattice case is of particular interest because the path-breaking work of Baxter [18, 19] provides a conjectured exact solution in the thermodynamic limit.

The study of the complex zeros of the chromatic polynomial is inspired by the Yang–Lee picture of phase transitions [20]. We study families of graphs $G_n$ for which the chromatic polynomial can be expressed via a transfer matrix of fixed size $M \times M$:

$$P_{G_n}(q) \;=\; \mathrm{tr}[A(q)\,T(q)^n] \tag{1.1a}$$

$$=\; \sum_{k=1}^{M} \alpha_k(q)\,\lambda_k(q)^n \;, \tag{1.1b}$$

where the transfer matrix $T(q)$ and the boundary-condition matrix $A(q)$ are polynomials in $q$, so that the eigenvalues $\{\lambda_k\}$ of $T$ and the amplitudes $\{\alpha_k\}$ are algebraic functions of $q$. Rather than using $T(q)$ to compute the zeros of the chromatic polynomial for a *finite* strip $m \times n$, we have focussed on the direct calculation of their accumulation points in the limit $n \to \infty$, i.e. for the case of an *semi-infinite* strip [21, 22, 23, 24, 16, 17]. According to the Beraha–Kahane–Weiss theorem [25, 26, 27], the accumulation points of zeros when $n \to \infty$ can either be isolated limiting points (when the amplitude associated to the dominant eigenvalue vanishes, or when all eigenvalues vanish simultaneously) or belong to a limiting curve $\mathcal{B}$ (when two dominant eigenvalues cross in modulus). By studying the limiting curves for different values of the strip width $m$, we hope to learn new features of the thermodynamic limit $m \to \infty$.

To determine the isolated limiting points, we shall take advantage of the following simple result [22]:

$$\det D = \prod_{k=1}^{M} \alpha_k \prod_{1 \le i \le j \le M} (\lambda_j - \lambda_i)^2 \;, \tag{1.2}$$

where $D$ is the $M \times M$ matrix with entries $D_{ij} = \sum_{k=1}^{M} \alpha_k (\lambda_k)^{i+j-2} = P_{G_{i+j-2}}$.

An important feature of the limiting curve $\mathcal{B}$ is that it typically crosses the positive real axis at a point $q_0(m)$.[1] Physically, $q_0(m)$ corresponds to a point of non-analyticity of the ground-state degeneracy per site [23, 28]. As the strip width $m$ grows, this crossing point $q_0(m)$ increases and presumably tends to a limiting value $q_0(\infty)$. On the other hand, as $m \to \infty$ the curve $\mathcal{B} = \mathcal{B}_m$ presumably tends to a thermodynamic-limit curve $\mathcal{B}_\infty$. We define $q_c$ to be the largest value where $\mathcal{B}_\infty$ crosses the real $q$-axis: please note that $q_c$ may or may not correspond to crossings of the real axis for any finite $m$. In general the value $q_0(\infty)$ is smaller than $q_c$, although for some lattices they may coincide (this depends on the shape of the curves $\mathcal{B}_m$ and $\mathcal{B}_\infty$). Indeed, in Ref. [17] evidence was presented suggesting that for the square lattice $q_0(\infty) = q_c = 3$.

The crucial role of $q_0$ is further emphasized by studying the relation between chromatic polynomials and the so-called *Beraha numbers*

$$ B_n \;=\; 4\cos^2 \frac{\pi}{n} \;=\; 2 + 2\cos \frac{2\pi}{n} \qquad \text{for } n = 2, 3, \ldots . \tag{1.3}$$

It has been found in a number of cases [29, 21, 22] that chromatic roots tend to accumulate at some of the Beraha numbers. In the case of the *square lattice*, we have found empirically [16, 17] that on a strip of width $m$ with either free or periodic transverse boundary conditions[2], there is at least one vanishing amplitude $\alpha_i(q)$ at each of the first $m$ Beraha numbers $B_2, \ldots, B_{m+1}$ (but not higher ones). It thus appears that in the limit $m \to \infty$ all the Beraha numbers will be zeros of some amplitude.[3] Moreover, we found that the vanishing amplitude corresponds to the eigenvalue obtained by analytic continuation in $q$ from the one that is dominant at small real $q$, in agreement with a conjecture of Baxter [19, p. 5255]. Thus, the first few Beraha numbers — namely, those (up to at most $B_{m+1}$) that lie below the point $q_0(m)$ — correspond to the vanishing of a dominant amplitude and hence, by the Beraha–Kahane–Weiss theorem, to a limit point of chromatic roots, while the remaining Beraha numbers do not. As the strip width $m$ grows, $q_0(m)$ tends to $q_0(\infty)$, and the limiting points of chromatic roots are thus constrained to be the points $B_2, B_3, \ldots, B_p < q_0(\infty)$. This scenario for the accumulation of chromatic roots at *some* of the Beraha numbers was set forth by Baxter [19] and elaborated by Saleur [8]; further references can be found in [16].

---

[1] If there is more than one such crossing, we define $q_0(m)$ to be the *smallest* such crossing. When no such crossing occurs, the limiting curve often includes a pair of complex-conjugate endpoints rather close to the positive real $q$-axis. In these cases, we define $q_0(m)$ to be the point closest to that axis with positive imaginary part.

[2] Let $m$ (resp. $n$) denote the number of sites in the transverse (resp. longitudinal) direction of the strip, and let F (resp. P) denote free (resp. periodic) boundary conditions in a given direction. Then we use the terminology: free ($m_F \times n_F$), cylindrical ($m_P \times n_F$), cyclic ($m_F \times n_P$), and toroidal ($m_P \times n_P$). In this paper we consider free and cylindrical boundary conditions, as well as a new type of boundary condition that we shall call "zig-zag" (Section 5).

[3] As we shall see, a similar (but not identical) statement appears to hold true also for the triangular lattice: see Section 7.2.

In the present publication we shall be concerned with the antiferromagnetic Potts model on the *triangular lattice*. For this case, Baxter and collaborators [30, 18, 19] have determined the exact free energy (among other quantities) on two special curves in the $(q, v)$-plane:

$$v^3 + 3v^2 - q = 0 \qquad (1.4)$$

$$v = -1 \qquad (1.5)$$

The uppermost branch $(v \geq 0)$ of curve (1.4) is known to correspond to the ferromagnetic critical point [30, 3], and Baxter [18] initially conjectured (following a hint of Nienhuis [31]) that the zero-temperature antiferromagnetic model (1.5) is critical in the interval $0 \leq q \leq 4$. This prediction is known to be correct for $q = 2$ [32, 33, 34] and is believed to be correct also for $q = 4$ [5, 35, 36]. On the other hand, for $q = 3$ the conjecture contradicts the rigorous result [37], based on Pirogov-Sinai theory, that there is a low-temperature phase with long-range order and small correlation length.[4] In any case, for $q > 4$ we expect that the triangular-lattice Potts model is noncritical even at zero temperature; this has recently been confirmed by Monte Carlo simulation of the models with $q = 5, 6$ [38]. We therefore expect that for the triangular lattice $q_c = 4$.

For the model (1.5), Baxter [18] used a Bethe Ansatz to compute three different expressions $g_i(q)$ $[i = 1, 2, 3]$ that he argued correspond to the dominant eigenvalues of the transfer matrix in different regions $\mathcal{D}_i$ of the complex $q$-plane; in a second paper [19] he provided corrected estimates for the precise locations of $\mathcal{D}_1, \mathcal{D}_2, \mathcal{D}_3$. Using these formulae, he determined the value of $q_0(\infty)$ as

$$q_0(\infty, \text{tri}) \approx 3.81967 \qquad (\text{Baxter}) \qquad (1.6)$$

One important outcome of the present paper (see Section 6.2) is that the "phase diagram" predicted by Baxter's formulae is actually more complicated than what Baxter found. In particular, it now appears that the correct value of $q_0(\infty, \text{tri})$ coming from Baxter's eigenvalues $g_i$ is slightly smaller than Baxter's value (1.6), the corrected value being

$$q_0(\infty, \text{tri}) = B_{12} = 2 + \sqrt{3} \approx 3.73205 \qquad (\text{this paper}) \qquad (1.7)$$

We therefore conjecture that the isolated limiting chromatic roots of the infinite-size triangular lattice are $B_2, \ldots, B_{11}$ and possibly $B_{12}$, rather than $B_2, \ldots, B_{14}$ as conjectured by Baxter.

To study the approach to the thermodynamic limit, we have computed the transfer matrix for triangular-lattice strips of widths $2 \leq m \leq 9$ with free boundary conditions and $2 \leq m \leq 12$ with cylindrical boundary conditions, and we have determined the corresponding limiting curves $\mathcal{B}$. We have also undertaken a detailed comparison of our finite-lattice eigenvalues with Baxter's eigenvalues $g_i$, and have found a surprising

---

[4]A Monte Carlo study of the $q = 3$ model found strong evidence for a first-order transition to an ordered phase at $\beta J \approx -1.594$ [10].

fact (Section 6.3): in the region of the $q$-plane corresponding to Baxter's $\mathcal{D}_3$, we find no evidence in our finite-lattice data of any eigenvalue corresponding to $g_1$. As a consequence, the "extra" branches of the phase diagram found in Section 6.2 appear to be absent after all! There seem to be two possibilities:

(a) The eigenvalue $g_1$ really is present in the region $\mathcal{D}_3$, but only for strip widths much larger than those we have studied. In this case, the limiting curve $\mathcal{B}_\infty$ really would exhibit all the complexities found in Section 6.2, and the correct value of $q_0$ would be given by (1.7) rather than (1.6).

(b) For some reason, the eigenvalue $g_1$ is not present in this region (though it is clearly present elsewhere). In this case, the limiting curve $\mathcal{B}_\infty$ would be similar to that depicted by Baxter, and the correct value of $q_0$ would be given by (1.6) after all.

We discuss these issues further in Section 6.4.

Our finite-lattice data also serve as a testing ground for the general conjectures on Beraha numbers as stated above (see Ref. [16] for further details). We discuss this further in Section 7.2.

Previous studies using a similar transfer-matrix approach have been made notably by Shrock and collaborators. In particular, they have considered triangular-lattice strips of width $m \leq 5$ for free and cylindrical boundary conditions [24, 41, 42, 43, 44].[5] They have also considered other boundary conditions for the same lattice [44, 45, 46, 47].[6] Generalizations to nonzero temperature for several boundary conditions have been carried out in Refs. [48, 49]. Finally, Refs. [47, 50] discuss some general structural properties of the Potts-model partition function and chromatic polynomial on square-lattice and triangular-lattice strips.

This paper is laid out as follows: In Section 2 we discuss some brief preliminaries. In Section 3 we give our numerical results for free transverse boundary conditions, and in Section 4 for periodic transverse (cylindrical) boundary conditions. We have also examined a third type of boundary conditions, called "zig-zag", which we introduce and motivate in Section 5. In Section 6 we analyze Baxter's [18, 19] exact solution for the thermodynamic limit and carefully recompute his phase diagram, finding interesting new features with possible physical consequences; we also compare his predictions for the dominant eigenvalues with our finite-lattice data and comment on the agreements and discrepancies. Finally, in Section 7 we present our conclusions.

---

[5]The case $m = 4$ with cylindrical boundary conditions was first done by Beraha and Kahane [21]. The case $m = 5$ with cylindrical boundary conditions was first done by Beraha, Kahane and Weiss [22].

[6]The case $2_\mathrm{F} \times n_\mathrm{P}$ (i.e., cyclic boundary conditions) was first done by Beraha, Kahane and Weiss [22].

# 2 Preliminaries

The general theory of the transfer-matrix method used here has been explained in Ref. [16], and the implementational details of an improved algorithm have been given in Ref. [17]. Suffice it here to mention that we have used the Fortuin–Kasteleyn representation [39, 40] of the Potts model in the computation of the transfer matrix; therefore, all quantities are expressed as polynomials in $q$.

To compute the limiting curves $\mathcal{B}$ we have used two different techniques: the resultant method and a direct-search method. These techniques have been described in [16, Section 4.1], and we use here the same conventions and notation.

Let us briefly mention a few improvements/additions to our methodology:

*Computation of T points.* We have adopted an improved method for locating T points, based on applying a numerical minimization algorithm (e.g. MATHEMATICA's `FindMinimum`) to the function

$$F(q) \;=\; (|\lambda_1(q)| - |\lambda_2(q)|)^2 \,+\, (|\lambda_1(q)| - |\lambda_3(q)|)^2 \,+\, (|\lambda_2(q)| - |\lambda_3(q)|)^2 \,, \quad (2.1)$$

where $\lambda_1, \lambda_2, \lambda_3$ are the three eigenvalues of the transfer matrix of largest modulus. At any given $q$ these eigenvalues can easily be computed numerically by finding the roots of the characteristic polynomial of the transfer matrix. Using this method, we are able to locate T points far more precisely than in our previous work.

*Fixed zeros.* When $q$ is an integer and the graph $G$ is not $q$-colorable, we have $P_G(q) = 0$. For this reason, certain small integers $q$ can be "fixed" zeros of the zero-temperature partition function, independent of the strip length $n$. In particular, $q = 0, 1$ are roots for all widths $m \geq 2$ and lengths $n \geq 1$. Furthermore, $q = 2$ is a root for all triangular-lattice strips of widths $m \geq 2$ and lengths $n \geq 2$, because the triangular lattice is not bipartite. Finally, $q = 3$ is a root for all *cylindrical* triangular-lattice strips of widths that are not multiples of 3 (with lengths $n \geq 2$), because these graphs are not 3-colorable.

It is interesting to see how these behaviors come about from the point of view of the transfer-matrix formalism. The partition function on a lattice of length $n$ has the form

$$Z_n \;=\; \sum_{k=1}^{M} \alpha_k(q)\, \lambda_k(q)^{n-1} \,, \quad (2.2)$$

where the $\{\lambda_k\}$ are the eigenvalues of the transfer matrix and the $\{\alpha_k\}$ are the corresponding amplitudes. A particular value $q$ can then be a "fixed" zero of $Z$ for any of three reasons:

1) All the amplitudes $\alpha_k$ vanish at $q$. Then $Z_n(q) = 0$ for all $n \geq 1$.

2) All the eigenvalues $\lambda_k$ vanish at $q$. Then $Z_n(q) = 0$ for all $n \geq 2$.

3) "Mixed case": Neither all the amplitudes nor all the eigenvalues vanish at $q$, but for each $k$ either $\alpha_k$ or $\lambda_k$ vanishes at $q$ (or both). Then $Z_n(q) = 0$ for all $n \geq 2$.

As we shall see, the points $q = 0$ and $q = 1$ will be fixed roots belonging to Case 1: all the amplitudes vanish due to an overall prefactor $q(q - 1)$. The point $q = 2$ will be a fixed root belonging sometimes to Case 1 and sometimes to Case 3 (and to Case 2 when $m = 2$ for all boundary conditions). For cylindrical strips where the width is not a multiple of 3, the point $q = 3$ will be a fixed root belonging to Case 2 for $m = 4_P$ and to Case 3 for $m \geq 5_P$. We shall endeavor to explain in each case the mechanism underlying the fixed zeros; these results will be summarized in Section 7.3.

*Computation of isolated limiting points.* To find the isolated limiting points, we first compute symbolically the determinant $\det D(q)$ defined by (1.2); this determinant is a polynomial in $q$ with integer coefficients, typically of very high degree. We then compute numerically the zeros of this polynomial, using the MPSolve 2.1.1 package [51, 52]; these zeros correspond to points $q$ where at least one amplitude $\alpha_k(q)$ vanishes. Finally, we test numerically each of these zeros to see whether the amplitude corresponding to the *dominant* eigenvalue is vanishing; if it is, then the point in question is an isolated limiting point. This method is guaranteed to discover *all* of the isolated limiting points. We shall not bother to report here all the zeros of $\det D(q)$, but only (a) the isolated limiting points and (b) the Beraha numbers $B_n$ that are zeros of some subdominant amplitude. Please note that whenever $B_n$ is a zero of $\det D(q)$, so are all the primitive generalized Beraha numbers

$$B_n^{(k)} = 4\cos^2 \frac{k\pi}{n} = 2 + 2\cos \frac{2\pi k}{n} \tag{2.3}$$

where $k$ is relatively prime to $n$, since they have the same minimal polynomial $p_n(q)$ [16, Section 2.3].

Unfortunately, in some cases the matrix $D(q)$ is so large that we have been unable to compute symbolically its determinant. In these cases, it is more convenient to compute numerically the eigenvalues $\{\lambda_j\}$ and their corresponding amplitudes $\{\alpha_j\}$ and check (a) whether any of the amplitudes vanish and (b) whether the amplitude $\alpha^\star$ associated to the dominant eigenvalue vanishes. We have restricted our search to certain "candidate" values of $q$ (or neighborhoods in the complex $q$-plane), namely (a) the Beraha numbers $B_n$ for $n \leq 50$, and (b) any real or complex values of $q \notin \mathcal{B}$ where zeros of $Z_n$ seem to be accumulating as $n$ gets large. When there is a exact candidate (such as the Beraha numbers $B_n$), we have computed the amplitudes with high-precision arithmetic (200 digits of precision at least). We considered that an amplitude is zero when its absolute value is less than (for instance) $10^{-190}$. When we do not have an exact candidate, we tried to minimize the dominant amplitude $|\alpha^\star|$ around a region where zeros of $Z_n$ tend to accumulate as $n$ grows. This situation occurred only for the strips of widths $8_Z$ and $10_Z$ ("zig-zag" boundary conditions, see Section 5). The condition $|\alpha^\star| \lesssim 10^{-52}$ holds for all the cases reported here.

In all the cases where we are unable to compute $\det D(q)$ symbolically, we are able to assert that certain points are indeed isolated limiting points, but we cannot claim with confidence that we have found *all* of the isolated limiting points.

# 3 Numerical Results for the Triangular-Lattice Chromatic Polynomial: Free Boundary Conditions

We have computed the transfer matrix $\mathsf{T}(m_{\mathrm{F}})$ and the limiting curves $\mathcal{B}$ for triangular-lattice strips of widths $2 \leq m \leq 9$ with free boundary conditions in both directions. We also write $L_x$ as a synonym for the strip width $m$.

As explained in Ref. [16], the chromatic polynomial for this family of strip lattices can be written as

$$Z(m_{\mathrm{F}} \times n_{\mathrm{F}}) = \mathbf{u}^{\mathrm{T}} \mathsf{H} \mathsf{T}(m_{\mathrm{F}})^{n-1} \mathbf{v}_{\mathrm{id}} \tag{3.1}$$

where $\mathbf{u}$ and $\mathbf{v}_{\mathrm{id}}$ are certain vectors, and $\mathsf{T}(m_{\mathrm{F}}) = \mathsf{V} \mathsf{H}$ is the transfer matrix. Here $\mathsf{H}$ (resp. $\mathsf{V}$) corresponds to adding one new layer of horizontal (resp. vertical and diagonal) bonds: see Figure 1(a). The matrices $\mathsf{H}$, $\mathsf{V}$ and $\mathsf{T}(m_{\mathrm{F}})$ act on the space of connectivities of sites in the top layer, whose basis elements $\mathbf{v}_{\mathcal{P}}$ are indexed by partitions $\mathcal{P}$ of the single-layer vertex set $\{1, 2, \ldots, m\}$. In particular, $\mathbf{v}_{\mathrm{id}} = \mathbf{v}_{\{\{1\}, \{2\}, \ldots, \{m\}\}}$. Since the strip lattices we are dealing with are planar, only *non-crossing* partitions $\mathcal{P}$ can occur.

In the particular case of the chromatic polynomial (i.e. the *zero-temperature* antiferromagnet), the horizontal operator $\mathsf{H}$ is a projection ($\mathsf{H}^2 = \mathsf{H}$), and we can work in its image subspace by using the modified transfer matrix $\mathsf{T}'(m_{\mathrm{F}}) = \mathsf{H} \mathsf{V} \mathsf{H}$ in place of $\mathsf{T}(m_{\mathrm{F}}) = \mathsf{V} \mathsf{H}$, and using the basis vectors

$$\mathbf{w}_{\mathcal{P}} = \mathsf{H} \mathbf{v}_{\mathcal{P}} \tag{3.2}$$

in place of $\mathbf{v}_{\mathcal{P}}$. Then we can rewrite (3.1) as

$$Z(m_{\mathrm{F}} \times n_{\mathrm{F}}) = \mathbf{u}^{\mathrm{T}} \mathsf{T}'(m_{\mathrm{F}})^{n-1} \mathbf{w}_{\mathrm{id}} \tag{3.3}$$

where $\mathbf{w}_{\mathrm{id}} = \mathsf{H} \mathbf{v}_{\mathrm{id}}$. Please note that $\mathbf{w}_{\mathcal{P}} = \mathsf{H} \mathbf{v}_{\mathcal{P}} = 0$ for any partition $\mathcal{P}$ that includes nearest-neighbor sites in the same block, so we can ignore all such partitions. The dimension of the transfer matrix $\mathsf{T}'(m_{\mathrm{F}})$ is therefore equal to the number of non-crossing non-nearest-neighbor partitions of the set $\{1, 2, \ldots, m\}$, which is given by the Motzkin number $M_{m-1}$ [16]. To simplify the notation, we will drop the prime in $\mathsf{T}'(m_{\mathrm{F}})$ and denote the basis elements $\mathbf{w}_{\mathcal{P}}$ by a shorthand using Kronecker delta functions: for instance, $\mathbf{w}_{\{\{1,3\}, \{2\}, \{4,6\}, \{5\}\}}$ will be written $\delta_{13} \delta_{46}$. We denote the set of basis elements for a given strip as $\mathbf{P} = \{\mathbf{w}_{\mathcal{P}}\}$. For instance, the basis for $m = 3$ is $\mathbf{P} = \{1, \delta_{13}\}$.

We have checked the self-consistency of our finite-lattice results using the trivial identity

$$Z(m_{\mathrm{F}} \times n_{\mathrm{F}}) = Z(n_{\mathrm{F}} \times m_{\mathrm{F}}) \tag{3.4}$$

for all pairs $2 \leq m, n \leq 9$.

## 3.1  $L_x = 2_F$

This case is trivial, as the transfer matrix is one-dimensional:

$$Z(2_F \times n_F) = q(q-1)(q-2)^{2(n-1)} \tag{3.5}$$

Since there is only one eigenvalue, there is obviously no crossing, hence $\mathcal{B} = \varnothing$. However, there are zeros for all $n$ at $q = 0, 1$ and for $n \geq 2$ at $q = 2$. The fixed zeros at $q = 0, 1$ arise from a vanishing amplitude, and the fixed zero at $q = 2$ arises from a vanishing eigenvalue.

## 3.2  $L_x = 3_F$

The transfer matrix is two-dimensional. In the basis $\mathbf{P} = \{1, \delta_{13}\}$ it can be written as

$$T(3_F) = \begin{pmatrix} q^3 - 7q^2 + 17q - 14 & q^2 - 6q + 9 \\ -q + 2 & q - 3 \end{pmatrix} \tag{3.6}$$

and the partition function is equal to

$$Z(3_F \times n_F) = q(q-1) \begin{pmatrix} q-1 \\ 1 \end{pmatrix}^{\mathrm{T}} \cdot T(3_F)^{n-1} \cdot \begin{pmatrix} 1 \\ 0 \end{pmatrix} \tag{3.7}$$

The limiting curve $\mathcal{B}$ (see Figure 2) contains three disconnected pieces and it crosses the real axis at $q_0 \approx 2.5698402910$. There are six endpoints:

$$q \approx 1.2047381150 \pm 1.1596169599\, i \tag{3.8a}$$
$$q \approx 2.3930361082 \pm 0.2538745688\, i \tag{3.8b}$$
$$q \approx 3.4022257768 \pm 0.5865084714\, i \tag{3.8c}$$

These results were previously obtained by Roček *et al.* [24].

The determinant $\det D(q)$ has the form

$$\det D(q) = q^2(q-1)^2(q-2)^3 \tag{3.9}$$

Thus, it vanishes at the first three Beraha numbers $q = 0, 1, 2$. At those points the dominant amplitude vanishes, hence they are isolated limiting points.

In fact, the partition function vanishes at $q = 0, 1$ for all $n$, and at $q = 2$ for all $n \geq 2$. Obviously, at $q = 0, 1$ both amplitudes vanish, due to the prefactor $q(q-1)$ in (3.7). [This happens for *all* strips of width $m \geq 2$; we will henceforth call these zeros "trivial".] At the fixed zero $q = 2$, there is one nonzero eigenvalue ($\lambda^\star = -1$) with a vanishing amplitude and one zero eigenvalue with a nonvanishing amplitude; we are therefore in Case 3 described in Section 2. The fourth real zero (see Table 1) converges at an approximate $1/n$ rate to the value $q_0 \approx 2.5698402910$.

## 3.3 $L_x = 4_{\mathrm{F}}$

The transfer matrix is four-dimensional. In the basis $\mathbf{P} = \{1, \delta_{13}, \delta_{24}, \delta_{14}\}$, it takes the form

$$
T(4_{\mathrm{F}}) \;=\; \begin{pmatrix} T_{11} & T_{12} & T_{13} & T_{14} \\ -q^2 + 5q - 6 & q^2 - 5q + 6 & -q + 3 & -2(q - 3) \\ -q^2 + 5q - 6 & q^2 - 5q + 6 & q^2 - 6q + 9 & q^2 - 8q + 15 \\ q - 2 & q^2 - 5q + 6 & -q + 3 & q^2 - 7q + 13 \end{pmatrix} \tag{3.10}
$$

where

$$
\begin{aligned}
T_{11} &= q^4 - 10q^3 + 39q^2 - 70q + 48 & \text{(3.11a)} \\
T_{12} &= q^3 - 9q^2 + 26q - 24 & \text{(3.11b)} \\
T_{13} &= q^3 - 9q^2 + 28q - 30 & \text{(3.11c)} \\
T_{14} &= q^3 - 10q^2 + 36q - 45 & \text{(3.11d)}
\end{aligned}
$$

The partition function is equal to

$$
Z(4_{\mathrm{F}} \times n_{\mathrm{F}}) \;=\; q(q - 1) \begin{pmatrix} (q - 1)^2 \\ q - 1 \\ q - 1 \\ q - 2 \end{pmatrix}^{\mathrm{T}} \cdot T(4_{\mathrm{F}})^{n-1} \cdot \begin{pmatrix} 1 \\ 0 \\ 0 \\ 0 \end{pmatrix} \tag{3.12}
$$

The limiting curve $\mathcal{B}$ (see Figure 3) contains two complex-conjugate disconnected pieces that do not cross the real axis. The closest points to the real axis are $q_0 \approx 2.7592502040 \pm 0.1544431251\,i$. There are six endpoints:

$$
\begin{aligned}
q &\approx 0.8164709452 \pm 1.2804094073\,i & \text{(3.13a)} \\
q &\approx 2.7592502040 \pm 0.1544431251\,i & \text{(3.13b)} \\
q &\approx 3.6398304896 \pm 0.5986827987\,i & \text{(3.13c)}
\end{aligned}
$$

There are T points at $q \approx 3.3341785562 \pm 0.8829730283\,i$. These results were previously obtained by Roček $et\ al.$ [24, 41].

The determinant $\det D(q)$ has the form

$$
\det D(q) = -q^4(q-1)^4(q-2)^{13}(q^2-3q+1)(q-3)^6(q^4-11q^3+46q^2-86q+61)^2 \tag{3.14}
$$

We recognize, as factors in (3.14), the first five minimal polynomials $p_k(q)$ for the Beraha numbers $B_k$ [16, Table 1]; therefore $\det D(q)$ vanishes at the first five Beraha numbers $q = 0, 1, 2, B_5, 3$. The dominant amplitude vanishes at $q = 0, 1, 2, B_5$, so these are isolated limiting points. At $q = 3$ only two subdominant amplitudes vanish, so this is not an isolated limiting point. Similarly, all of the zeros of the last factor in (3.14) correspond to the vanishing of subdominant amplitudes only, so none of them is an isolated limiting point.

In fact, the partition function vanishes at $q = 0, 1$ for all $n$, and at $q = 2$ for all $n \geq 2$. The fixed zeros at $q = 0, 1$ are trivial. At $q = 2$, there are three zero

10

eigenvalues and a unique leading eigenvalue $\lambda^\star = 4$ with zero amplitude. Notice that the transfer matrix is not diagonal for $q = 2$: there is a $2 \times 2$ nontrivial Jordan block corresponding to $\lambda = 0$ and whose contribution to the partition function is zero for all $n$. The amplitude corresponding to the other $\lambda = 0$ eigenvalue is 2; we are therefore in Case 3 described in Section 2. Finally, the fourth real zero converges exponentially fast to $B_5$ (see Table 1).

Please note that for this strip there is a vanishing subdominant amplitude at $q = B_k$ for a Beraha number $k$ *greater than* $m + 1$ (namely, $B_6 = 3$). As we shall see, this occurs frequently for the triangular lattice, and contrasts with the behavior observed for the square lattice [16, 17].

## 3.4 $L_x = 5_\mathrm{F}$

The transfer matrix is nine-dimensional; it can be found in the MATHEMATICA file `transfer3.m` available as part of the electronic version of this paper in the `cond-mat` archive. This strip has been previously studied by Chang and Shrock [44]; but they did not compute the limiting curve.

The limiting curve $\mathcal{B}$ is connected (see Figure 4). It crosses the real axis at $q_0 = 3$. There are six endpoints:

$$q \approx 0.5586170364 \pm 1.2816149610\,i \tag{3.15a}$$
$$q \approx 3.0474871745 \pm 0.8171660680\,i \tag{3.15b}$$
$$q \approx 3.7782975917 \pm 0.5699779858\,i \tag{3.15c}$$

The topology of the limiting curve is rather involved. It has 12 T points: $q \approx 3.1572589261 \pm 0.7951215102\,i$, $q \approx 3.1251751109 \pm 0.8152460413\,i$, $q \approx 3.2093444343 \pm 0.9296294663\,i$, $q \approx 3.3452062643 \pm 0.9758086833\,i$, $q \approx 3.3248793469 \pm 0.9987588766\,i$, and $q \approx 3.2492362818 \pm 1.1185073809\,i$. These points define four closed regions. The first five T points are the vertices of two complex-conjugate regions which look approximately like rectangular bands. The third, fifth and sixth T points above define two complex-conjugate triangular-like regions.

The determinant $\det D(q)$ is given by

$$\det D(q) = q^9(q-1)^9(q-2)^{66}(q^2-3q+1)^4(q-3)^{61}P(q)^2 \tag{3.16}$$

where the polynomial $P(q)$ can be found in the MATHEMATICA file `transfer3.m`. The factors appearing in $\det D(q)$ are the first five polynomials $p_k(q)$ given in [16, Table 1]; therefore $\det D(q)$ vanishes at $q = 0, 1, 2, B_5, 3$. The dominant amplitude vanishes at the first four of them (but not at $q = 3$), so that $q = 0, 1, 2, B_5$ are isolated limiting points. All of the zeros of $P(q)$ correspond to the vanishing of subdominant amplitudes only, so none of them is an isolated limiting point.

The first two real zeros $q = 0, 1$ are trivial ones. At $q = 2$ there are two nonzero eigenvalues with zero amplitudes and seven zero eigenvalues. The transfer matrix is not diagonalizable: there are two Jordan blocks of dimension 3 and 2, respectively, associated to the eigenvalue $\lambda = 0$. The contribution of these blocks to the partition

11

function vanishes for all $n$. In addition, the amplitude corresponding to the other two zero eigenvalues are 0 and 2; we are therefore in Case 3 described in Section 2. The fourth real zero converges exponentially fast to the value $q = B_5$ (see Table 1); and the fifth real zero converges at an approximate $1/n$ rate to the value $q_0 = 3$. This agrees with the fact that $q = 3$ is a regular limiting point and not an isolated limiting point.

## 3.5 $L_x = 6_F$

The transfer matrix is 21-dimensional; it can be found in the MATHEMATICA file `transfer3.m`.

The limiting curve $\mathcal{B}$ is connected (see Figure 5). It crosses the real axis at $q_0 \approx 3.1609256737$. There are six endpoints:

$$q \approx 0.3796307748 \pm 1.2450702104\,i \tag{3.17a}$$
$$q \approx 2.9641235697 \pm 1.1179839989\,i \tag{3.17b}$$
$$q \approx 3.8664092416 \pm 0.5329463088\,i \tag{3.17c}$$

There are four T points at $q \approx 3.3081144403 \pm 1.2171494282\,i$, and $q \approx 3.5005856709 \pm 0.9442298756\,i$.

The determinant $\det D(q)$ is given by

$$\det D(q) = q^{21}(q-1)^{21}(q-2)^{360}(q^2-3q+1)^{13}(q-3)^{503}(q^3-5q^2+6q-1)P(q)^2 \tag{3.18}$$

where the polynomial $P(q)$ can be found in the MATHEMATICA file `transfer3.m`. The factors appearing in $\det D(q)$ are the first six polynomials $p_k(q)$ given in [16, Table 1]. Thus, $\det D(q)$ vanishes at $q = 0, 1, 2, B_5, 3, B_7$. The dominant amplitude vanishes at the first five of them (but not at $B_7$), so that $q = 0, 1, 2, B_5, 3$ are isolated limiting points. All of the zeros of $P(q)$ correspond to the vanishing of subdominant amplitudes only, so none of them is an isolated limiting point.

The first two real zeros $q = 0, 1$ are trivial ones. At $q = 2$ we get six nonzero eigenvalues with zero amplitudes and 15 zero eigenvalues. We find again that the transfer matrix is not diagonalizable for $q = 2$: there are five nontrivial Jordan blocks (one of dimension 3 and four of dimension 2) corresponding to the eigenvalue $\lambda = 0$, and whose contribution to the partition function always vanishes. The amplitudes of the other four zero eigenvalues are (0,0,0,2). This combination seems to be the generic case for free boundary conditions: all amplitudes vanish except one corresponding to a zero eigenvalue. When the transfer matrix is not diagonalizable, then the nontrivial Jordan blocks correspond to $\lambda = 0$ and their contribution is always zero. The fourth and fifth real zeros converge exponentially fast to the values $q = B_5$ and $q = 3$, respectively (see Table 1); the sixth real zero converges at an approximate $1/n$ rate to the value $q_0 \approx 3.1609256737$.

## 3.6 $L_x = 7_F$

The transfer matrix is 51-dimensional; it can be found in the MATHEMATICA file `transfer3.m`. In this case we have been unable to compute symbolically the

resultant, hence the computation of the limiting curve has been performed using the direct-search method.

The limiting curve $\mathcal{B}$ is connected (see Figure 6). It crosses the real axis at $q_0 \approx 3.2764013231$. There are six endpoints:

$$q \approx 0.250538 \pm 1.196864\,i \tag{3.19a}$$

$$q \approx 3.925804 \pm 0.496672\,i \tag{3.19b}$$

$$q \approx 2.878928 \pm 1.343851\,i \tag{3.19c}$$

There are four T points at $q \approx 3.6146786603 \pm 0.9081562491\,i$ and $q \approx 3.2704141478 \pm 1.5194310419\,i$.

We have been unable to compute the determinant $\det D(q)$. However, we computed the amplitudes numerically at each of the Beraha numbers $B_n$ up to $B_{50}$ and determined in particular whether it is an isolated limiting point or not. As always, $q = 0, 1$ are trivial isolated limiting points where all the amplitudes vanish. The dominant amplitude also vanishes at $q = 2, B_5, 3, B_7$, so they are isolated limiting points too. Finally, a subdominant amplitude vanishes at $q = B_8$.

The first two real zeros $q = 0, 1$ are trivial ones. At $q = 2$, all amplitudes vanish except one corresponding to a zero eigenvalue. In particular, there are 12 nonzero eigenvalues with zero amplitudes, 8 zero eigenvalues with zero amplitudes, and one zero eigenvalue with nonzero amplitude. We also find 12 nontrivial Jordan blocks corresponding to $\lambda = 0$, whose contribution to the partition function is always zero. The fourth, fifth and sixth real zeros converge exponentially fast to the values $B_5$, 3 and $B_7$, respectively (see Table 2); however, the convergence to $B_7 \approx 3.246979603717$ is slowed by its nearness to the regular limiting point $q_0 \approx 3.2764013231$. For lengths $n \gtrsim 77$, a seventh real zero appears: it converges (at an approximate $1/n$ rate) to $q_0$.

## 3.7  $L_x = 8_{\mathrm{F}}$

The transfer matrix is 127-dimensional; it can be found in the MATHEMATICA file `transfer3.m`. Again we have used the direct-search method to locate the points of the limiting curve $\mathcal{B}$.

The limiting curve $\mathcal{B}$ is connected (see Figure 7). It crosses the real axis at $q_0 \approx 3.3610599515$. There are six endpoints:

$$q \approx 0.154432 \pm 1.146669\,i \tag{3.20a}$$

$$q \approx 2.793496 \pm 1.521468\,i \tag{3.20b}$$

$$q \approx 3.967566 \pm 0.463648\,i \tag{3.20c}$$

There are four T points at $q \approx 3.2555859898 \pm 1.7000353877\,i$ and $q \approx 3.6703287722 \pm 0.8845072864\,i$.

We were unable to compute the determinant $\det D(q)$. However, we computed the amplitudes numerically at each of the Beraha numbers $B_n$ up to $B_{50}$ and determined in particular whether it is an isolated limiting point or not. As always, $q = 0, 1$ are trivial isolated limiting points where all the amplitudes vanish. The dominant

13

amplitude vanishes also at $q = 2, B_5, 3, B_7$, so they are isolated limiting points too. Finally, some subdominant amplitudes vanish at $q = B_8, B_9$; they are not isolated limiting points.

The first two real zeros $q = 0, 1$ are trivial ones. At the third real zero $q = 2$, all amplitudes vanish except one corresponding to a zero eigenvalue. At $q = 2$ the transfer matrix is not diagonalizable: we find 30 nontrivial Jordan blocks corresponding to $\lambda = 0$, but their contribution to the partition function vanishes for all $n \geq 1$. We also get 33 nonzero eigenvalues with zero amplitudes, 20 zero eigenvalues with zero amplitudes, and one zero eigenvalue with nonzero amplitude. The fourth, fifth and sixth real zeros converge exponentially fast to the values $B_5$, 3 and $B_7$, respectively (see Table 2). We also expect a seventh real zero converging (at an approximate $1/n$ rate) to $q_0 \approx 3.3610599515$. Such zero does not appear up to lengths $n = 96$ (see Table 2). We would need to go to very large $n$ to observe this additional zero.

## 3.8 $L_x = 9_\mathrm{F}$

The transfer matrix is 323-dimensional; it can be found in the MATHEMATICA file `transfer3.m`. The size of this transfer matrix prevented us from computing the limiting curve $\mathcal{B}$. However, we were able to compute the point where the limiting curve crosses the real axis: it is $q_0 \approx 3.4251304673$. In Figure 8 we show the zeros of $Z$ for the finite lattices $9_\mathrm{F} \times 45_\mathrm{F}$ and $9_\mathrm{F} \times 90_\mathrm{F}$.

The first two real zeros $q = 0, 1$ are trivial ones. We have checked numerically that the dominant amplitude vanishes at $q = 2, B_5, 3, B_7, B_8$ (and at no other Beraha numbers up to $B_{50}$); these are therefore isolated limiting points. By inspection of Figure 8 we do not find any candidate for a non-Beraha real isolated limiting point or for a complex isolated limiting point. A subdominant amplitude vanishes for $q = B_9$ and $B_{10}$.

At $q = 2$ the transfer matrix is not diagonalizable: we find 76 nontrivial Jordan blocks (up to dimension $5 \times 5$) corresponding to $\lambda = 0$; none of these blocks contribute to the partition function for any $n \geq 1$. We also get 74 nonzero eigenvalues with zero amplitudes, 50 zero eigenvalues with zero amplitudes, and one zero eigenvalue with nonzero amplitude. The fourth, fifth, and sixth real zeros converge exponentially fast to the values $B_5$, 3 and $B_7$, respectively (see Table 2). We expect that the seventh real zero will converge exponentially fast to $B_8 = 2 + \sqrt{2}$ and that there will be (for large enough length $n$) an additional real zero that will eventually converge to the value $q \approx 3.4251304673 > B_8$ at an approximate $1/n$ rate. However, we would probably need to go to very large lengths $n$ in order to observe this behavior.

14

# 4 Numerical Results for the Triangular-Lattice Chromatic Polynomial: Cylindrical Boundary Conditions

We have also computed the transfer matrix $\mathsf{T}(m_{\mathrm{P}})$ and the limiting curves $\mathcal{B}$ for triangular-lattice strips of widths $2 \leq m \equiv L_x \leq 12$ with cylindrical boundary conditions, i.e. periodic b.c. in the transverse direction and free b.c. in the longitudinal direction.

The partition function can be written analogously to (3.3) as

$$Z(m_{\mathrm{P}} \times n_{\mathrm{F}}) = \mathbf{u}^{\mathrm{T}} \mathsf{T}(m_{\mathrm{P}})^{n-1} \mathbf{w}_{\mathrm{id}} \tag{4.1}$$

where $\mathsf{T}(m_{\mathrm{P}}) = \mathsf{HVH}$. (See [16, Section 3.1] for some remarks about the actual computation of this transfer matrix.) Since $\mathsf{T}(m_{\mathrm{P}})$ commutes with translations (due to the periodic b.c.) and the vectors $\mathbf{u}$ and $\mathbf{w}_{\mathrm{id}}$ are translation-invariant, we can restrict attention to the translation-invariant subspace. The dimension of $\mathsf{T}(m_{\mathrm{P}})$ is therefore given by the number of equivalence classes modulo translation of non-crossing non-nearest-neighbor partitions. This number is denoted by $\mathrm{TriCyl}(m)$ in [16, Table 2]. A general analytic expression for $\mathrm{TriCyl}(m)$ is not known, although such a formula has been obtained for prime values of $m$ [53, Theorem 3].

We have checked our results for widths $2 \leq m_{\mathrm{P}} \leq 12$ and lengths $n_{\mathrm{F}} = 2, 3, 4$ by comparing to the results of Beraha–Kahane–Weiss [22] (resp. Chang–Shrock [44]) for *width* $n_{\mathrm{F}} = 2$ (resp. $n_{\mathrm{F}} = 3, 4$) and *length* $m_{\mathrm{P}}$ (i.e. cyclic boundary conditions), using the trivial identity

$$Z(m_{\mathrm{P}} \times n_{\mathrm{F}}) = Z(n_{\mathrm{F}} \times m_{\mathrm{P}}) . \tag{4.2}$$

This is a highly non-trivial check of the correctness of our results.

The triangular lattice with cylindrical boundary conditions possesses a curious reflection symmetry that we shall now explain. Note first that the triangular lattice is *not* invariant under reflection in the transverse direction[7], since reflection changes the direction of the diagonal bonds. Nevertheless, *in the translation-invariant subspace* the transfer matrix does commute with reflection, because by translating the upper row (of a pair of rows) by one unit, one can change $\diagdown$ into $\diagup$, thereby converting the triangular lattice into a reflected triangular lattice! Because the transfer matrix (in the translation-invariant subspace) commutes with reflection, we can pass to a new basis consisting of connectivities that are either even or odd under reflection.[8]

---

[7]More precisely, if the strip width is even, one can choose to reflect either through a pair of lattice sites or through a pair of bisectors (sites with half-integer coordinates); the two choices differ by a subsequent translation. If the strip width is odd, then every reflection axis passes through one lattice site and one bisector.

[8]Let us call $\{v_j\}_{j=1}^{M}$ the connectivity basis in the translation-invariant subspace. Some of these basis elements are invariant under reflection; the rest can be grouped into pairs $(v_\alpha, v_\beta)$ that map into each other under reflection. A basis for the reflection-even (i.e. reflection-invariant) subspace is then given by the basis elements in the first set together with the combinations $v_\alpha + v_\beta$ from the second set. A basis for the reflection-odd subspace is given by the combinations $v_\alpha - v_\beta$ from the second set.

In this new basis, the transfer matrix $\mathsf{T}(m_{\mathrm{P}})$ is block-diagonal:

$$\mathsf{T}(m_{\mathrm{P}}) \;=\; \begin{pmatrix} \mathsf{T}_+(m_{\mathrm{P}}) & 0 \\ 0 & \mathsf{T}_-(m_{\mathrm{P}}) \end{pmatrix}, \tag{4.3}$$

where $\mathsf{T}_+$ (resp. $\mathsf{T}_-$) corresponds to the reflection-even (resp. reflection-odd) sub-space. Furthermore, the reflection-odd components of the start vector $\mathbf{w}_{\mathrm{id}} = \mathsf{H}\mathbf{v}_{\mathrm{id}}$ are identically zero, since both $\mathbf{v}_{\mathrm{id}}$ and $\mathsf{H}$ are manifestly reflection-invariant. Likewise, the reflection-odd components of the final vector $\mathbf{u}$ are identically zero, since the definition of $\mathbf{u}$ involves only $\mathsf{H}$ and not $\mathsf{V}$. Therefore (for either of these two reasons), the amplitudes $\alpha_k(q)$ corresponding to the reflection-odd subspace are all identically vanishing; these eigenvalues make no contribution whatsoever to the partition function. It follows that we can work entirely within the reflection-invariant subspace, which has dimension $\mathrm{SqCyl}(m)$ [16, Table 2]. For strip widths $m \geq 8$, $\mathrm{SqCyl}(m)$ is strictly smaller than $\mathrm{TriCyl}(m)$, so that the matrix $\mathsf{T}_-$ is nontrivial.

## 4.1 $L_x = 2_{\mathrm{P}}$

This case is trivial, as the transfer matrix is one-dimensional:

$$Z(2_{\mathrm{P}} \times n_{\mathrm{F}}) \;=\; q(q-1)[(q-2)(q-3)]^{n-1}. \tag{4.4}$$

Please note that the triangular-lattice strip $2_{\mathrm{P}} \times n_{\mathrm{F}}$ is *not* equivalent to the strip $2_{\mathrm{F}} \times n_{\mathrm{F}}$ for any length $n \geq 2$.

Since there is only one eigenvalue, there is obviously no crossing, hence $\mathcal{B} = \varnothing$. However, there are zeros for all $n$ at $q = 0, 1$ and for $n \geq 2$ at $q = 2, 3$.

## 4.2 $L_x = 3_{\mathrm{P}}$

This case is also trivial, as the transfer matrix is again one-dimensional:

$$Z(3_{\mathrm{P}} \times n_{\mathrm{F}}) \;=\; q(q-1)(q-2)(q^3 - 9q^2 + 29q - 32)^{n-1}. \tag{4.5}$$

Again $\mathcal{B} = \varnothing$, and the amplitude vanishes at $q = 0, 1, 2$ (which are the first three Beraha numbers). For $n \geq 2$ there are additional fixed zeros at $q \approx 2.5466023485$ and $q \approx 3.2266988258 \pm 1.4677115087\,i$, where the eigenvalue vanishes. This strip was studied by Roček *et al.* [41].

## 4.3 $L_x = 4_{\mathrm{P}}$

The transfer matrix is two-dimensional. In the basis $\mathbf{P} = \{1, \delta_{13} + \delta_{24}\}$ it can be written as

$$T(4_{\mathrm{P}}) = \begin{pmatrix} q^4 - 12q^3 + 58q^2 - 135q + 126 & 2(q^3 - 10q^2 + 33q - 36) \\ -2(q^2 - 7q + 12) & 2(q^2 - 6q + 9) \end{pmatrix} \tag{4.6}$$

16

and the partition function is equal to

$$Z(4_P \times n_F) = q(q-1) \begin{pmatrix} q^2 - 3q + 3 \\ 2(q-1) \end{pmatrix}^T \cdot T(4_P)^{n-1} \cdot \begin{pmatrix} 1 \\ 0 \end{pmatrix} \qquad (4.7)$$

The limiting curve $\mathcal{B}$ (see Figure 9) contains three pieces: two complex-conjugate arcs and a self-conjugate loop. In addition, at the point $q = 3$ both eigenvalues vanish simultaneously (i.e. the transfer matrix $T(4_P)$ itself vanishes); this is a special (degenerate) species of isolated limiting point [27]. (One of the amplitudes does not vanish at $q = 3$, but that is irrelevant.) The self-conjugate loop-like component crosses the real axis at $q_0 \approx 3.4814056002$ and $q = 4$. There are four endpoints:

$$q \approx 1.3705340683 \pm 2.7508526144\,i \qquad (4.8a)$$
$$q \approx 3.6294659317 \pm 0.6958422780\,i \qquad (4.8b)$$

This limiting curve was first obtained in the pioneering paper of Beraha and Kahane [21] (see also [41]). They drew the important conclusion that $q = 4$ is a limiting point of (complex) chromatic roots for the sequence $4_P \times n_F$ of *planar* graphs — hence the wonderful title of their paper, "Is the Four-Color Conjecture Almost False?"[9]

The determinant $\det D(q)$ has the form

$$\det D(q) = 8q^2(q-1)^2(q-2)(q^2 - 3q + 1)(q-3)^2(q-4)^2 \qquad (4.9)$$

We recognize the first five minimal polynomials $p_k(q)$ given in [16, Table 1]. Hence, the determinant vanishes at the first five Beraha numbers $q = 0, 1, 2, B_5, 3$. It also vanishes at $q = 4$, which corresponds to $B_\infty$. The dominant amplitude vanishes only at $q = 0, 1, 2, B_5$; these values of $q$ correspond to isolated limiting points.

The fixed zeros at $q = 0, 1$ are trivial ones. At the fixed zero $q = 2$, there is one nonzero eigenvalue ($\lambda^\star = 10$) with a vanishing amplitude and one zero eigenvalue with a nonvanishing amplitude ($\alpha = 2$); we are therefore in Case 3 described in Section 2. The fourth real zero converges exponentially fast to $B_5$ (see Table 3), in agreement with the fact that this is an isolated limiting point. The fifth real zero, at $q = 3$, is a fixed zero where both eigenvalues vanish (one of the amplitudes is 0 and the other is 18); we are therefore on Case 2 described in Section 2. The fact that $q = 3$ is a fixed zero is due to the width not being a multiple of 3. Finally, $q = 4$ is a crossing point where both eigenvalues take the value $\lambda = 2$ and one of the amplitudes vanishes. The sixth real zero in Table 3 converges at an approximate $1/n$ rate to the value $q_0 \approx 3.4814056002$.

For this strip there is a vanishing subdominant amplitude at $q = B_6 = 3$, which is *greater than* $B_{m+1} = B_5$, in contrast with the behavior observed for the square lattice [16, 17].

---

[9]Ironically, by the time that this article was published, the Four-Color Conjecture had become the Four-Color Theorem. The Beraha–Kahane article was submitted in 1976 but not published until 1979.

## 4.4   $L_x = 5_P$

The transfer matrix is two-dimensional. In the basis $\mathbf{P} = \{1, \delta_{13} + \text{perm.}\}$ it can be written as

$$T(5_P) = \begin{pmatrix} T_{11} & 5(q^4 - 14q^3 + 76q^2 - 187q + 174) \\ -q^3 + 11q^2 - 43q + 58 & 3q^3 - 35q^2 + 132q - 162 \end{pmatrix} \quad (4.10)$$

where

$$T_{11} = q^5 - 15q^4 + 95q^3 - 320q^2 + 579q - 452 , \quad (4.11)$$

and the partition function is equal to

$$Z(5_P \times n_F) = q(q-1)(q-2) \begin{pmatrix} q^2 - 2q + 2 \\ 5(q-1) \end{pmatrix}^{\mathrm{T}} \cdot T(5_P)^{n-1} \cdot \begin{pmatrix} 1 \\ 0 \end{pmatrix} \quad (4.12)$$

The limiting curve $\mathcal{B}$ (see Figure 10) contains three disconnected pieces: two complex-conjugate arcs and a self-conjugate loop-like arc. This latter piece crosses the real axis at $q_0 \approx 3.2072219810$ and at $q \approx 3.2847747616$. There are four endpoints:

$$q \approx 0.4772525688 \pm 2.5694937945\,i \quad (4.13\text{a})$$
$$q \approx 3.5227474312 \pm 0.1876729035\,i \quad (4.13\text{b})$$

The limiting curve was first obtained in [44]. [10]

The determinant $\det D(q)$ has the form

$$\det D(q) = 5q^2(q-1)^2(q-2)^2(q^2 - 3q + 1)(q-3)(q^3 - 11q^2 + 43q - 58)^2 \quad (4.14)$$

We recognize the first five minimal polynomials $p_k(q)$ given in [16, Table 1]. Hence, the determinant vanishes at the first five Beraha numbers $q = 0, 1, 2, B_5, 3$. Furthermore, the dominant amplitude vanishes at all these points; hence they are isolated limiting points. The last factor of the determinant does not provide additional isolated limiting points.

The fixed zeros at $q = 0, 1, 2$ are trivial ones where all amplitudes vanish due to the prefactor $q(q-1)(q-2)$ in (4.12). The fourth real zero converges exponentially fast to $B_5$ (see Table 3). The fifth real zero, at $q = 3$, is a fixed zero where there is one nonzero eigenvalue ($\lambda^\star = -2$) with a vanishing amplitude and one zero eigenvalue with a nonvanishing amplitude ($\alpha = 30$); we are therefore in Case 3 described in Section 2. The fact that $q = 3$ is a fixed zero is due to the width not being a multiple of 3. Finally, the sixth real zero in Table 3 converges at an approximate $1/n$ rate to the value $q_0 \approx 3.2072219810$.

---

[10]Two decades earlier, Beraha, Kahane and Weiss [22] computed the transfer matrix and reported the crossings of the limiting curve $\mathcal{B}$ with the real axis. But they did not show a plot of the limiting curve.

## 4.5  $L_x = 6_{\mathrm{P}}$

The transfer matrix is five-dimensional; it can be found in the MATHEMATICA file `transfer3.m`. This strip has been previously studied by Chang and Shrock [44]; but they did not compute the limiting curve.

The limiting curve $\mathcal{B}$ is connected (see Figure 11). It crosses the real axis at $q_0 \approx 3.2524186216$. There are four endpoints:

$$q \approx 0.0207708231 \pm 2.2756742729\, i \tag{4.15a}$$

$$q \approx 4.2838551928 \pm 0.6111544521\, i \tag{4.15b}$$

There are T points at $q \approx 3.9766954928 \pm 0.9167681670\, i$.

The determinant $\det D(q)$ has the form

$$
\begin{aligned}
\det D(q) \;=\; & 1769472 q^5 (q-1)^5 (q-2)^6 (q^2 - 3q + 1)^3 (q-3)^{15} (q^3 - 5q^2 + 6q - 1) \\
& \times (q^2 - 5q + 5)^2 (q-4)^8 P(q)^2
\end{aligned}
\tag{4.16}
$$

where the polynomial $P(q)$ can be found in the file `transfer3.m`. The first six factors in (4.16) are the first six minimal polynomials given in [16, Table 1]; hence the determinant vanishes at the first six Beraha numbers $q = 0, 1, 2, B_5, 3, B_7$. It also vanishes at the Beraha number $B_{10}$, whose minimal polynomial is $q^2 - 5q + 5$, and at $q = 4$. The dominant amplitude vanishes only at the first six Beraha numbers, so these values are the only isolated limiting points. The polynomial $P(q)$ does not provide additional isolated limiting points.

The first two zeros $q = 0, 1$ are trivial ones. At $q = 2$ we have three nonzero eigenvalues with vanishing amplitudes, one zero eigenvalue with zero amplitude, and one zero eigenvalue with nonzero amplitude; we therefore fall in Case 3 of Section 2. The fourth and fifth real zeros converge exponentially fast to $q = B_5, 3$ (see Table 3). The next Beraha number $B_7 \approx 3.2469796037$ is very close to the value $q_0 \approx 3.2524186216$ where the limiting curve $\mathcal{B}$ crosses the real axis. This explains why the convergence rate to the sixth real zero in Table 3 is not as fast as expected (empirically the convergence is roughly $\sim n^{-1.9}$); but we expect that it will be ultimately exponential (for very large $n$). We also expect a seventh real zero for large enough $n$; this zero is expected to converge (at an approximate $1/n$ rate) to the value $q_0 \approx 3.2524186216$. We would need to go to very large $n$ to observe this additional zero.

Finally, for this strip there is a vanishing subdominant amplitude at $q = B_{10}$, which is *greater than* $B_{m+1} = B_7$, in contrast with the behavior observed for the square lattice [16, 17].

## 4.6  $L_x = 7_{\mathrm{P}}$

The transfer matrix is six-dimensional; it can be found in the MATHEMATICA file `transfer3.m`.

The limiting curve $\mathcal{B}$ is connected (see Figure 12). It crosses the real axis at $q_0 \approx 3.4790022937$ and $q \approx 3.6798199576$. It enters the half-plane $\mathrm{Re}(q) < 0$, and

19

there are four endpoints

$$q \approx -0.2279183274 \pm 2.0134503491\, i \qquad (4.17a)$$
$$q \approx \phantom{-}3.9930118897 \pm 0.6273386181\, i \qquad (4.17b)$$

There are four T points at $q \approx 3.6222949363 \pm 0.1398555812\, i$ and $q \approx 3.9816630253 \pm 0.8993269516\, i$. Finally, it is worth noticing that the limiting curve encloses a small region around $3.479 \lesssim \mathrm{Re}(q) \lesssim 3.680$ and $|\mathrm{Im}(q)| \lesssim 0.14$.

The determinant $\det D(q)$ has the form

$$
\begin{aligned}
\det D(q) \;=\; & 68841472 q^6 (q-1)^6 (q-2)^6 (q^2 - 3q + 1)^4 (q-3)^{21} (q^3 - 5q^2 + 6q - 1) \\
& \times (q^2 - 4q + 2)(q^2 - 5q + 5)^2 P(q)^2
\end{aligned}
\qquad (4.18)
$$

where the polynomial $P(q)$ can be found in the file `transfer3.m`. The first seven factors in (4.18) are precisely the first minimal polynomials given in [16, Table 1]. The next one $(q^2 - 5q + 5)$ is the tenth minimal polynomial in [16, Table 1]. Hence, the determinant $\det D(q)$ vanishes at the Beraha numbers $q = 0, 1, 2, B_5, 3, B_7, B_8, B_{10}$. However, the dominant amplitude vanishes only at the first seven Beraha numbers $q = 0, 1, 2, B_5, 3, B_7, B_8$; these values are the only isolated limiting points for this strip. The polynomial $P(q)$ does not provide additional isolated limiting points.

The first three zeros $q = 0, 1, 2$ are trivial ones. The fifth real zero, at $q = 3$, is a fixed zero where there are 2 nonzero eigenvalues with zero amplitudes, one zero eigenvalue with zero amplitude, and 3 zero eigenvalues with nonzero amplitudes. The fourth, sixth and seventh real zeros converge exponentially fast to $q = B_5, B_7, B_8$ (see Table 3). The eighth real zero seems to converge at an approximate $1/n$ rate to the value $q_0 \approx 3.4790022937$.

In contrast with the behavior observed for the square lattice, we find a vanishing subdominant amplitude at $q = B_{10}$, which is greater than $B_{m+1} = B_8$.

## 4.7  $L_x = 8_{\mathrm{P}}$

The transfer matrix $T(8_{\mathrm{P}})$ is 15-dimensional. As discussed at the beginning of this section, the transfer matrix can be brought into block-diagonal form

$$
T(8_{\mathrm{P}}) \;=\; \begin{pmatrix} T_+(8_{\mathrm{P}}) & 0 \\ 0 & T_-(8_{\mathrm{P}}) \end{pmatrix}
\qquad (4.19)
$$

where the block $T_+$ (resp. $T_-$) is 14-dimensional (resp. 1-dimensional) and corresponds to the subspace of reflection-invariant (resp. reflection-odd) connectivities. Moreover, the amplitude corresponding to the reflection-odd eigenvalue is identically vanishing; this eigenvalue therefore makes no contribution to the partition function. The reduced transfer matrix $T_+(8_{\mathrm{P}})$ can be found in the MATHEMATICA file `transfer3.m`. The one-dimensional block is $T_-(8_{\mathrm{P}}) = -q^3 + 6q^2 - 8q - 3$.

There are, however, two further curious features for which we have, as yet, no explanation. First of all, we find *another* eigenvalue $\lambda = -q^3 + 6q^2 - 8q - 3$, this time inside the reflection-invariant subspace. Secondly (and even more mysteriously),

this eigenvalue too has an identically vanishing amplitude. (We have checked this fact numerically.) The pair of eigenvalues $\lambda = -q^3 + 6q^2 - 8q - 3$ can be observed explicitly by forming the characteristic polynomial of the transfer matrix, which can be factored as[11]

$$\det[T(8_P) - \lambda\mathbf{1}] \;=\; (\lambda + q^3 - 6q^2 + 8q + 3)^2 \, Q_2(q,\lambda) \qquad (4.20)$$

where $Q_2(q,\lambda)$ is a polynomial in $q$ and $\lambda$ (it is obviously of degree 13 in $\lambda$). Unfortunately, we have been unable to find a further change of basis to make $T_+(8_P)$ block-diagonal and thereby bring out explicitly the eigenvalue $\lambda = -q^3 + 6q^2 - 8q - 3$ lying inside that subspace.

In order to compute the limiting curve $\mathcal{B}$ we have mainly used the resultant method. The existence of a double eigenvalue $\lambda = -q^3 + 6q^2 - 8q - 3$ in the full transfer matrix $T(8_P)$ makes the resultant identically zero for $\theta = 0$. However, this problem does not arise if we consider the reduced matrix $T_+(8_P)$. Nevertheless, the existence of an identically zero amplitude within the reduced subspace makes the computation of the limiting curve $\mathcal{B}$ not completely straightforward, as only those eigenvalues with non-identically-vanishing amplitudes should be taken into account in computing $\mathcal{B}$. A simple solution is devised by noting that the resultant method uses only the characteristic polynomial of the transfer matrix. Therefore, we can drop the factor $(\lambda + q^3 - 6q^2 + 8q + 3)^2$ in (4.20) and compute the resultant using the polynomial $Q_2(q,\lambda)$. In this way, we obtain a nonzero resultant, into which the zero-amplitude eigenvalues do not enter.[12]

The limiting curve $\mathcal{B}$ is connected (see Figure 13). It crosses the real axis at $q_0 \approx 3.5147694243$. It enters the half-plane $\mathrm{Re}(q) < 0$, and there are four endpoints

$$
\begin{aligned}
q &\approx\; -0.3713655472 \pm 1.7983425919\,i & (4.21a)\\
q &\approx\;\;\;\; 4.0496984440 \pm 0.7359317819\,i & (4.21b)
\end{aligned}
$$

There are cusp-like structures around $q \approx 4.04 \pm 0.74\,i$. A closer look shows that these structures are in fact T points located at $q \approx 4.0428606488 \pm 0.7417105390\,i$, from which there emerge very short branches terminating at the endpoints $q \approx 4.0496984440 \pm 0.7359317819\,i$.

We form a matrix $D(q)$ of dimension 13 rather than 15; in this way we can avoid

---

[11] In most of the previously studied cases with cylindrical boundary conditions (namely, triangular-lattice strips of widths $4_P \leq m \leq 7_P$ and square-lattice strips of widths $4_P \leq m \leq 9_P$), the characteristic polynomial associated to the transfer matrix cannot be factored as in (4.20). In other words, none of the eigenvalues $\lambda$ is a polynomial in $q$. The cases with $m \leq 3_P$ are trivial as the transfer matrix is one-dimensional: there is a single eigenvalue, which is indeed a polynomial in $q$.

[12] We also checked — though this is not relevant to computing $\mathcal{B}$ for the boundary conditions being considered here — that the zero-amplitude eigenvalue $\lambda = -q^3 + 6q^2 - 8q - 3$ is not dominant at any of the zeros of our resultant. If the zero-amplitude eigenvalue $\lambda = -q^3 + 6q^2 - 8q - 3$ were in fact dominant somewhere in the complex $q$-plane, then by modifying the top and bottom endgraphs (as shown in [41]) it might be possible to make that eigenvalue (in either the reflection-even or reflection-odd sector or both) contribute to the chromatic polynomial and thereby obtain a *different* limiting curve $\mathcal{B}$ for the different choice of endgraphs.

the two identically vanishing amplitudes.[13] Its determinant has the form

$$
\begin{aligned}
\det D(q) \;=\;\; &\text{const.} \times q^{13}(q-1)^{13}(q-2)^{24}(q^2-3q+1)^{10}(q-3)^{191} \\
&\times (q^3-5q^2+6q-1)^4(q^2-4q+2)(q^3-6q^2+9q-1) \\
&\times (q^2-5q+5)^{14}(q^3-7q^2+14q-7)^2(q-4)^{54} \\
&\times (12q^6-196q^5+1355q^4-5126q^3+11337q^2-14086q+7755) \\
&\times P_1(q)^2
\end{aligned}
\tag{4.22}
$$

where the polynomial $P_1(q)$ can be found in the file `transfer3.m`. The first nine factors in (4.22) are precisely the first minimal polynomials given in [16, Table 1]; therefore, $\det D(q)$ vanishes at the Beraha numbers $q = B_2, \ldots, B_{10}$. The next factor is the square of the polynomial $q^3 - 7q^2 + 14q - 7$, which is $p_{14}(q)$ [16, Table 1], so that $\det D(q)$ also vanishes at $q = B_{14}$. Finally, the determinant also vanishes at $q = 4 = B_\infty$. Unlike what we have seen for cylindrical strips of smaller width, in this case the remaining part of $\det D(q)$ is *not* the square of a polynomial with integer coefficients; rather, there is the additional degree-6 factor preceding $P_1(q)^2$. The dominant amplitude vanishes only at the first seven Beraha numbers $q = 0, 1, 2, B_5, 3, B_7, B_8$, so these values are the only isolated limiting points for this strip. The degree-6 factor and the polynomial $P_1(q)$ do not provide additional isolated limiting points.

The first two zeros $q = 0, 1$ are trivial ones. At $q = 2, 3$, all amplitudes vanish except for a few corresponding to zero eigenvalues; we are thus in Case 3 of Section 2. At $q = 2$, there are 10 nonzero eigenvalues with zero amplitudes, 3 zero eigenvalues with zero amplitudes, and one zero eigenvalue with nonzero amplitude. At $q = 3$ the transfer matrix is not diagonalizable: there are 2 nonzero eigenvalues with zero amplitudes, one $2 \times 2$ nontrivial Jordan block corresponding to $\lambda = 0$ with no contribution at all to the partition function for all $n$, and 10 zero eigenvalues with nonzero amplitudes. The fourth, sixth and seventh real zeros converge exponentially fast to $q = B_5, B_7, B_8$ (see Table 3). The eighth real zero seems to converge at an approximate $1/n$ rate to the value $q_0 \approx 3.5147694243$.

Finally, we find vanishing subdominant amplitudes at $q = B_{10}, B_{14}$, which are greater than $B_{m+1} = B_9$.

## 4.8 $\quad L_x = 9_{\rm P}$

The transfer matrix $T(9_{\rm P})$ is 28-dimensional. It can be brought into block-diagonal form

$$
T(9_{\rm P}) \;=\; \begin{pmatrix} T_+(9_{\rm P}) & 0 \\ 0 & T_-(9_{\rm P}) \end{pmatrix} ,
\tag{4.23}
$$

where the block $T_+$ (resp. $T_-$) is 22-dimensional (resp. 6-dimensional) and corresponds to the subspace of reflection-invariant (resp. reflection-odd) connectivities. Moreover,

---

[13]If we were to form a 15-dimensional or 14-dimensional matrix $D(q)$, its determinant would be identically zero. This tells us (in case we did not know it already) that two of the amplitudes are identically zero.

all the amplitudes corresponding to the reflection-odd subspace are identically vanishing; this subspace therefore makes no contribution to the partition function. The reduced transfer matrix $T_+(9_{\mathrm{P}})$ can be found in the MATHEMATICA file `transfer3.m`.

Mysteriously, all of the eigenvalues in the reflection-odd subspace have "copies" in the reflection-even subspace. This can be seen by computing the characteristic polynomial associated to the transfer matrix $T(9_{\mathrm{P}})$, which can be factored as follows:

$$\det[T(9_{\mathrm{P}}) - \lambda\mathbf{1}] \;=\; Q_1(q,\lambda)^2\, Q_2(q,\lambda) \tag{4.24}$$

where $Q_1(q,\lambda)$ and $Q_2(q,\lambda)$ are polynomials in $q$ and $\lambda$; here $Q_1$ (resp. $Q_2$) is of degree 6 (resp. 16) in $\lambda$. More specifically, $Q_1$ (resp. $Q_1Q_2$) is the characteristic polynomial of $T_-$ (resp. $T_+$); the fact that $Q_1$ appears as a factor in the characteristic polynomial of $T_+$ is direct proof of the just-mentioned "copying" of eigenvalues. Even more mysteriously, our numerical checks suggest that all the eigenvalues coming from $Q_1$ have identically zero amplitudes — not only in the reflection-odd subspace (where this is well understood) but also in the reflection-invariant subspace. We thus find 6 pairs of equal eigenvalues with identically vanishing amplitudes.

In order to be able to use the resultant method in this case, we proceed as in the previous subsection: we drop the polynomial $Q_1(q,\lambda)^2$ (which contains the zero-amplitude eigenvalues) from the characteristic polynomial associated to $T(9_{\mathrm{P}})$ and compute the resultant with the polynomial $Q_2(q,\lambda)$ (which contains the eigenvalues with nonzero amplitudes). We have computed the points with $\theta = 0$ with the resultant method; the points with other values of $\theta$ have been computed using the direct-search method.

The limiting curve $\mathcal{B}$ is connected (see Figure 14). It crosses the real axis at $q_0 \approx 3.5270636990$. It enters the half-plane $\mathrm{Re}(q) < 0$, and there are four endpoints

$$q \;\approx\; -0.4576020413 \pm 1.6238415411\,i \tag{4.25a}$$

$$q \;\approx\; \phantom{-}4.2828643197 \pm 0.3823491910\,i \tag{4.25b}$$

There are T points located at $q \approx 4.0160853030 \pm 0.7870153859\,i$.

We form a matrix $D(q)$ of dimension 16 rather than 28, in order to avoid the 12 identically zero amplitudes. Its determinant has the form

$$\begin{aligned}
\det D(q) \;=\; & \mathrm{const} \times q^{16}(q-1)^{16}(q-2)^{16}(q^2-3q+1)^{13}(q-3)^{173} \\
& \times (q^3-5q^2+6q-1)^5(q^2-4q+2)^4(q^3-6q^2+9q-1) \\
& \times (q^2-5q+5)^7(q^3-7q^2+14q-7)^2 P(q)\,, \tag{4.26}
\end{aligned}$$

where the polynomial $P(q)$ can be found in the file `transfer3.m`. We find the same "Beraha factors" as in the triangular-lattice strip of width $8_{\mathrm{P}}$ (Section 4.7). Thus, $\det D(q)$ vanishes at the Beraha numbers $q = B_2, \ldots, B_{10}, B_{14}$. The polynomial $P(q)$ is not the square of any polynomial with integer coefficients; rather it can be written as $P_1(q)P_2(q)^2$ where $P_1$ and $P_2$ are integer-coefficient polynomials. The dominant amplitude vanishes only at the first seven Beraha numbers $q = 0, 1, 2, B_5, 3, B_7, B_8$; thus, these values are the only isolated limiting points for this strip. The polynomial $P(q)$ does not provide additional isolated limiting points.

The first three zeros $q = 0, 1, 2$ are trivial ones (i.e., all amplitudes vanish identically). The fourth, fifth, sixth and seventh real zeros converge exponentially fast to $q = B_5, 3, B_7, B_8$ (see Table 4). The eighth real zero seems to converge at an approximate $1/n$ rate to the value $q_0 \approx 3.5270636990$.

We again find a vanishing subdominant amplitude at $q = B_{14}$, which is greater than $B_{m+1} = B_{10}$.

## 4.9   $L_x = 10_P$

The transfer matrix $T(10_P)$ is 67-dimensional. It can be brought into block-diagonal form

$$T(10_P) \;=\; \begin{pmatrix} T_+(10_P) & 0 \\ 0 & T_-(10_P) \end{pmatrix} \;, \tag{4.27}$$

where the block $T_+$ (resp. $T_-$) is 51-dimensional (resp. 16-dimensional) and corresponds to the subspace of reflection-invariant (resp. reflection-odd) connectivities. All the amplitudes corresponding to the reflection-odd subspace are identically vanishing; this subspace therefore makes no contribution to the partition function. The reduced transfer matrix $T_+(10_P)$ can be found in the MATHEMATICA file `transfer3.m`.

The characteristic polynomial of the transfer matrix $T(10_P)$ obviously factors as $\det[T(10_P) - \lambda \mathbf{1}] = Q_1(q, \lambda) \, Q(q, \lambda)$, where $Q_1$ (resp. $Q$) is the characteristic polynomial of $T_-$ (resp. $T_+$). Numerically we have found, once again, that all the eigenvalues in the reflection-odd subspace have "copies" in the reflection-even subspace. Therefore, the polynomial $Q(q, \lambda)$ should have $Q_1(q, \lambda)$ as a factor, so that

$$\det[T(10_P) - \lambda \mathbf{1}] \;=\; Q_1(q, \lambda)^2 \, Q_2(q, \lambda) \tag{4.28}$$

where $Q_2(q, \lambda)$ is a polynomial of degree 35 in $\lambda$. Unfortunately, we have been unable to compute the characteristic polynomial $Q(q, \lambda)$ of the reduced transfer matrix $T_+(10_P)$ and verify the conjectured factorization (4.28).

Once again, we have found numerically that the "copied" eigenvalues have identically vanishing amplitudes. We thus find 16 pairs of equal eigenvalues with identically vanishing amplitudes.

We have used the direct-search method in the computation of $\mathcal{B}$. The limiting curve $\mathcal{B}$ is connected (see Figure 15). It crosses the real axis at $q_0 \approx 3.6348299654$. It enters the half-plane $\mathrm{Re}(q) < 0$, and there are four endpoints

$$q \;\approx\; -0.510807 \pm 1.481233 \, i \tag{4.29a}$$
$$q \;\approx\; \phantom{-}4.113231 \pm 0.492835 \, i \tag{4.29b}$$

There are T points located at $q \approx 4.0632619066 \pm 0.8803786140 \, i$.

We have numerically checked that the dominant amplitude vanishes at the first nine Beraha numbers $q = 0, 1, 2, B_5, 3, B_7, B_8, B_9, B_{10}$ (and at no others); therefore, these values are the only isolated limiting points for this strip. We have found no evidence of complex isolated limiting points from the zeros of the finite-length strips.

The first two zeros $q = 0, 1$ are trivial ones. At $q = 2, 3$ we are in Case 3 described in Section 2. At $q = 2$, there are 38 nonzero eigenvalues with zero amplitudes, 12 zero

eigenvalues with zero amplitudes and one zero eigenvalue with a nonzero amplitude. At $q = 3$ the transfer matrix is not diagonalizable: we find 4 nonzero eigenvalues with zero amplitudes, one $2 \times 2$ nontrivial Jordan block corresponding to $\lambda = -3$ which does not contribute to the partition function for any $n$, 40 zero eigenvalues with nonzero amplitudes, and two nontrivial Jordan blocks (of dimensions 3 and 2 respectively) corresponding to $\lambda = 0$. The contribution of these later blocks is zero except for $n = 1$. The fourth, sixth, seventh, eight and ninth real zeros converge exponentially fast to $q = B_5, B_7, B_8, B_9, B_{10}$ (see Table 4). The tenth real zero seems to converge at an approximate $1/n$ rate to the value $q_0 \approx 3.6348299654$.

Finally, we have also checked that there are vanishing amplitudes (in addition to the trivial 32 identically zero amplitudes) for $q = B_{11}$, $B_{14}$, and $B_{18}$. In all these cases, the vanishing amplitude corresponds to a subdominant eigenvalue; thus, none of these points is an isolated limiting point. Please note that the last two values (namely, $B_{14}$ and $B_{18}$) are greater than $B_{m+1} = B_{11}$.

## 4.10 $L_x = 11_\mathrm{P}$

The transfer matrix $T(11_\mathrm{P})$ is 145-dimensional. It can be brought into block-diagonal form

$$T(11_\mathrm{P}) \;=\; \begin{pmatrix} T_+(11_\mathrm{P}) & 0 \\ 0 & T_-(11_\mathrm{P}) \end{pmatrix} \,, \tag{4.30}$$

where the block $T_+$ (resp. $T_-$) is 95-dimensional (resp. 50-dimensional) and corresponds to the subspace of reflection-invariant (resp. reflection-odd) connectivities. All the amplitudes corresponding to the reflection-odd subspace are identically vanishing; this subspace therefore makes no contribution to the partition function. The reduced transfer matrix $T_+(11_\mathrm{P})$ can be found in the MATHEMATICA file `transfer3.m`.

The characteristic polynomial of the transfer matrix $T(11_\mathrm{P})$ obviously factors as $\det[T(11_\mathrm{P}) - \lambda\mathbf{1}] = Q_1(q, \lambda)\, Q(q, \lambda)$, where $Q_1$ (resp. $Q$) is the characteristic polynomial of $T_-$ (resp. $T_+$). Numerically we have found, once again, that all the eigenvalues in the reflection-odd subspace have "copies" in the reflection-even subspace. Therefore, the polynomial $Q(q, \lambda)$ should have $Q_1(q, \lambda)$ as a factor, so that

$$\det[T(11_\mathrm{P}) - \lambda\mathbf{1}] \;=\; Q_1(q, \lambda)^2\, Q_2(q, \lambda) \tag{4.31}$$

where $Q_2(q, \lambda)$ is a polynomial of degree 45 in $\lambda$. Unfortunately, we have been unable to compute the characteristic polynomial $Q(q, \lambda)$ of the reduced transfer matrix $T_+(11_\mathrm{P})$ and verify the conjectured factorization (4.31).

Once again, we have found numerically that the "copied" eigenvalues have identically vanishing amplitudes. We thus find 50 pairs of equal eigenvalues with identically vanishing amplitudes.

As in the preceding subsection, we used the direct-search method in the computation of $\mathcal{B}$. This curve crosses the real $q$-axis at $q_0 \approx 3.6441399017$ (see Figure 16). It enters the half-plane $\mathrm{Re}(q) < 0$, and there are four endpoints

$$q \;\approx\; -0.543988 \pm 1.363241\, i \tag{4.32a}$$

$$q \;\approx\; 4.156093 \pm 0.529420\, i \tag{4.32b}$$

There are T points located at $q \approx 4.0425923021 \pm 0.6927608569\,i$.

We have numerically checked that the dominant amplitude vanishes at the first nine Beraha numbers $q = 0, 1, 2, B_5, 3, B_7, B_8, B_9, B_{10}$ (and at no others), so that these values are the only real isolated limiting points for this strip. We inspected the zeros of the finite-length strips and found no evidence of complex isolated limiting points.

The first three zeros $q = 0, 1, 2$ are trivial ones, as all amplitude vanish. At $q = 3$ the transfer matrix is not diagonalizable. There are four nontrivial Jordan blocks corresponding to four nonzero eigenvalues. Furthermore, the contribution of these Jordan blocks to the partition function vanishes for all $n \geq 1$. We also find 8 nonzero eigenvalues with zero amplitudes, 30 zero eigenvalues with nonzero amplitudes, and 30 zero eigenvalues with zero amplitudes. The fourth, sixth, seventh, eighth and ninth real zeros converge exponentially fast to $q = B_5, B_7, B_8, B_9, B_{10}$ (see Table 4). The tenth real zero seems to converge at an approximate $1/n$ rate to the value $q_0 \approx 3.6441399017$.

Finally, we have also checked that there are vanishing amplitudes (in addition to the trivial 100 identically zero amplitudes) for $q = B_{11}, B_{12}, B_{14}, B_{18}$. In all these cases, the vanishing amplitude is subdominant; thus, none of these points is an isolated limiting point. Again, the values $B_{14}$ and $B_{18}$ are greater than $B_{m+1} = B_{12}$.

## 4.11   $L_x = 12_{\mathrm{P}}$

The transfer matrix $T(12_{\mathrm{P}})$ is 368-dimensional. It can be brought into block-diagonal form

$$T(12_{\mathrm{P}}) \;=\; \begin{pmatrix} T_+(12_{\mathrm{P}}) & 0 \\ 0 & T_-(12_{\mathrm{P}}) \end{pmatrix}\,, \tag{4.33}$$

where the block $T_+$ (resp. $T_-$) is 232-dimensional (resp. 136-dimensional) and corresponds to the subspace of reflection-invariant (resp. reflection-odd) connectivities. All the amplitudes corresponding to the reflection-odd subspace are identically vanishing; this subspace therefore makes no contribution to the partition function. The reduced transfer matrix $T_+(12_{\mathrm{P}})$ can be found in the MATHEMATICA file `transfer3.m`.

The characteristic polynomial of the transfer matrix $T(12_{\mathrm{P}})$ obviously factors as $\det[T(12_{\mathrm{P}}) - \lambda\mathbf{1}] = Q_1(q, \lambda)\,Q(q, \lambda)$, where $Q_1$ (resp. $Q$) is the characteristic polynomial of $T_-$ (resp. $T_+$). Numerically we have found, once again, that all the eigenvalues in the reflection-odd subspace have "copies" in the reflection-even subspace. Therefore, the polynomial $Q(q, \lambda)$ should have $Q_1(q, \lambda)$ as a factor, so that

$$\det[T(12_{\mathrm{P}}) - \lambda\mathbf{1}] \;=\; Q_1(q, \lambda)^2\, Q_2(q, \lambda) \tag{4.34}$$

where $Q_2(q, \lambda)$ is a polynomial of degree 96 in $\lambda$. Unfortunately, we have been unable to compute the characteristic polynomial $Q(q, \lambda)$ of the reduced transfer matrix $T_+(12_{\mathrm{P}})$ and verify the conjectured factorization (4.34).

Once again, we have found numerically that the "copied" eigenvalues have identically vanishing amplitudes. We thus find 136 pairs of equal eigenvalues with identically vanishing amplitudes.

Due to the large dimension of the transfer matrix, we have been unable to compute the limiting curve. However, we have managed using the direct-search method to compute the point where $\mathcal{B}$ crosses the real $q$-axis: $q_0 \approx 3.6431658979$. We have also computed the position of the pair of complex-conjugate T points that are obvious in Figure 16; the result is $q \approx 4.05713658 \pm 0.73432479\,i$.

We have numerically checked that the dominant amplitude vanishes at the first nine Beraha numbers $q = 0, 1, 2, B_5, 3, B_7, B_8, B_9$, and $B_{10}$. These values are the only isolated limiting points for this strip. We have found no evidence of complex isolated limiting points by inspecting the zeros of the finite-length strips.

The first two zeros $q = 0, 1$ are trivial ones. At $q = 2$ there are 164 nonzero eigenvalues with zero amplitudes, 2 zero eigenvalues with nonzero amplitudes, and 66 zero eigenvalues with zero amplitudes. The convergence to $q = B_5, 3, B_7, B_8, B_9$, $B_{10}$ is exponentially fast (see Table 4). The tenth real zero seems to converge at an approximate $1/n$ rate to the value $q_0 \approx 3.6431658979$.

Finally, we have also checked that there are vanishing amplitudes (in addition to the trivial 272 identically zero amplitudes) for $q = B_{11}, B_{12}, B_{13}, B_{14}, B_{18}, B_{22}$. In all these cases, the vanishing amplitude is subdominant; thus, none of these points is an isolated limiting point.

In this case we find three vanishing subdominant amplitudes ($B_{14}$, $B_{18}$, and $B_{22}$) that are greater than the value $B_{m+1} = B_{13}$.

# 5 Numerical Results for the Triangular-Lattice Chromatic Polynomial: Zig–Zag Boundary Conditions

Until now, we have built up the triangular lattice by transferring along a direction that is perpendicular to one of the principal directions of the lattice. An alternative choice, of course, would be to transfer along a direction that is *parallel* to a principal direction. When periodic boundary conditions are imposed across the strip, these two constructions are inequivalent: they yield different finite graphs. We shall refer to this alternative construction, with periodic boundary conditions in the transversal direction and free boundary conditions in the longitudinal direction, as "zig–zag" boundary conditions, and it will be denoted by the subscript Z. Note that the lattice width $m$ must be *even*.

For zig–zag boundary conditions, the transfer matrix is not given by the formulae of Ref. [16]. Rather, as is evident from Figure 1(b), the transfer matrix now takes the following form

$$\mathsf{T}(m_{\mathrm{Z}}) = \mathsf{H}\mathsf{V}_{\mathrm{even}}\mathsf{H}\mathsf{V}_{\mathrm{odd}} \;, \tag{5.1}$$

where $\mathsf{V}_{\mathrm{even}}$ (resp. $\mathsf{V}_{\mathrm{odd}}$) is the product of the matrices associated to the vertical bonds located at even (resp. odd) sites of the lattice. With this definition, all the formulae applied in the previous sections hold.

Our original motivation for introducing this new construction was the following: It is clear from Sections 3 and 4 that the limiting curves for the strips with free and

cylindrical boundary conditions differ qualitatively by the existence of a small additional inward-pointing branch for the case of free b.c., which is absent for cylindrical b.c. In the limit of infinite width, one might wonder whether this branch extends to $q = 2$, as the triangular-lattice Ising model is known to have a zero-temperature critical point [32]. We found it interesting to examine whether we can recover such a branch by imposing zig–zag boundary conditions. The answer turns out to be negative; but it seems to us that zig–zag b.c. are interesting in their own right, irrespective of this initial motivation.

We have computed the transfer matrix $T(m_Z)$ and the limiting curves $\mathcal{B}$ for triangular-lattice strips of even widths $2 \leq m \equiv L_x \leq 10$. It is interesting to note that the trick discussed in [16, Sections 3.1 and 3.3] for the standard construction of a cylindrical triangular-lattice strip is not necessary here. On the other hand, the dimension of the transfer matrix $T(m_Z)$ is in general different from $\mathrm{TriCyl}(m)$, because the invariances are different: for zig-zag boundary conditions, the system is invariant under translations of *even* (but not odd) length and under reflections.

## 5.1   $L_x = 2_Z$

This case is trivial, as the transfer matrix is one-dimensional:

$$Z(2_Z \times n_F) = q(q-1)(q-2)^{2(n-1)} \tag{5.2}$$

Please note that the strip $2_Z \times n_F$ is equivalent to $2_F \times n_F$. Since there is only one eigenvalue, there is obviously no crossing, hence $\mathcal{B} = \varnothing$. However, there are zeros for all $n$ at $q = 0, 1$ and for $n \geq 2$ at $q = 2$.

## 5.2   $L_x = 4_Z$

The transfer matrix is three-dimensional. In the basis $\mathbf{P} = \{1, \delta_{13}, \delta_{24}\}$ it can be written as

$$T(4_Z) = \begin{pmatrix} T_{11} & T_{12} & T_{13} \\ 2q-5 & q^2-4q+4 & 1 \\ T_{31} & q^2-4q+4 & 3q^2-17q+25 \end{pmatrix} \tag{5.3}$$

where

$$
\begin{align}
T_{11} &= q^4 - 12q^3 + 56q^2 - 121q + 101 \tag{5.4a} \\
T_{12} &= q^3 - 8q^2 + 20q - 16 \tag{5.4b} \\
T_{13} &= q^3 - 10q^2 + 34q - 40 \tag{5.4c} \\
T_{31} &= 2q^3 - 17q^2 + 50q - 50 \tag{5.4d}
\end{align}
$$

and the partition function is equal to

$$Z(4_P \times n_Z) = q(q-1) \begin{pmatrix} q^2-3q+3 \\ q-1 \\ q-1 \end{pmatrix}^{\mathrm{T}} \cdot T(4_Z)^{n-1} \cdot \begin{pmatrix} 1 \\ 0 \\ 0 \end{pmatrix} \tag{5.5}$$

The limiting curve $\mathcal{B}$ (see Figure 18) contains two complex-conjugate arcs, which do not cross the real $q$-axis. There are four endpoints:

$$q \approx 2.0991442518 \pm 2.5589234827\,i \qquad (5.6a)$$
$$q \approx 2.7371672817 \pm 0.1723332852\,i \qquad (5.6b)$$

We have found a complex-conjugate pair of double zeros of the resultant for $\theta = 0$ (see [16, Section 4.1.1]) at $q \approx 3.7718445063 \pm 1.1151425080\,i$. At these values the limiting curve appears at first glance to be singular (see Figure 18). However, a closer look reveals that this is *not* the case; in fact, the limiting curve is perfectly analytic around these two points.[14]

The determinant $\det D(q)$ has the form

$$\begin{aligned} \det D(q) &= -q^3(q-1)^3(q-2)^2(q^2-3q+1)(q-3)^2(2q-5)^4 \\ &\quad \times (q^3 - 10q^2 + 34q - 38)^2 \end{aligned} \qquad (5.7)$$

We recognize the first five minimal polynomials $p_k(q)$ given in [16, Table 1]. Hence, the determinant vanishes at the first five Beraha numbers $q = 0, 1, 2, B_5, 3$. The dominant amplitude vanishes at all these points except at $q = 3$; therefore, $q = 0, 1, 2, B_5$ are isolated limiting points. It is interesting to note that the dominant amplitude vanishes also at $q = 5/2$, so that this too is an isolated limiting point. This is the first time we have found a real isolated limiting point that is not a Beraha number. (For the square lattice, we did not find any non-Beraha real isolated limiting point [16, 17].) There are no additional isolated limiting points coming from the last factor $q^3 - 10q^2 + 34q - 38$, as the vanishing amplitudes in question all correspond to subdominant eigenvalues.

The first two real zeros $q = 0, 1$ are trivial as all the amplitudes vanish. The third real zero $q = 2$ belongs to Case 3 of Section 2: the two nonzero eigenvalues have zero amplitude, and there is an additional zero eigenvalue with a nonzero amplitude. Finally, the fourth and fifth real zeros converge exponentially fast to the values $5/2$ and $B_5$, respectively. In summary, we find five isolated limiting points $q = 0, 1, 2, 5/2$ and $B_5$. This is in agreement with Table 5.

Please note that there is a vanishing subdominant amplitude at $q = B_6 = 3$. This value is greater than $B_{m+1} = B_5$, in contrast with the observed behavior for the square lattice [16, 17].

## 5.3 $\quad L_x = 6_{\mathrm{Z}}$

The transfer matrix is seven-dimensional; it can be found in the MATHEMATICA file `transfer3.m`.

---

[14]In the notation of [16, Section 4.2], the characteristic polynomial of $T(4_{\mathrm{Z}})$ can be expanded as

$$P(\lambda, q) = c(\lambda - \lambda_0)^2 + d(q - q_0)^2 + e(q - q_0)(\lambda - \lambda_0) + \ldots$$

around the points $q_0 \approx 3.7718445063 \pm 1.1151425080\,i$ and the dominant (double) eigenvalue $\lambda_0 = -0.5237532362 + 4.5580089825\,i$ (the linear terms in $\lambda - \lambda_0$ and $q - q_0$ vanish). This expansion leads to analytic eigenvalues $\lambda_{\pm}(q)$ around $q = q_0$ and to an analytic equimodular locus around $q = q_0$.

The limiting curve $\mathcal{B}$ is connected (see Figure 19). It crosses the real axis at $q \approx 3.1752579126$. There are four endpoints:

$$q \approx 0.3618461880 \pm 2.5093731708\,i \qquad (5.8a)$$

$$q \approx 4.2589504182 \pm 0.7015734543\,i \qquad (5.8b)$$

There are T points at $q \approx 3.8395346820 \pm 1.1149959335\,i$.

The determinant $\det D(q)$ has the form

$$\det D(q) = 81q^7(q-1)^7(q-2)^{18}(q^2-3q+1)^4(q-3)^{44}(q^3-5q^2+6q-1)P(q)^2 \quad (5.9)$$

where the polynomial $P(q)$ can be found in the file `transfer3.m`. The first six polynomial are the first six minimal polynomials given in [16, Table 1]; hence the determinant vanishes at the first six Beraha numbers $q = 0, 1, 2, B_5, 3, B_7$. The dominant amplitude vanishes at the first five Beraha numbers $q = 0, 1, 2, B_5, 3$ as well as at three of the zeros of $P(q)$, namely $q \approx 2.7226328355$ and $q \approx 3.6696077451 \pm 0.9506864736\,i$. This is the first triangular-lattice strip where we find complex isolated limiting points. In the square-lattice case, complex isolated limiting points were quite common: we found such limiting points for $L \geq 6$ with both free and cylindrical boundary conditions [16, 17].

The first two real zeros $q = 0, 1$ are trivial ones. The third real zero $q = 2$ falls in Case 3 of Section 2: there are four nonzero eigenvalues with zero amplitudes, two zero eigenvalues with nonzero amplitudes, and one zero eigenvalue with zero amplitude. The convergence of the fourth, fifth and sixth real zeros to their corresponding limiting values (namely, $B_5, 2.7226328355$, and 3) is exponentially fast, as shown in Table 5. Finally, the seventh real zero converges at an approximate $1/n$ rate to the value $q \approx 3.1752579126$.

In summary, we find six real isolated limiting points at $q = 0, 1, 2, B_5, 2.7226328355, 3$ and $B_7$ (see Table 5) and two complex isolated limiting points at $q \approx 3.6696077451 \pm 0.9506864736\,i$. However, since the complex isolated limiting points are very near $\mathcal{B}$, it is very difficult to observe the convergence to them as distinct from the convergence to $\mathcal{B}$ (see Figure 19).

## 5.4 $L_x = 8_Z$

The transfer matrix is 24-dimensional; it can be found in the MATHEMATICA file `transfer3.m`.

The limiting curve $\mathcal{B}$ is connected (see Figure 20). It crosses the real axis at $q \approx 3.3941047539$. There are four endpoints:

$$q \approx -0.2143469947 \pm 2.0301412598\,i \qquad (5.10a)$$

$$q \approx 4.2899063418 \pm 0.5046183096\,i \qquad (5.10b)$$

There are T points at $q \approx 4.0055796610 \pm 0.8830638824\,i$.

In this case we were unable to compute the determinant $\det D(q)$. However, we checked numerically whether any of the amplitudes vanishes at the Beraha numbers

$B_n$, and if this occurs, whether the vanishing amplitude is the leading one or not. We have made this check up to $n = 50$. We have found that at least one amplitude vanishes at the Beraha numbers $q = 0, 1, 2, B_5, 3, B_7, B_8, B_9$. The dominant amplitude vanishes only at the first six (namely, $q = 0, 1, 2, B_5, 3, B_7$), so that these latter numbers are isolated limiting points (see Table 5). In Table 5 we also notice an additional isolated zero at $q \approx 2.8214204955$. We have numerically confirmed that this point is indeed an isolated limiting point by minimizing the absolute value of the dominant amplitude $\alpha^\star$ in a neighborhood of that point.

The first two real zeros $q = 0, 1$ are trivial ones. At $q = 2$, there are 13 nonzero eigenvalues with zero amplitudes, 2 zero eigenvalues with nonzero amplitudes, and 9 zero eigenvalues with zero amplitudes. Finally, the other real zeros in Table 5 converge exponentially fast to their corresponding limiting values (namely, $B_5, 2.8214204955, 3$, and $B_7$). We expect, for sufficiently larger lengths $n$, an additional real zero larger than $B_7$ and converging to $q \approx 3.3941047539$; but we apparently need to go beyond $n = 80$ to see it. In summary, there are seven real isolated limiting points at $q = 0$, 1, 2, $B_5$, 2.8214204955, 3, and $B_7$.

By minimizing the absolute value of the dominant amplitude $\alpha^\star$, we have found a pair of complex-conjugate isolated limiting points at $q \approx 3.8327415674 \pm 0.73050211595\,i$ (See Figure 20). Again, we are not sure that we have found all complex isolated limiting points for this strip.

## 5.5 $\quad L_x = 10_{\mathrm{Z}}$

The transfer matrix is 87-dimensional; it can be found in the MATHEMATICA file `transfer3.m`.

In this case we were unable to compute the limiting curve. However, we were able to compute the value of $q$ where that curve crosses the real axis: $q \approx 3.5204366907$.

The matrix $D(q)$ is too large for us to compute its determinant. Instead, we have checked numerically the eigenvalues and amplitudes of the transfer matrix at the Beraha numbers $B_n$ with $2 \leq n \leq 50$. We have found that at least one amplitude vanishes at the Beraha numbers $q = 0, 1, 2, B_5, 3, B_7, B_8, B_9, B_{10}, B_{11}$. The dominant amplitude vanishes only at the first seven (namely, $q = 0, 1, 2, B_5, 3, B_7, B_8$), so that these latter numbers are isolated limiting points (see Table 5). In Table 5 we also notice two additional isolated zeros at $q \approx 2.8737312493$ and $q \approx 3.3831285312$. We have numerically checked that in both cases the leading amplitudes vanish, so they too are isolated limiting points.

The first two real zeros $q = 0, 1$ are trivial. At $q = 2$, there are 35 nonzero eigenvalues with zero amplitudes, 31 zero eigenvalues with zero amplitudes, and 21 zero eigenvalues with nonzero amplitudes. The convergence of the fourth through ninth real zeros to their corresponding limiting values (namely, $B_5, 2.8737312493, 3, B_7, 3.3831285312, B_8$) is exponentially fast as shown in Table 5. Finally, the tenth real zero converges at an approximate $1/n$ rate to the value $q \approx 3.5204366907$.

In summary, there are nine real isolated limiting points at $q = 0$, 1, 2, $B_5$, 2.8737312493, 3, $B_7$, 3.3831285312, and $B_8$. We have been unable to say whether

or not there are any complex isolated limiting points; but we do not see any candidate in Figure 21.

# 6   Thermodynamic Limit

In this section we will review the Bethe-Ansatz solution found by Baxter [18, 19] for the thermodynamic limit of the zero-temperature triangular-lattice Potts antiferromagnet (Section 6.1), and carefully recalculate Baxter's predictions for the limiting curve $\mathcal{B}_\infty$ where the chromatic roots are expected to accumulate (Section 6.2). The resulting picture will be substantially similar to that set forth by Baxter [19], but with a few important qualitative differences. Next we will compare Baxter's predictions for the dominant eigenvalues with our finite-lattice data (Section 6.3), and comment on the agreements and discrepancies (Section 6.4).

## 6.1   Baxter's solution

In terms of the variables $x$ and $\theta$ defined by

$$q \;=\; 2 - x - x^{-1} \;=\; 2 + 2\cos\theta \tag{6.1}$$

with $|x| < 1$ and $0 < \mathrm{Re}\,\theta < \pi$, Baxter defined three functions (eigenvalues) $g_i(q)$ as follows:

$$g_1(q) \;=\; -\frac{1}{x}\prod_{j=1}^{\infty}\frac{(1 - x^{6j-3})(1 - x^{6j-2})^2(1 - x^{6j-1})}{(1 - x^{6j-5})(1 - x^{6j-4})(1 - x^{6j})(1 - x^{6j+1})} \tag{6.2a}$$

$$\log g_2(q) \;=\; \int_{-\infty}^{\infty} dk\,\frac{\sinh k\theta}{2k}\left(\frac{\sinh[k(\pi - 2\theta)/2]}{(2\cosh k\theta - 1)\sinh(\pi k/2)}\right.$$
$$\left. -\,\frac{\cosh[k(\pi - 2\theta)/2]}{(2\cosh k\theta + 1)\cosh(\pi k/2)}\right) \tag{6.2b}$$

$$\log g_3(q) \;=\; \int_{-\infty}^{\infty} dk\,\frac{\sinh k\theta\,[\sinh k(\pi - \theta)]}{k\sinh \pi k\,[2\cosh k(\pi - \theta) - 1]} \tag{6.2c}$$

These formulae were obtained in [18], but the corresponding ranges of validity were established only in [19]. In particular, Baxter found that the complex $q$-plane can be divided into three domains $\mathcal{D}_i$ $[i = 1, 2, 3]$, in each of which the dominant eigenvalue is $g_i$. According to Baxter [19], the intersections of these regions with the real axis are as follows:

$$\mathcal{D}_1 \cap \mathbb{R} \;=\; \{q > 4\} \cup \{q < 0\} \tag{6.3a}$$
$$\mathcal{D}_2 \cap \mathbb{R} \;=\; \{q_0 < q < 4\} \tag{6.3b}$$
$$\mathcal{D}_3 \cap \mathbb{R} \;=\; \{0 < q < q_0\} \tag{6.3c}$$

Baxter therefore determined the parameter $q_0$ by solving the equation

$$g_2(q_0) = g_3(q_0) \qquad (6.4)$$

via Newton's method and numerical integration of (6.2b)/(6.2c), and found $q_0 \approx$ 3.81967. We have refined this computation using the same method, and find

$$q_0(\text{Baxter}) \approx 3.819671731239719 . \qquad (6.5)$$

This point is labelled F in Figures 24 and 26 ($\theta_{\mathrm{F}} \approx 0.427907971348122$). We have also plotted the eigenvalues $g_2$ and $g_3$ over the entire range $0 < \theta < \pi$ and verified that there is only one crossing point, namely (6.5). However, as we will argue later, the intersections $\mathcal{D}_i \cap \mathbb{R}$ are in fact more complicated than what is claimed in (6.3), so that (6.5) is *not* in fact the correct value of $q_0$ *if Baxter's three eigenvalues are in fact the dominant ones*. (See Sections 6.3 and 6.4 for further discussion.)

In order to obtain the limiting curve $\mathcal{B}_\infty$ in the complex $q$-plane, Baxter [19] took advantage of the following simpler expressions for the ratios of eigenvalues:

$$\frac{g_2(q)}{g_1(q)} = \prod_{j=1}^{\infty} \left( \frac{1 - \omega p^{2j-1}}{1 - \omega p^{2j}} \right)^3 \frac{1 - p^{6j}}{1 - p^{6j-3}} \qquad (6.6a)$$

$$\frac{g_3(q)}{g_1(q)} = \prod_{j=1}^{\infty} \left( \frac{1 + \omega^2 y^j}{1 - \omega^2 y^j} \right)^3 \frac{1 - y^{3j}}{1 + y^{3j}} \qquad (6.6b)$$

where

$$p = -e^{i\pi^2/3\theta} \qquad (6.7a)$$
$$y = e^{-2i\pi^2/3(\pi-\theta)} \qquad (6.7b)$$
$$\omega = e^{2\pi i/3} \qquad (6.7c)$$

In these equations we require that $|p| < 1$ and $|y| < 1$ so that the products converge; this corresponds to $\operatorname{Im} \theta < 0$.

As Baxter [19] noted, the parameter $\theta$ enters into the products (6.6a,b) only via $p$ or $y$, respectively, and these two variables are invariant under the transformations

$$\frac{\pi}{\theta} \to \frac{\pi}{\theta} + 6k \qquad \Longrightarrow \qquad p \to p \qquad (6.8a)$$

$$\frac{\pi}{\pi - \theta} \to \frac{\pi}{\pi - \theta} + 3k' \qquad \Longrightarrow \qquad y \to y \qquad (6.8b)$$

for any integers $k, k'$. Thus, each solution of $|g_2/g_1| = 1$ in the complex $p$-plane corresponds to an infinite family of solutions in the complex $\theta$-plane: these can be thought of as a "primary" solution (namely, the one with largest $\operatorname{Re} \theta$ contained in the physical region $0 < \operatorname{Re} \theta < \pi$) and its "images" under the transformation (6.8a) with $k \geq 1$. As $k \to \infty$ these "image" curves converge to $\theta = 0$ ($q = 4$). Likewise, each solution of $|g_3/g_1| = 1$ in the complex $y$-plane corresponds to an infinite family

33

of solutions in the complex $\theta$-plane: a "primary" solution (the one with smallest $\mathrm{Re}\,\theta$ contained in the physical region) and its "images" under the transformation (6.8b) with $k' \geq 1$. As $k' \to \infty$ these "image" curves converge to $\theta = \pi$ ($q = 0$). It is important to note that the transformations (6.8) do *not* tell anything about the dominant or subdominant character of the equimodular curve at the transformed value of $\theta$; this property has to be checked by other means.

Let us emphasize that the symmetries (6.8) play no essential logical role in our analysis: one can, in principle, discover all the equimodular curves by direct search, without any reference to these symmetries. But it is *useful* to know, once one has discovered one equimodular curve, that in certain circumstances there must exist others as well (and to know their exact location).

**Important Remark.** Neither the eigenvalues (6.2b,c) nor the eigenvalue ratios (6.6a,b) or $g_3/g_1 = (6.6a)/(6.6b)$ — nor even their absolute values — are invariant under the transformation $\theta \to \theta + 2\pi k''$ that leaves $q$ invariant. Therefore, we *must* require $0 < \mathrm{Re}\,\theta < \pi$ when using these formulae.

**Remarks.** 1. The formula $q = 2 - x - x^{-1}$ maps the disc $|x| < 1$ one-to-one onto the $q$-plane cut along the interval $[0, 4]$. Therefore (as Baxter observed [19]), when $q$ is real and $q > 4$ or $q < 0$, the parameter $x$ is also real, as is the eigenvalue $g_1$ defined in (6.2a).

2. The formula $q = 2 + 2\cos\theta$ maps the strip $0 < \mathrm{Re}\,\theta < \pi$ one-to-one onto the $q$-plane cut along the intervals $(-\infty, 0]$ and $[4, \infty)$. In particular, when $q$ is real and $0 < q < 4$, the parameter $\theta$ is real ($0 < \theta < \pi$), as are the eigenvalues $g_2$ and $g_3$ defined in (6.2b)/(6.2c).

3. The definitions (6.2a), (6.6a) and (6.6b) cannot be applied directly *on* the real $q$-axis for $0 < q < 4$; rather, one must consider a limit in which $\mathrm{Im}\,\theta \uparrow 0$ and hence $|x|, |p|, |y| \uparrow 1$.

## 6.2 Recomputation of Baxter's phase diagram

In this subsection we will carefully recompute the limiting curve $\mathcal{B}_\infty$ *under the tentative hypothesis that Baxter's three eigenvalues are in fact the dominant ones.* (In Section 6.3 we will test this hypothesis against our finite-lattice data.)

### 6.2.1 Computation of limiting curves

Our goal is to compute the locus of points where two or more of the eigenvalues $g_i$ are equimodular, and to determine at each such point whether these equimodular eigenvalues are dominant or subdominant. We carry out this procedure as follows:

1) We use (6.6a) to compute the locus $|g_2/g_1| = 1$ in the complex $p$-plane (Figure 22); we then transform the resulting plot to the complex $\theta$-plane using (6.7a). As noted above, each curve in the $p$-plane corresponds to an infinite family of curves in the $\theta$-plane. Along each of these latter curves, we compute $|g_3/g_1|$ and classify the curve (or portions of it) as dominant or subdominant.

2) We use (6.6b) to compute the locus $|g_3/g_1| = 1$ in the complex $y$-plane (Figure 23); we then transform the resulting plot to the complex $\theta$-plane using (6.7b). Each curve in the $y$-plane corresponds to an infinite family of curves in the $\theta$-plane. Along each of these latter curves, we compute $|g_2/g_1|$ and classify the curve (or portions of it) as dominant or subdominant.

3) We use (6.6a,b) to compute the locus $|g_3/g_2| = 1$ directly in the complex $\theta$-plane and to determine dominance or subdominance.

4) We combine the three families of equimodular curves into a single $\theta$-plane plot (Figure 24).

5) Finally, we transform the resulting curves to the complex $q$-plane using (6.1). The resulting "phase diagram" is shown in Figure 25; a detailed view near the point $q = 4$ is shown in Figure 26.

Despite the explicit formulae (6.6), these computations are far from straightforward, due to the slow convergence of the products when $|p|$ or $|y|$ is near 1 (i.e. when $q$ is near the interval $0 < q < 4$ of the real axis) and to the need for very high numerical precision in intermediate stages of the computation. We discuss these technical points in the Appendix.

The equimodular curves $|g_2/g_1| = 1$ in the complex $p$-plane are shown in Figure 22. Each equimodular curve $C_n$ has exactly two endpoints. As we approach the circle $|p| = 1$, more smaller equimodular curves appear. In order to disentangle the larger curves from these new smaller curves, we have followed each equimodular curve carefully as it approaches the $|p| = 1$ limit. In Figure 22 we have shown all equimodular curves that intersect the circle $|p| = 0.99$.

The principal feature is a curve $C_1$ running from point G ($p = -1$, $\theta = \pi/6$ and images) via the origin ($p = 0$, $\theta = -i0$) to point H ($p = -i$, $\theta = 2\pi/3$ and images). The next-longest curve ($C_2$) runs from point I ($p = i$, $\theta = 2\pi/9$ and images) to point J ($p = e^{3\pi i/7}$, $\theta = 7\pi/30$ and images). The third-longest curve ($C_3$) runs from point K ($p = e^{-\pi i/5}$, $\theta = 5\pi/12$ and images) to point L ($p = e^{-\pi i/4}$, $\theta = 4\pi/9$ and images). Some further equimodular curves and their endpoints are shown on Figure 22 and enumerated in Table 8. In this table we have first shown the curves $C_n$ for which both endpoints are reasonably well determined (see below). Then we have listed some other well-determined endpoints whose counterparts could not be estimated with sufficient accuracy; these points are grouped into the category "Others".

It is curious that all these endpoints appear to lie at $p = e^{i\varphi}$ where $\varphi$ is a rational multiple of $\pi$ (with a small denominator). In order to test this conjecture, we have performed detailed fits as follows: For each endpoint we first obtained ten nearby equimodular points $p$ with $|p| = 0.990, 0.991, \ldots, 0.999$. Then we performed a least-

squares fit of the data[15] using the polynomial Ansatz

$$\frac{\operatorname{Arg} p}{\pi} \;=\; \frac{\operatorname{Arg} p_{\text{Fit}}}{\pi} + \sum_{k=1}^{8} a_k (1 - |p|)^k \tag{6.9}$$

in order to estimate the phase $\varphi = \operatorname{Arg} p_{\text{Fit}}$ at the endpoint. If the equimodular curve is smooth close to $|p| = 1$, this Ansatz is expected to work well. We have chosen an eighth-order polynomial in order to take into account as many data points as possible while allowing a little freedom (we have one degree of freedom in the fits). As a check, we have repeated this computation with lower-degree polynomial Ansätze and dropping the data with the smallest values of $|p|$ (in order to have at least one degree of freedom in the fit). We have used the stability of the estimates for $\operatorname{Arg} p_{\text{Fit}}$ as a guideline to decide whether a fit is good or not (see below).

We next asked whether the estimated value of $\operatorname{Arg} p_{\text{Fit}}/\pi$ is or is not close to a rational number with a small denominator. We have used the following basic criterion: the real number $x$ is "close" to the rational number $m/n$ whenever the

$$\text{"discrepancy"} \;\equiv\; |nx - m| \tag{6.10}$$

is sufficiently small. In order to make precise what we mean by "sufficiently small", let us first define

$$d_n(x) \;=\; \min_{m \in \mathbb{Z}} |nx - m| \,. \tag{6.11}$$

Clearly, for *every* real number $x$ and *every* integer $n$, we have $d_n(x) \leq 1/2$; so, if we are to have good evidence that $x = m/n$, we will need to insist, at the very least, that the "discrepancy" be $\ll 1/2$. But this requirement is, in fact, nowhere near stringent enough: the trouble is that, in our procedure, the denominator $n$ is not fixed in advance; rather, we start from the number $x$ and we ask whether there *exists* a (small) integer $n$ such that $d_n(x) \ll 1$. And the occurrence of *some* integers $n$ such that $d_n(x) \ll 1$ is by no means a rare event. Indeed, a theorem of Hurwitz (1891) asserts that for *every* real number $x$, *there exist* infinitely many integers $n$ such that $d_n(x) < 1/(\sqrt{5}\,n)$.[16] So we will need to demand that $d_n(x) \ll 1/n$. This suggests using the criterion $d_n(x) \leq \delta/n^s$ for some $\delta > 0$ and some $s > 1$.

Suppose, in fact, that $x$ is a *randomly chosen* real number (from a uniform distribution). Then it is not hard to show that

$$\text{Prob(there exists an integer } n \text{ with } d_n(x) \leq \delta/n^s) \;\leq\; \sum_{n=1}^{\infty} \frac{2\delta\phi(n)}{n^{s+1}} \tag{6.12a}$$

$$=\; \frac{2\delta\zeta(s)}{\zeta(s+1)} \,, \tag{6.12b}$$

---

[15] We have made the computations with data truncated to eight decimal digits, hence the error of the input data is $10^{-8}$. Note, however, that the deviations from (6.9) are *not* statistical fluctuations; rather, they are "corrections to scaling", i.e. due to neglected higher-order terms in (6.9). A large value of the $\chi^2$ is thus a signal that we need to include higher-order terms in our Ansatz.

[16] The constant $\sqrt{5}$ is best possible, as is shown by $x = (1 + \sqrt{5})/2$. For a proof of Hurwitz's theorem, see [54, Chapter 1], [55, Chapters 5 and 6] or [56, Chapter I].

where $\phi(n)$ is the Euler totient function (i.e. the number of integers $1 \le k \le n$ that are relatively prime to $n$) and $\zeta(s)$ is the Riemann zeta function.[17] Therefore, if we insist that

$$\text{``discrepancy''} \quad \le \quad \frac{\epsilon \zeta(s+1)}{2\zeta(s)n^s} \ , \tag{6.13}$$

we are following a procedure whose probability of yielding a "false positive signal" is less than $\epsilon$ (if $x$ is chosen uniformly at random). Otherwise put, we can define a "significance level"

$$\epsilon \quad = \quad \frac{2\zeta(s)n^s}{\zeta(s+1)} \ \times \ \text{``discrepancy''} \ . \tag{6.14}$$

For concreteness, we have chosen $s = 3/2$. Roughly speaking, we consider the equality $x = m/n$ to be very strongly supported if $\epsilon \lesssim 0.001$, strongly supported if $\epsilon \lesssim 0.01$, and a plausible guess if $\epsilon \lesssim 0.05$.

We have been able to fit the data corresponding to 42 endpoints. (We have numerically located additional endpoints, but we have not included here those endpoints that correspond to very small equimodular curves close to the circle $|p| = 1$.) Of these 42 endpoints, we have obtained a reasonably good fit for the 28 points displayed in Table 8: here a "reasonably good fit" is defined as one for which $\epsilon \le 0.05$ and for which the values of $\mathrm{Arg}\, p_{\mathrm{Fit}}$ and $\epsilon$ are stable under changes in the degree of the polynomial Ansatz (6.9). We find that 18 points have $\epsilon \le 10^{-3}$ (eight of them even have $\epsilon \le 10^{-4}$), while 10 points have $10^{-3} < \epsilon \le 0.05$.

We have found several smaller equimodular curves that are hard to see on Figure 22, and we suspect that they too have rational endpoints. Indeed, we would not be surprised to learn that such rational endpoints are *dense* in the unit circle (though we have no idea how to prove this conjecture).

The equimodular curves $|g_3/g_1| = 1$ in the complex $y$-plane are shown in Figure 23. Again, each equimodular curve $D_n$ has exactly two endpoints, and smaller equimodular curves appear as we approach the $|y| = 1$ limit. We have shown in Figure 22 all equimodular curves that intersect the circle $|y| = 0.99$.

The principal feature is again a curve $D_1$ running from point G ($y = e^{-4\pi i/5}$, $\theta = \pi/6$ and images) via the origin ($p = 0$, $\theta = \pi - i0$) to point H ($y = 1$, $\theta = 2\pi/3$ and images). The next-longest curve ($D_2$) runs from point K ($y = e^{6\pi i/7}$, $\theta = 5\pi/12$ and images) to point L ($y = e^{4\pi i/5}$, $\theta = 4\pi/9$ and images). Finally, a small curve ($D_4$) runs from point G' ($y = e^{-8\pi i/11}$, $\theta = \pi/12$ and images) to point H' ($y = e^{-10\pi i/13}$, $\theta = 2\pi/15$ and images); we call these points G' and H' because they correspond to $\theta$

---

[17]PROOF OF (6.12): Let $x$ be a uniform random number in $[0, 1]$; we do all our arithmetic in the real numbers modulo 1. For any fixed $m$ and $n$, we clearly have $\mathrm{Prob}(|nx - m| \le \delta/n^s) = \min[2\delta/n^{s+1}, 1]$. Now we need to sum over pairs $(m, n)$ with $1 \le m \le n$; in doing this, it suffices to consider only pairs $(m, n)$ that are *relatively prime*, since if $m/n = m'/n'$ with $n' < n$, then the interval $|nx - m| \le \delta/n^s$ is entirely contained in the larger interval $|n'x - m'| \le \delta/n'^s$. This proves (6.12a). The equality with (6.12b) is a standard identity in analytic number theory: see e.g. [57, p. 371].

Of course, (6.12) is still an overestimate, because it neglects the overlaps between intervals whose denominators $n$ and $n'$ do not divide each other. It would be interesting to know what the true behavior of this probability is.

values that are images of the points G and H under the $p$-plane transformation (6.8a) [though they are not images in the $y$-plane].

Once again, all the endpoints appear to lie at $y = e^{i\psi}$ where $\psi$ is a rational multiple of $\pi$ with small denominator. Even more curiously, many of these endpoints correspond to $\theta$ values that are also observed as endpoints in the $|g_2/g_1| = 1$ plot (e.g., all points with a label in Tables 8 and 9). We performed fits to those endpoints in the same manner as just explained for the $p$-plane. We found 44 endpoints, and of these we obtained reasonably good fits for the 23 endpoints displayed in Table 9. All these points satisfy the criterion $\epsilon \leq 0.05$, and both $\mathrm{Arg}\, p_{\mathrm{Fit}}$ and $\epsilon$ are rather stable as we vary the degree of the polynomial Ansatz (6.9). Of these 23 endpoints, we find 12 satisfying $\epsilon \leq 10^{-3}$ (six of them satisfy the stronger condition $\epsilon \leq 10^{-4}$), while the other 11 endpoints satisfy $10^{-3} < \epsilon \leq 0.05$.

We have also found more smaller equimodular curves that are hard to see on Figure 23; we conjecture that they have rational endpoints and we wonder whether these rational endpoints are dense in the unit circle.

**Remark**. It is important to note that the two main points in Figures 24–25 (namely, G and H) are extremely well determined in both the $p$- and $y$-planes. In particular, their $\epsilon$ values range from $4 \times 10^{-5}$ down to $6 \times 10^{-8}$. Thus, we can trust that the values of $\theta$ for these two points are given *exactly* by $\theta_G = \pi/6$ and $\theta_H = 2\pi/3$ (see Tables 8–9).

### 6.2.2 Summary of $\theta$-plane phase diagram

Let us now describe the resulting zero-temperature "phase diagram" in the complex $\theta$-plane (Figure 24) and discuss the agreements and discrepancies with respect to Baxter [19]. For simplicity we have labelled the points by the same letters as in Figure 5 of [19]. The portions of curves where the equimodular eigenvalues are dominant (resp. subdominant) are depicted in black (resp. pink).

The curve A–B (resp. B–C) corresponds to the dominant equimodularity of $g_3$ (resp. $g_2$) and $g_1$. These two curves together with the real $\theta$ axis enclose the rest of the dominant curves. The position of these points is

$$
\begin{aligned}
\theta_A &= \pi & \text{(6.15a)} \\
\theta_B &\approx 0.508588719845180 - 0.625516375803391\, i & \text{(6.15b)} \\
\theta_C &= 0 & \text{(6.15c)}
\end{aligned}
$$

The point B is triply equimodular (i.e. a T point), so that three equimodular curves cross there:

1) C–B–H, which corresponds to $|g_1| = |g_2|$ (it is dominant along C–B and subdominant along B–H); and

2) A–B–Q–G, which corresponds to $|g_1| = |g_3|$ (it is dominant along A–B, subdominant along B–Q, and dominant again along Q–G);

38

3) R–B–Q–F, which corresponds to $|g_2| = |g_3|$ (it is subdominant along R–B, dominant along B–Q, and subdominant again along Q–F). Point R corresponds to $\theta = -i\infty$.

This last result contradicts [19], where the entire curve B–Q–F is claimed to be dominant. The position of these points is[18]

$$\theta_Q \approx 0.440568708859061 - 0.235993788540783\,i \qquad (6.16a)$$
$$\theta_F \approx 0.427907971348122 \qquad (6.16b)$$

The point Q is also triply equimodular, so that three equimodular curves cross there. Two of them have just been discussed: A–B–Q–G and R–B–Q–F. The third is C–Q–G, which corresponds to $|g_1| = |g_2|$; it is dominant along C–Q and subdominant along Q–G. Please note that the subdominant curve Q–G lies always to the right of (but very close to) the dominant curve Q–G.

There are infinitely many equimodular curves $|g_1| = |g_2|$ terminating at point C ($q = 4$) and converging to it: they are images under (6.8a) of the two curves C–B–H and C–Q–G. The dominant eigenvalue alternates between $g_1$ and $g_2$ as these curves are crossed. For simplicity, we have shown in Figure 24 only the first few of these image curves. The endpoints of these curves can be obtained easily using the values of $\theta_G = \pi/6$ and $\theta_H = 2\pi/3$ (see Table 8) and transformation (6.8a). The result is

$$\theta_{G,k} = \frac{\pi}{6(1+k)} \qquad (6.17a)$$
$$\theta_{H,k} = \frac{2\pi}{3(1+4k)} \qquad (6.17b)$$

According to (1.3)/(6.1), they correspond to Beraha numbers: $\theta_{G,k}$ is $B_{12+12k}$, and $\theta_{H,k}$ is $B_{3+12k}$.

Likewise, there are infinitely many equimodular curves $|g_1| = |g_3|$ terminating at point A ($q = 0$) and converging to it: they are images under (6.8b) of the two curves A–B–Q–G and A–H. The dominant eigenvalue alternates between $g_1$ and $g_3$ as these curves are crossed. Once again, we have shown in Figure 24 only the first few of these image curves. The endpoints of these curves can be obtained easily using the values of $\theta_G = \pi/6$ and $\theta_H = 2\pi/3$ (see Table 9) and transformation (6.8b). The result is

$$\theta_{G,k'} = \frac{1 + 15k'}{6 + 15k'}\pi \qquad (6.18a)$$
$$\theta_{H,k'} = \frac{2 + 3k'}{3 + 3k'}\pi \qquad (6.18b)$$

In this case, none of them corresponds to a Beraha number.

There are also many small equimodular curves lying near the real $\theta$-axis, some of which are dominant; they arise from the curves I–J, K–L, etc. in Figures 22 and

---

[18]Despite appearances, the point F in Figure 24 is *not* triply equimodular: the dominant equimodular curve $|g_1| = |g_2|$ meets the real axis at H' ($\theta = 2\pi/15 \approx 0.41888$), i.e. slightly *below* point F; this is discussed below at (6.17b) ff. This splitting is somewhat more visible on Figure 26.

39

23. The number of these curves grows rapidly as $|\operatorname{Im}\theta| \to 0$, so we cannot possibly compute all of them; moreover, the computation becomes increasingly difficult as $|\operatorname{Im}\theta| \to 0$, since $|p|$ and $|y|$ are tending to 1. We have, in any case, shown in Figure 24 all those curves in the range $0.2 \le \operatorname{Re}\theta \le 2.3$ that intersect the half-plane $\operatorname{Im}\theta \le -0.01$. Again, one can obtain the endpoints of these curves by applying transformations (6.8) to the corresponding $\theta$ values in Tables 8 and 9. These endpoints are not in general Beraha numbers. Only point I ($\theta_I = 2\pi/9$) and its transformed values under (6.8a),

$$\theta_{I,k} = \frac{2\pi}{9+12k} \,, \tag{6.19}$$

are Beraha numbers (namely, $B_{9+12k}$).

It follows from Figure 24 that the point $q_0$ should not be identified with F (as Baxter [19] did), but rather with the point G at position

$$\theta_{\mathrm{G}} = \frac{\pi}{6} \approx 0.523598775598299 \tag{6.20}$$

(see Tables 8 and 9).

### 6.2.3 Summary of $q$-plane phase diagram

In Figure 25 we show the above "phase diagram" in the $q$-plane (for clarity, only the dominant equimodular curves have been depicted). This is quite similar to Figure 5 of [19], except for four issues:

1) The "phase diagram" around point C ($q = 4$) is richer than the one found by Baxter (see Figure 26 for a detailed plot of this region). The largest components of the region $\mathcal{D}_2$ (where $g_2$ is dominant) are bounded by C–B–Q–C and its complex-conjugate counterpart C–E–Q$'$–C. The points B and Q take the values

$$q_{\mathrm{B}} \approx 4.099903170634857 + 0.649694690705481\,i \tag{6.21a}$$
$$q_{\mathrm{Q}} \approx 3.859627688708099 + 0.203154495450945\,i \tag{6.21b}$$

However, there are additional components of $\mathcal{D}_1$ and $\mathcal{D}_2$ near point C; indeed, as we approach point C the dominant eigenvalue alternates between $g_1$ and $g_2$. Thus, $g_1$ is dominant on the region lying between C–Q–G–Q$'$–C and C–$B_{15}$–C; $g_2$ is dominant on the region between the curve C–$B_{15}$–C and the next curve we find towards C, etc. Baxter found [via the transformation (6.8a)] only half of the curves around point C, namely, those curves that are images of C–B–H and past through the Beraha numbers $B_{3+12k}$. (In Figure 26 we have shown two of these curves, corresponding to $B_{15}$ and $B_{27}$.)

2) If we define $q_0$ as the point on the real $q$-axis where the region $\mathcal{D}_3$ ends, then the above discussion implies that $q_0$ is not given by $q_{\mathrm{F}} \approx 3.819671731239719$ as Baxter believed [cf. (6.5)], but rather by

$$q_0 = q_{\mathrm{G}} = B_{12} = 2 + \sqrt{3} \approx 3.732050807568877 \tag{6.22}$$

[cf. (6.20)].

40

3) The "phase diagram" around point A ($q = 0$) is also richer than the one found by Baxter. The analytic structure is similar to the one already discussed for the point C, except for the fact that now the dominant eigenvalue alternates between $g_1$ and $g_3$. Again, Baxter found [via (6.8b)] only some of the equimodular curves in this region. The physical meaning of these new curves is not clear to us.

4) We also find many new dominant equimodular curves lying very close to the real $q$-axis between points A and C. Some of them (lying between H and G) have been depicted in Figure 25. These curves were missed by Baxter and their physical meaning is unclear.

Let us stress that Baxter was aware of some (though not all) of the "extra" equimodular curves discussed here. He said [19, p. 5252]:

> We have ignored those alternative curves as the finite lattice calculations give no evidence of there being zeros on them, and the full set of complex zeros just fits onto BAE, BCE, BFE.

It is an open question whether ignoring these curves is indeed the correct thing to do; we shall address this question more fully in Sections 6.3 and 6.4.

On Figure 25 we have also superposed the limiting curve for $L = 11_{\rm P}$ (see Figure 16).[19] This curve lies quite close to the main parts of the infinite-strip-width limiting curve obtained in this section. The point $q_0$ for the $L = 11_{\rm P}$ strip (as well as for the rest of the strips considered in this paper: see Table 6) lies below both Baxter's prediction (6.5) and our somewhat lower prediction (6.22). So our results in Sections 3–5 are compatible with both predictions; unfortunately our strips are not yet wide enough to distinguish between them. On the other hand, it is precisely around points A and C that the finite-strip limiting curve is not defined, so our transfer-matrix results do not give any clue as to whether the additional dominant equimodular curves we have found there can be neglected (as Baxter did) or not.

Another way of discovering whether the true value of $q_0$ is given by point F (6.5) or by point G (6.22) is to consider the isolated limiting points of wide triangular-lattice strips. We expect that all *real* isolated limiting points are smaller than $q_0$. Thus, if we find any isolated limiting point larger than (6.22) [and smaller than (6.5)], then we should conclude that our prediction is false. In Tables 1, 3, 4 and 5 we do not find any such zero. The largest real zero we have found is $\approx 3.6345747 < q_{\rm G} = B_{12} \approx 3.7320508\ldots$. On the other hand, for free and cylindrical boundary conditions, all real isolated limiting points are expected to be Beraha numbers. Thus, if $q_0$ were given by F, as Baxter predicts, then the largest real isolated limiting point would be $B_{14} \approx 3.801938$. On the other hand, if $q_0$ is given by G, as we predict, then the largest real isolated limiting point would be $B_{11} \approx 3.682507$ (or perhaps $B_{12} \approx 3.732051$). In Figure 26 we have also depicted the position of the Beraha numbers $B_{11}, \ldots, B_{16}$ to make easier the comparison with the two alternative values of $q_0$.

---

[19] $L = 12_{\rm P}$ would be substantially similar, had we been able to compute the limiting curve for it (compare Figures 16 and 17).

## 6.3 Comparison of Baxter's eigenvalues with finite-lattice data

Let us now compare Baxter's predictions for the leading eigenvalues $g_i(q)$ [$i = 1, 2, 3$] with our finite-lattice data on strips up to width $L = 12$ (with cylindrical boundary conditions). We shall consider slices of fixed $\operatorname{Im} q$, and plot $\log |g_i(q)|$ as a function of $\operatorname{Re} q$. Simultaneously, we shall also plot $f_k(q, L) = L^{-1} \log |\lambda_k(q)|$ for the five largest (in modulus) eigenvalues of the transfer matrix. Our goal is to see whether analogues of Baxter's eigenvalues $g_1, g_2, g_3$ can be observed in our finite-lattice data.

Let us begin at large $\operatorname{Im} q$, where the behavior is simplest. A plot for $\operatorname{Im} q = 2$ is shown in Figure 30. Baxter's eigenvalues $g_1, g_2, g_3$ are shown as a solid blue line, a dashed black line, and a dashed-dotted red line, respectively. The eigenvalue $g_1$ is dominant for $\operatorname{Re} q \lesssim -0.52$, the eigenvalue $g_3$ is dominant for $-0.52 \lesssim \operatorname{Re} q \lesssim 3.82$, and the eigenvalue $g_1$ is once again dominant for $\operatorname{Re} q \gtrsim 3.82$. The eigenvalue $g_2$ is everywhere strongly subdominant. Comparing these curves with our finite-lattice eigenvalues, we see that:

- In the region $\operatorname{Re} q \lesssim -0.52$, the leading eigenvalue agrees almost perfectly with $g_1$, and the second eigenvalue agrees very closely with $g_3$.

- In the region $-0.52 \lesssim \operatorname{Re} q \lesssim 3.82$, the leading eigenvalue agrees quite well (though not perfectly) with $g_3$. Moreover, in a small part of this region near its two extremes, we can identify a subleading eigenvalue that appears to correspond to $g_1$. However, in most of this region we are unable to identify an eigenvalue corresponding to $g_1$ — conceivably it exists but is hidden under too many other subleading eigenvalues.

- In the region $\operatorname{Re} q \gtrsim 3.82$, the leading eigenvalue almost perfectly with $g_1$. However, we are unable to identify any eigenvalue corresponding to $g_3$, except perhaps for $\operatorname{Re} q$ just above the crossover point $\approx 3.82$.

We have also extrapolated to the infinite-volume limit $L \to \infty$ the values of the free energy $f_1(L)$ corresponding to the leading eigenvalue. At values of $q$ where the theory is critical, conformal field theory predicts that the finite-size corrections to the bulk free energy should be of the form

$$f_1(L) \;=\; f_1(\infty) + \frac{\pi G}{6}\, \frac{c}{L^2} + \cdots \tag{6.23}$$

where $c$ is the system's conformal charge, $G$ is a geometrical factor that equals $\sqrt{3}/2$ on the triangular lattice, and the dots stand for higher-order corrections. At values of $q$ where the theory is noncritical, the finite-volume effects should decay exponentially as $L \to \infty$, so one may expect that the Ansatz (6.23) will again work well (and simply yield a very small number for $c$). We therefore estimated the free energy $f_1(\infty)$ by inserting the data points $L = 11, 12$ into the Ansatz (6.23). The results are shown as solid green dots on Figure 30.

For $\operatorname{Re} q \lesssim -0.52$ and $\operatorname{Re} q \gtrsim 3.82$, the extrapolated free energy $f_1(\infty)$ coincides almost exactly with the value for $L = 12$ (as well as with Baxter's eigenvalue $g_1$), in

accordance with our expectation that the region outside the curve ABCEA is noncritical and hence has exponentially rapid convergence to the infinite-volume limit. In the intermediate regime $-0.52 \lesssim \operatorname{Re} q \lesssim 3.82$, the extrapolated free energy coincides almost exactly with Baxter's eigenvalue $g_3$ (except near the boundaries of this regime, where the extrapolation behaves less well); indeed, it coincides with $g_3$ substantially better than $L = 12$ points did, suggesting that the theory in this region is indeed critical and satisfies (6.23) with $c \neq 0$.

The behavior is similar at $\operatorname{Im} q = 1.5$ (Figure 31) and $\operatorname{Im} q = 1$ (Figure 32); the main difference is that the subleading eigenvalue in the region $\operatorname{Re} q \lesssim -0.5$ is more distant from $g_3$ than it was for $\operatorname{Im} q = 2$. In particular, for $\operatorname{Im} q = 1$ the two leading finite-volume eigenvalues do not even cross; this reflects the fact that $\operatorname{Im} q = 1$ lies below the leftmost endpoint of the equimodular curve (see Figure 17). However, this is almost certainly an effect that will go away for larger strip widths $L$, as the equimodular curve closes up towards $q = 0$ (compare Figures 28 and 25). The leading finite-volume eigenvalue agrees almost perfectly with $g_1$ for $\operatorname{Re} q \lesssim -0.5$ and agrees quite well with $g_3$ for $-0.5 \lesssim \operatorname{Re} q \lesssim 4$, despite the lack of crossing; moreover, the agreement with $g_3$ in the latter interval is almost perfect (except near the endpoints) after extrapolation to $L = \infty$. All this is exactly the behavior one would expect when a curve such as Figure 17 is trying to approximate that of Figure 25. The agreement in the region $\operatorname{Re} q \lesssim -0.5$ of the two leading eigenvalues with $g_1$ and $g_3$ must therefore be reckoned as excellent. Please note that all these slices lie well above the point B and the curve AH.

Consider now the slice $\operatorname{Im} q = 0.5$, which crosses the curves BQ and BC and twice crosses the curve AH; the corresponding eigenvalues are plotted in Figure 33. Here the eigenvalue $g_1$ is dominant for $\operatorname{Re} q \lesssim -0.56$; the eigenvalue $g_3$ becomes ever-so-slightly dominant for $-0.56 \lesssim \operatorname{Re} q \lesssim -0.09$; the eigenvalue $g_1$ again becomes dominant in the interval $-0.09 \lesssim \operatorname{Re} q \lesssim 0.95$ (between the two crossings of the curve AH), where it has a sharp peak; the eigenvalue $g_3$ is dominant for $0.95 \lesssim \operatorname{Re} q \lesssim 4.01$; the eigenvalue $g_2$ is briefly dominant in the interval $4.01 \lesssim \operatorname{Re} q \lesssim 4.17$; and finally, the eigenvalue $g_1$ is dominant for $\operatorname{Re} q \gtrsim 4.17$. But very little of this complexity is seen in our finite-lattice eigenvalues:

- In the region $\operatorname{Re} q \lesssim -0.56$, the leading eigenvalue agrees almost perfectly with $g_1$.

- In the entire region $-0.56 \lesssim \operatorname{Re} q \lesssim 4.01$, we see no sign whatsoever of $g_1$; in particular, *we see no sign of the sharp peak in the interval $-0.09 \lesssim \operatorname{Re} q \lesssim 0.95$.* Rather, the leading eigenvalue everywhere agrees closely (though not perfectly) with $g_3$.

- The region $\operatorname{Re} q \approx 4$ is very hard to disentangle.

- For $\operatorname{Re} q \gtrsim 4.17$, the leading eigenvalue agrees almost perfectly with $g_1$. There may conceivably be one or more eigenvalues corresponding to $g_2$; this is uncertain.

When we extrapolate the leading eigenvalue to $L \to \infty$, there is essentially no change in the regions $\operatorname{Re} q \lesssim -0.56$ and $\operatorname{Re} q \gtrsim 4.17$ (where the agreement with $g_1$ was essentially perfect anyway); on the other hand, we obtain an even better agreement with $g_3$ in the intermediate region $-0.56 \lesssim \operatorname{Re} q \lesssim 4.01$, except near the endpoint $\operatorname{Re} q \approx 4$ where the extrapolation goes haywire.

The behavior is similar at $\operatorname{Im} q = 0.35$ (Figure 34). The peak in $g_1$ is even sharper, and once again no sign of it is seen in the finite-lattice data. Please note that the slice at $\operatorname{Im} q = 0.35$ intersects only the outermost curve AH, but it is very close to the next curve AH$'$ (the maximum value of $\operatorname{Im} q$ along this second curve is $\approx 0.3435$).

Likewise at $\operatorname{Im} q = 0.2$ (Figure 35): this slice intersects *two* of the curves (AH and AH$'$), corresponding to a sharp dip in $g_1$ near $\operatorname{Re} q \approx 0.36$, followed by an even sharper rise near $\operatorname{Re} q \approx 0.89$ and then another precipitous dip. Once again, we see no sign of this behavior in the finite-lattice eigenvalues or in the extrapolated leading eigenvalue. The same situation holds for $\operatorname{Im} q = 0.1$ (Figure 36): there are more and sharper dips and rises in $g_1$, including some near $\operatorname{Re} q \approx 4$; but there is no sign of this abrupt behavior in the finite-size data or the extrapolated data.

Finally, let us consider $\operatorname{Im} q = 0$ (Figure 37). Here $g_1$ is well-defined only for $q < 0$ and $q > 4$ [cf. (6.2a)], while $g_2$ and $g_3$ are well-defined only for $0 < q < 4$ [cf. (6.2b,c)]. The eigenvalues $g_2$ and $g_3$ cross at the point $q_F \approx 3.819671731239719$ found by Baxter [cf. (6.5)]. The leading eigenvalue $f_1$ for $L = 12_P$ reproduces well Baxter's prediction for the leading eigenvalue nearly everywhere (namely, $g_1$ for $q \le 0$ and $q \ge 4$, $g_3$ for $0 \le q \le q_F$, and $g_2$ for $q_F \le q \le 4$). The main discrepancy occurs around $q = q_F$: we find that our finite-size data agree with $g_2$ in the interval $q_0(L = 12_P) \approx 3.64317 < q < 4$, which is somewhat larger than the interval $q_F \approx 3.81967 < q < 4$ predicted by Baxter. But this is perfectly understandable as a finite-size effect due to the fact that $q_0(L = 12_P)$ is smaller than $q_F$. If we look at the extrapolation to infinite volume of the leading eigenvalue, we observe an even better agreement with Baxter's prediction in the interval $0 \lesssim \operatorname{Re} q \lesssim 3$; but in a wide interval around $q = q_F$ the extrapolation looks horrible. This is probably due to the large finite-size effects that characterize that region where three eigenvalues are closely competing for dominance and there is a complicated pattern of level crossings.

In summary, our finite-lattice data are in excellent agreement with Baxter's predictions, *except on one major point*: we find no evidence of an eigenvalue corresponding to $g_1$ in the region of the $q$-plane enclosed by the curve ABCEA. As a consequence, we find no evidence of the equimodular curves in this region that should correspond to the crossings of $g_1$ and $g_3$ (e.g. AHA and its images, LK, etc.) or of $g_1$ and $g_2$ (e.g. CQGQ$'$C and its images, etc.). There seem to be two possibilities:

(a) The eigenvalue $g_1$ really is present in this region, but only for strip widths $L$ larger than those we have studied (possibly *much* larger). In this case, the limiting curve $\mathcal{B}_\infty$ really would exhibit all the complexities shown in Figures 25 and 26, and the correct value of $q_0$ would be given by $q_G = 2 + \sqrt{3} \approx 3.73205$ rather than by $q_F \approx 3.81967$ as predicted by Baxter.

(b) For some reason, the eigenvalue $g_1$ is not present in this region (though it is clearly present elsewhere). In this case, the limiting curve $\mathcal{B}_\infty$ would be given by

44

ABCEA and CBQFQ′EC only, and the correct value of $q_0$ would be $q_F \approx 3.81967$ after all.

At present our numerical data are insufficient to distinguish definitively between these two scenarios. But some relevant theoretical considerations will be presented in the next subsection.

## 6.4   Critical discussion

Baxter [19, p. 5242] stresses that

> we expect the results to be exact: the only way they could be wrong would be if the domain structure were more complicated. For instance, we cannot rule out the existence of a fourth domain within which $W(q)$ [the "partition function per site"] has some yet different form. All we can say is that we have seen no sign of it.

But the trouble seems to be not that a fourth dominant eigenvalue appears in some part of the complex plane — we see no sign of that either — but rather that in part of the complex plane one of Baxter's three eigenvalues (namely, $g_1$) does *not* appear!

One possible explanation may have been hinted at by Baxter in his first paper, where he points out [18, p. 2823] that the equivalence between Nienhuis' loop model and the triangular-lattice chromatic polynomial "should be treated with caution"; indeed he observes that it gives manifestly *wrong* answers on a finite lattice when $q = 1$ or 3. He then gives the following explanation for this discrepancy, which we now find strikingly prescient:

> We can resolve this apparent contradiction by repeating Nienhuis' argument for a finite lattice. We start by writing the triangular Potts model as a Kagomé lattice six-vertex model, as has been done by Baxter *et al* (1976).[20] We interpret this as an SOS model by placing spins on the faces of the Kagomé lattice, adjacent spins differing by $\frac{1}{2}$, the greater being to the left of the intervening arrow. Choosing the hexagonal (triangular) faces to have integer (half-integer) spins and taking $J = -\infty$, we can sum over the half-integer spins to obtain Nienhuis' SOS form of the loop model, *but with special boundary weights* [emphasis added]. For $0 < q < 4$ these boundary weights are complex, so it is possible for them to modify the bulk behaviour. Obviously this is happening in the $q = 1$ and 3 cases mentioned above.
>
> In terms of the loop model transfer matrices, these boundary conditions may mean that not all eigenvalues contribute to the partition function. (If an eigenvector is 'orthogonal to the boundary vector', then it never enters the calculation of $Z_{\text{Loop}}$.) This must be happening in the $q = 1$ and 3 cases, so is presumably a general phenomenon. (Similar problems with using the six-vertex form of the Potts model have previous[ly] been observed (see Baxter 1982b).[21])

---

[20]The reference being cited here is Baxter, Kelland and Wu [58].

[21]The reference being cited here is [59].

Thus not only is care necessary to select the largest eigenvalue of the loop model transfer matrix but one should also verify that it is a contributing eigenvalue.

Indeed, it is quite possible that Baxter's solution of the hexagonal-lattice loop model corresponds to some unusual boundary condition for the triangular-lattice chromatic polynomial — different from the free and cylindrical boundary conditions studied here — in which one or more eigenvalues present in the latter are entirely absent in the former (or vice versa). The presence or absence of such eigenvalues can, of course, radically change the limiting curve $\mathcal{B}$ in case the "missing" eigenvalue becomes dominant somewhere in the complex $q$-plane.[22]

But this explanation has a severe defect: if true, it would suggest that the "missing" eigenvalue should be absent *throughout* the complex $q$-plane (corresponding to an *identically* vanishing amplitude). In our case, by contrast, the eigenvalue $g_1$ is unambiguously observed outside the curve ABCEA; it is only inside this curve that the eigenvalue $g_1$ "disappears". It is hard to see how such a $q$-dependent effect could be caused by boundary conditions.

There remains, of course, the other possibility noted earlier: namely, that the eigenvalue $g_1$ really is present inside the curve ABCEA as well, but only for strip widths $L$ larger than those we have studied. Indeed, it is not so surprising that on lattices $L \leq 12$ we have failed to see the gyrations of $g_1$ that give rise to the equimodular curves AH, AH′, . . . : after all, in this same neighborhood ($q \approx 0$) we also fail to see the crossing of $g_1$ and $g_3$ that corresponds to the completion of the equimodular curve BA at $q = 0$, and there is little doubt that *this* feature will be restored in the limit $L \to \infty$.

Light could perhaps be shed on this issue by a more detailed examination of Baxter's Bethe Ansatz for finite-width strips [18] and a comparison of his finite-width results with our own. It could also be useful to study boundary conditions that are periodic in the longitudinal direction (e.g. cyclic or toroidal), as these seem to lead to curves $\mathcal{B}$ that close at $q = 0$ already for finite $L$ [45, 46, 47]. The trouble is that these studies are restricted, at present, to very small $L$ (namely, $L \leq 4$).

---

[22] Here is an example of such a situation: In computing the triangular-lattice chromatic polynomial with cylindrical boundary conditions, one has the choice of working entirely within the translation-invariant subspace (as we have done) or else working in a larger space that includes non-translation-invariant connectivities (as Roček *et al.* [41] have done). If one takes the latter approach, one will find that one of the eigenvalues has an identically vanishing amplitude (provided that translation-invariant endgraphs are used); when this non-contributing eigenvalue is ignored (as it should be), both approaches will give the same limiting curve $\mathcal{B}$. On the other hand, the latter approach allows one to consider also the use of *non*-translation-invariant endgraphs; and it can sometimes be arranged for the "extra" eigenvalue to contribute and indeed be dominant in some region of the complex $q$-plane, with the result that the limiting curve $\mathcal{B}$ is *different* from what it was without that eigenvalue. Compare, for example, [41, Figures 4(a) and (b)], which show the limiting curves $\mathcal{B}$ for the triangular lattice of width $L = 4_\mathrm{P}$ with different endgraphs.

# 7  Summary and Outlook

## 7.1  Behavior of dominant-eigenvalue-crossing curves $\mathcal{B}$

In this paper we have computed the transfer matrix for triangular-lattice strips of width $3 \leq L_x \leq 9$ for free boundary conditions, $4 \leq L_x \leq 12$ for cylindrical boundary conditions, and $L_x = 4, 6, 8, 10$ for "zig–zag" boundary conditions. The transfer matrix allows the computation of the chromatic zeros for strips of arbitrary length $L_y$. As the length $L_y$ tends to infinity (for fixed width $L_x$), the chromatic zeros accumulate along certain curves (limiting curves $\mathcal{B}$) and around certain points (isolated limiting points) according to the Beraha–Kahane–Weiss theorem [25, 26, 27]. For all the above strips except $L_x = 10_{\mathrm{F}}, 12_{\mathrm{P}}, 10_{\mathrm{Z}}$, we have been able to compute the limiting curves $\mathcal{B}$. The exact computation of all the isolated limiting points has been carried out for $L_x \leq 6_{\mathrm{F}}$, $L_x \leq 9_{\mathrm{P}}$ and $L_x \leq 6_{\mathrm{Z}}$; for the larger strips we were able to check that certain values of $q$ are isolated limiting points, but we cannot be certain that we have found all of them. By studying the behavior of the limiting curves and isolated limiting points as a function of the strip width $L_x$ (and boundary conditions), we hope to shed light on the thermodynamic limit $L_x, L_y \to \infty$.

The basic properties of both limiting curves and isolated limiting points are summarized in Table 6. In all cases the identity

$$
\begin{aligned}
\text{endpoints} \;=\;\; & (2 \times \text{components}) + (2 \times \text{double points}) + (\text{T points}) \\
& - (2 \times \text{enclosed regions})
\end{aligned}
\tag{7.1}
$$

holds. This identity can be derived by simple topological/graph-theoretic arguments.

By inspection of Table 6, we observe some regularities when $L_x$ becomes large. For all three boundary conditions, the curve $\mathcal{B}$ appears to become connected ($\#\mathrm{C} = 1$) when $L_x$ is large enough. For all $L_x$, the number of endpoints ($\#\mathrm{E}$) is 6 for free boundary conditions and 4 for the other two boundary conditions. (Note, however, that for $L_x \geq 7_{\mathrm{F}}$, $L_x \geq 10_{\mathrm{P}}$ and $L_x = 8_{\mathrm{Z}}$ our counts on the number of endpoints are only lower bounds: we may have missed some.) When $L_x$ is large enough, the number of T points ($\#\mathrm{T}$) is 4 for free boundary conditions and 2 for the other boundary conditions. We have found no evidence of double points for any of the strips considered. Finally, the number of enclosed regions is zero except for $L_x = 5_{\mathrm{F}}$, $L_x \leq 5_{\mathrm{P}}$ and $L_x = 7_{\mathrm{P}}$. These regularities are in sharp contrast with the square-lattice case [16, 17], where the number of connected components and endpoints seems to grow with the strip width. In particular, we have not found in the triangular-lattice limiting curves any trace of the small gaps and bulb-like regions that are so common in the square-lattice case. It therefore seems that the thermodynamic limit may be achieved in a smoother way for the triangular lattice than for the square lattice. Finally, it is worth mentioning that in all cases except $L_x = 4_{\mathrm{F}}$ and $4_{\mathrm{Z}}$, the limiting curve $\mathcal{B}$ crosses the real $q$-axis, thus defining $q_0$. By contrast, for the square lattice, $q_0$ is well-defined only for odd widths; for even widths with both free and cylindrical boundary conditions, we found either that $\mathcal{B}$ fails to intersect the real axis or that it contains a segment of the real axis passing through a double point [16, 17].

Let us also note that, as in the square-lattice case [16, 17], we find chromatic zeros with $\text{Re}\,q < 0$. Indeed, for $L_x \geq 7_{\text{P}}$ and $L_x \geq 8_{\text{Z}}$ we find that the limiting curve $\mathcal{B}$ intersects the half-plane $\text{Re}\,q < 0$. For free boundary conditions, none of our limiting curves ($L_x \leq 8_{\text{F}}$) reach this half-plane; but from Table 6 we can see that $\min \text{Re}\,q$ is decreasing and we expect that it will be $< 0$ for $L_x \geq 10_{\text{F}}$ (and possibly already for $9_{\text{F}}$).

The regularities exhibited by the limiting curves become clearer when we superpose them all (with fixed boundary conditions). This is done in Figures 27, 28 and 29 for free, cylindrical and zig-zag b.c., respectively. We find an overall behavior similar to that found for the square lattice [16, 17]. For free boundary conditions (Figure 27), we find a monotonic behavior with the width $L_x$: both the leftmost arcs and the rightmost arcs move outwards as $L_x$ is increased (see also the columns labelled $\min \text{Re}\,q$ and $\max \text{Re}\,q$ in Table 6). The value of $q_0$ (or $\text{Re}\,q_0$ for $L_x = 4_{\text{F}}$) is also monotonically increasing in $L_x$. The overall shape of the limiting curves is similar to the expected limiting curve in the thermodynamic limit (Figure 25). We expect that as $L_x$ grows, the leftmost endpoints will tend towards $q = 0$, while the rightmost endpoints will go to $q = q_c(\text{tri}) = 4$. The crossing point $q_0$ will eventually go to either point F [cf. (6.5)] or point G [cf. (6.22)] in Figure 25. Unfortunately, our numerical data are not good enough to tell unambiguously the true limit. There is additional one feature of the limiting curves with free boundary conditions that does *not* correspond to any feature of the predicted thermodynamic-limit curve: namely, a pair of small complex-conjugate branches emerging from T points and pointing inwards. From Figure 27, it seems that the size of these branches does not go to zero as $L_x$ is increased (at least up to 8 or 9); rather their size stays more or less constant. We are unable to say whether these branches will get shorter for larger $L_x$ and ultimately disappear in the limit $L_x \to \infty$.

In Figure 28 we superpose all the limiting curves with cylindrical boundary conditions. As in the square-lattice case, the behavior of the leftmost part of these curves seems to be monotonic: the arcs move outwards as $L_x$ is increased. In particular, $\min \text{Re}\,q$ decreases monotonically with the strip width (see Table 6). However, the behavior on the right side of the plot is clearly not monotonic: there are differences depending on the quantity $L_x \bmod 3$. This is to be expected, since with periodic boundary conditions in the transversal direction, strip widths that are not multiples of 3 are somewhat *unnatural* as they introduce frustration in the 3-state Potts antiferromagnet. Thus, the dependence on $L_x$ in the interval $3 \lesssim \text{Re}\,q \lesssim 4.5$ is not a surprise (the same feature is present in the square-lattice case, where we find an even-odd dependence on the limiting curves [16, 17]). For fixed values of $L_x \bmod 3$, we find that $q_0$ is monotonic in $L_x$: for $L_x = 1 \bmod 3$ it decreases, while for $L_x = 0$ or $2 \bmod 3$ it increases. The shape of the limiting curves for $L_x = 0 \bmod 3$ is very similar to the expected thermodynamic limit (Figure 25), while in the other cases we find stronger finite-size effects that we expect to disappear in the limit $L_x \to \infty$. Finally, it is worth mentioning the absence of the extra branches that appear for free boundary conditions.

In Figure 29 we superpose the limiting curves for "zig-zag" boundary conditions. In this case we only have three curves, so we are unable to extract any definitive

conclusion. We can only confirm the monotonic behavior on the leftmost side of the curves and the absence of any extra branches. Again, the overall shape is similar to the expected thermodynamic limit depicted in Figure 25.

If we compare the limiting curves for different boundary conditions, we see that the thermodynamic limit is achieved faster for cylindrical and "zig-zag" boundary conditions than for free boundary conditions (due to existence of "surface" effects in the later). This is similar to the behavior observed in the square-lattice case.

The main unsolved problem is, of course, whether the extra equimodular curves predicted by Baxter's formulae (Figure 25) are really there for large enough $L$. Unfortunately, the evidence from strip widths $L \leq 12$ is inconclusive (Sections 6.3 and 6.4).

**Remark**. In the computation of the limiting curves $\mathcal{B}$ for triangular-lattice strips with *cylindrical* boundary conditions, we have found a curious behavior involving identically vanishing amplitudes. (This is important, because the eigenvalues corresponding to the identically vanishing amplitudes must be *excluded* from the computation of the equimodular curves. For square-lattice strips, by contrast, we have not observed any identically vanishing amplitudes [16, 17].) As explained in the introduction to Section 4, the transfer matrix can be written (after a change of basis) in the block-diagonal form

$$\mathsf{T}(m_{\mathrm{P}}) = \begin{pmatrix} \mathsf{T}_+(m_{\mathrm{P}}) & 0 \\ 0 & \mathsf{T}_-(m_{\mathrm{P}}) \end{pmatrix} , \tag{7.2}$$

where the matrix $\mathsf{T}_+(m_{\mathrm{P}})$ lives on the subspace of reflection-invariant connectivities and has dimension SqCyl($m$) [i.e., the dimension of the transfer matrix for a square-lattice strip of width $m$ with cylindrical boundary conditions], while the matrix $\mathsf{T}_-(m_{\mathrm{P}})$ lives on the subspace of reflection-odd connectivities and has dimension TriCyl($m$) − SqCyl($m$). For $m \geq 8_{\mathrm{P}}$ we have TriCyl($m$) > SqCyl($m$) and this decomposition becomes nontrivial. Now, simple symmetry arguments (see Section 4) explain why all the eigenvalues in the reflection-odd subspace should have identically vanishing amplitudes. But what is curious and mysterious is that each of these eigenvalues has an identical "partner" in the reflection-even subspace, also with identically vanishing amplitude. This means that the characteristic polynomial associated to the transfer matrix $\mathsf{T}(m_{\mathrm{P}})$ can be factored as

$$\det[\mathsf{T}(m_{\mathrm{P}}) - \lambda \mathbf{1}] = Q_1(q,\lambda)^2 \, Q_2(q,\lambda) , \tag{7.3}$$

where the zero-amplitude eigenvalues are those coming from the factor $Q_1(q,\lambda)^2$. In particular, the number of eigenvalues with zero amplitude (# VA) is always even, and it equals twice the dimension of the reflection-odd subspace:

$$\#\mathrm{VA}(m) = 2 \times [\mathrm{TriCyl}(m) - \mathrm{SqCyl}(m)] \tag{7.4}$$

(see Table 7). This is, at any rate, what we have found for $8_{\mathrm{P}} \leq m \leq 12_{\mathrm{P}}$ (see Sections 4.7–4.11); we conjecture that it holds for larger widths as well. It follows that the effective dimension of the transfer matrix TriCyl$'(m)$ is given by

$$\mathrm{TriCyl}'(m) = 2\mathrm{SqCyl}(m) - \mathrm{TriCyl}(m) . \tag{7.5}$$

49

Numerical values for all these quantities are displayed in Table 7; of course, the values of # VA and TriCyl$'(m)$ for $m = 13, 14$ are *conjectures*.

Numerical values of TriCyl$(m)$ and SqCyl$(m)$ were first reported in [16, Table 2]. An analytic formula of TriCyl$(m)$ for prime values of $m$ has been obtained in [53, Theorem 3]. This paper also contains a conjecture for SqCyl$(m)$ with prime $m \geq 3$ [53, Conjecture 2]. Finally, an analytic formula for TriCyl$'(m)$ has been conjectured for arbitrary values of $m$ [53, Conjecture 1].

## 7.2   Behavior of amplitudes and the Beraha conjecture

Let us now discuss the isolated limiting points and the role of the Beraha numbers in the triangular-lattice strips. Our results show that the number of isolated limiting points is a non-decreasing function of the strip width $L_x$ (for each boundary condition), at least up to the maximum $L_x$ we have been able to investigate. For free and cylindrical boundary conditions we did not find any complex isolated limiting points (see Table 6). For "zig-zag" boundary conditions we find a pair of complex-conjugate isolated limiting points for $L_x = 6_Z$, and we have evidence of the existence of another pair of complex-conjugate isolated limiting points for $L_x = 8_Z$.

Concerning the real isolated limiting points, most of them are Beraha numbers (1.3). It is only for "zig-zag" boundary conditions that we find real isolated limiting points that are *not* Beraha numbers: for $L_x = 4_Z$ we find $q = 5/2$; for $L_x = 6_Z$, $q \approx 2.722633$; for $L_x = 8_Z$, $q \approx 2.821420$; and for $L_x = 10_Z$, we find two such points, $q \approx 2.873731$ and $q \approx 3.383129$. It is not clear to us how these non-Beraha real isolated limiting points behave as $L_x \to \infty$, e.g., whether their number is bounded or unbounded.

For all the lattices we have studied, we observed empirically that there is at least one vanishing amplitude $\alpha_i(q)$ at each of the Beraha numbers up to $B_{L+1}$ (see Table 10). It is reasonable to conjecture that this holds for all $L$ (in agreement with a similar conjecture for the square lattice [16, Conjecture 7.1]):

**Conjecture 7.1** *For a triangular-lattice strip of width $L$ with free, cylindrical or "zig-zag" boundary conditions, at each Beraha number $q = B_2, \ldots, B_{L+1}$ there is at least one vanishing amplitude $\alpha_i(q)$. That is, $\det D(q) = 0$ for $q = B_2, \ldots, B_{L+1}$.*

In contrast with the square-lattice case [16, Conjectures 7.2 and 7.3], however, we find that there is a vanishing amplitude [hence $\det D(q) = 0$] also at some Beraha numbers *larger* than $B_{L+1}$. Indeed, we find examples for each boundary condition (see Table 10):

- For free boundary conditions, $q = B_6$ is a zero of $\det D(q)$ for $L = 4_F$.

- For cylindrical boundary conditions, $q = B_6$ is a zero of $\det D(q)$ for $L = 4_P$; $q = B_{10}$ is a zero for $L = 6_P, 7_P, 8_P$; $q = B_{14}$ is a zero for $L = 8_P, 9_P, 10_P, 11_P, 12_P$; $q = B_{18}$ is a zero for $L = 10_P, 11_P, 12_P$; and finally, $q = B_{22}$ is a zero for $L = 12_P$.

- For "zig-zag" boundary conditions, $q = B_6$ is a zero of $\det D(q)$ for $L = 4_Z$.

We have systematically checked all Beraha numbers up to $B_{50}$ to make this list.

Please note that for free and "zig-zag" boundary conditions, we have found only *one* case each in which a Beraha number beyond $B_{L+1}$ is a zero of $\det D(q)$, namely the relatively small value of $L = 4$. It is conceivable that for all larger $L$ there are no such Beraha zeros, as is conjectured for all $L$ for the square lattice [16, Conjecture 7.2]. However, this conjecture clearly cannot be true for cylindrical boundary conditions. There is presumably some pattern that tells us *which* Beraha numbers $q = B_k$ with $k > L+1$ can be zeros of $\det D(q)$. Thus far only a few Beraha numbers $(B_6, B_{10}, B_{14}, B_{18}, B_{22})$ have appeared on that list. Indeed, we conjecture that the pattern is the following:

**Conjecture 7.2** *For a triangular-lattice strip of width $L$ with cylindrical boundary conditions, the Beraha numbers where $\det D(q)$ vanishes is given by the union of the sets $\{B_2, B_3, ..., B_{L+1}\}$ and $\{B_{4k-2} \mid k = 1, 2, ..., \lfloor L/2 \rfloor\}$, the upper limit on $k$ being the integer part of $L/2$.*

## 7.3 Nature of the fixed zeros

In Section 2 we discussed the "fixed" zeros that occur at small integers $q$ (here $q = 0, 1, 2, 3$) when the graph fails to be $q$-colorable. From the point of view of the transfer-matrix formalism, these fixed zeros can arise in either of three ways:

1) All the amplitudes $\alpha_k$ vanish at $q$. Then $Z_n(q) = 0$ for all lengths $n \geq 1$.

2) All the eigenvalues $\lambda_k$ vanish at $q$. Then $Z_n(q) = 0$ for all $n \geq 2$.

3) "Mixed case": Neither all the amplitudes nor all the eigenvalues vanish at $q$, but for each $k$ either $\alpha_k$ or $\lambda_k$ vanishes at $q$ (or both). Then $Z_n(q) = 0$ for all $n \geq 2$.

Let us now summarize what we have found concerning the nature of these fixed zeros for triangular-lattice strips:

$\boldsymbol{q = 0, 1.}$ At $q = 0, 1$ all the amplitudes vanish, due to the prefactor $q(q - 1)$ in the left vector $\mathbf{u}$. These points therefore belong to Case 1.

$\boldsymbol{q = 2.}$ At $q = 2$ the behavior depends on the boundary conditions and on the strip width $L_x$:

- Free boundary conditions:

    - $L_x = 2_F$: The one eigenvalue vanishes at $q = 2$ (Case 2).
    - $L_x = 3_F$: There is one nonzero eigenvalue with a zero amplitude, and one zero eigenvalue with a nonzero amplitude (Case 3).
    - $L_x = 4_F$: There is at least one nonzero eigenvalue with a zero amplitude and exactly one zero eigenvalue with a nonzero amplitude (Case 3). The transfer matrix at $q = 2$ is not diagonalizable: it has a nontrivial Jordan block corresponding to $\lambda = 0$.

- $L_x \geq 5_\mathrm{F}$: There is at least one nonzero eigenvalue with a zero amplitude, at least one zero eigenvalue with a zero amplitude, and exactly one zero eigenvalue with a nonzero amplitude (Case 3). We also find that for all $L_x \geq 4_\mathrm{F}$ the transfer matrix at $q = 2$ is not diagonalizable, i.e. it has nontrivial Jordan blocks (all corresponding to eigenvalue $\lambda = 0$).

- Cylindrical boundary conditions:

  - $L_x$ odd: All the amplitudes vanish, due to the prefactor $q(q-1)(q-2)$ in the left vector $\mathbf{u}$ (Case 1).

  - $L_x = 2_\mathrm{P}$: The one eigenvalue vanishes at $q = 2$ (Case 2).

  - $L_x = 4_\mathrm{P}$: There is one nonzero eigenvalue with a zero amplitude, and one zero eigenvalue with a nonzero amplitude (Case 3).

  - $L_x$ even $\geq 6_\mathrm{P}$: There is at least one nonzero eigenvalue with a zero amplitude, at least one zero eigenvalue with a zero amplitude, and at least one zero eigenvalue with a nonzero amplitude (Case 3).

- Zig-zag boundary conditions:

  - $L_x = 2_\mathrm{Z}$: This is identical to $L_x = 2_\mathrm{F}$ (Case 2).

  - $L_x = 4_\mathrm{Z}$: There are two nonzero eigenvalues with zero amplitudes, and one zero eigenvalue with a nonzero amplitude (Case 3).

  - $L_x$ even $\geq 6_\mathrm{Z}$: There is at least one nonzero eigenvalue with a zero amplitude, at least one zero eigenvalue with a zero amplitude, and at least one zero eigenvalue with a nonzero amplitude (Case 3).

$\boldsymbol{q = 3.}$ The point $q = 3$ is a fixed zero only for cylindrical boundary conditions with strip widths $L_x$ that are not a multiple of 3. There are two distinct situations:

- $L_x = 4_\mathrm{P}$: Both eigenvalues vanish, so that the whole transfer matrix vanishes (Case 2).

- $L_x = 5_\mathrm{P}$: There is one nonzero eigenvalue with a zero amplitude, and one zero eigenvalue with a nonzero amplitude (Case 3).

- $L_x = 7_\mathrm{P}, 8_\mathrm{P}, 10_\mathrm{P}, 11_\mathrm{P}$: There is at least one nonzero eigenvalue with zero amplitude, at least one zero eigenvalue with a nonzero amplitude, and at least one zero eigenvalue with a zero amplitude [or nontrivial Jordan block corresponding to $\lambda = 0$ with no contribution to the partition function for any $n \geq 1$] (Case 3). We also find that for $L_x \geq 8_\mathrm{P}$ the transfer matrix at $q = 3$ is not diagonalizable, i.e. it has nontrivial Jordan blocks.

# Acknowledgments

# A  Numerical Computation of $\prod\limits_{n=1}^{\infty}(1 - tx^n)$

In this appendix we discuss briefly some of the technical issues involved in the numerical computation of Baxter's products (6.6). Everything can be expressed in terms of the function

$$R(t,x) \;=\; \prod_{n=1}^{\infty}(1 - tx^n) \;, \tag{A.1}$$

which is defined for complex $t$ and $x$ satisfying $|x| < 1$ and was first studied by Euler [60]. Here we need the cases $t = \pm 1$ and $t = \pm$ a cube root of unity. A more detailed discussion, including proofs, can be found in [61].

The numerical computation of $R(t,x)$ clearly becomes delicate when $|x| \uparrow 1$. In particular, direct use of the product (A.1) gives an algorithm that is only "linearly convergent", i.e. the number of significant digits in the answer grows linearly with the number of terms taken. Moreover, the constant of proportionality in this relation is proportional to $1 - |x|$, and thus deteriorates linearly as $|x| \uparrow 1$. Finally, there is severe loss of numerical precision when multiplying numbers that are very near 1. An alternative approach can be based on the representation

$$\log R(t,x) \;=\; -\sum_{k=1}^{\infty} \frac{t^k}{k}\, \frac{x^k}{1 - x^k} \;, \tag{A.2}$$

which is valid whenever $|x| < 1$ and $|tx| < 1$. This sum is again only linearly convergent, but the problem of loss of numerical precision is alleviated by use of the logarithm.

A much more efficient algorithm can be based on the identity

$$R(t,x) \;=\; \sum_{n=0}^{\infty} \frac{(-t)^n x^{n(n+1)/2}}{(1 - x)(1 - x^2)\cdots(1 - x^n)} \tag{A.3}$$

53

due to Euler.[23] Because of the $x^{n(n+1)/2}$ factor in the numerator, this algorithm is "quadratically convergent":

**Proposition A.1 ([61])** *Define*

$$a_n = \frac{(-t)^n x^{n(n+1)/2}}{(1-x)(1-x^2)\cdots(1-x^n)} \; . \tag{A.4}$$

*Then, for $|t| \le 1$ and $|x| \le e^{-\gamma}$ $(\gamma > 0)$, we have*

*(a)* $\Delta_N \equiv \left| \sum_{n=N}^{\infty} a_n \right| \le \dfrac{e^{\pi^2/6\gamma - N(N+1)\gamma/2}}{1 - e^{-(N+1)\gamma}}$

*(b)* $\delta_N \equiv \dfrac{\left| \sum_{n=N}^{\infty} a_n \right|}{|R(t,x)|} \le \dfrac{e^{\pi^2/3\gamma - N(N+1)\gamma/2}}{1 - e^{-(N+1)\gamma}}$

**Corollary A.2 ([61])** *Let $K \ge 0$, and suppose that $|t| \le 1$ and $|x| \le e^{-\gamma}$ $(\gamma > 0)$.*

*(a) If $N \ge \sqrt{\dfrac{\pi^2}{3\gamma^2} + \dfrac{2K}{\gamma}}$, then $\Delta_N \le e^{-K}$.*

*(b) If $N \ge \sqrt{\dfrac{2\pi^2}{3\gamma^2} + \dfrac{2K}{\gamma}}$, then $\delta_N \le e^{-K}$.*

It turns out [61] that the *a priori* bound of Proposition A.1(b) is asymptotically within 9.1% of being sharp when $t = 1$, $0 < x = e^{-\gamma} < 1$ and $N \gg 1/\gamma$ (moreover, in this case it is asymptotically sharp as $\gamma \downarrow 0$). But since this bound is overly pessimistic in other cases, it is of some value to provide an *a posteriori* bound on the truncation error that is more realistic, when $x \notin (0,1)$, than the *a priori* bound. Here is such a bound, which can be used a stopping criterion in the numerical algorithm:

**Proposition A.3 ([61])** *Let $|t| \le 1$, $|x| \le e^{-\gamma}$ $(\gamma > 0)$ and $N > (\log 2)/\gamma$. Then:*

*(a)* $\Delta_N \equiv \left| \sum_{n=N}^{\infty} a_n \right| \le |a_{N-1}| \dfrac{e^{-N\gamma}}{1 - 2e^{-N\gamma}}$

*(b)* $\delta'_N \equiv \dfrac{\left| \sum_{n=N}^{\infty} a_n \right|}{|S_N|} \le \dfrac{|a_{N-1}|}{|S_N|} \dfrac{e^{-N\gamma}}{1 - 2e^{-N\gamma}}$ *where $S_N \equiv \sum_{n=0}^{N-1} a_n$*

*[Note also that $\delta_N \le \delta'_N/(1 - \delta'_N)$.]*

*In particular, if $N \ge (\log 3)/\gamma$, we have $\Delta_N \le |a_{N-1}|$ and $\delta'_N \le |a_{N-1}|/|S_N|$.*

[23]For a proof of (A.3), see e.g. [62, p. 19, Corollary 2.2], [63, p. 34, Lemma 4(a)] or [64, pp. 22–23].

Let us conclude by making some brief remarks about the numerical precision that is required in intermediate stages of the calculation based on (A.3). It turns out [61] that the largest term $\max_{n} |a_n|$ can be as large in magnitude as $e^{\pi^2/12\gamma}$ (and is indeed of this order when $0 < x < 1$), while the answer $R(t, x)$ can be as small in magnitude as $e^{-\pi^2/6\gamma}$ (and is indeed of this order when $t = 1$ and $0 < x < 1$). It is therefore necessary to maintain, in intermediate stages of the calculation, approximately $(\pi^2/4\gamma)/\log 10 \approx 1.07/\gamma$ digits of working precision beyond the number of significant digits desired in the final answer.

We used all three algorithms — the product (A.1), the logarithmic sum (A.2) and the quadratically convergent sum (A.3) — and carefully cross-checked the value of $R(t, x)$; we also verified numerically the error bounds of Proposition A.1, Corollary A.2 and Proposition A.3. In order to guarantee that the roundoff error is under control, we performed all computations using MATHEMATICA with a working precision of at least 100 digits and often much more (increasing the working precision until the answer is independent of the precision used).

# References

[1] F.Y. Wu, Rev. Mod. Phys. **54**, 235 (1982); **55**, 315 (E) (1983).

[2] F.Y. Wu, J. Appl. Phys. **55**, 2421 (1984).

[3] R.J. Baxter, *Exactly Solved Models in Statistical Mechanics* (Academic Press, London–New York, 1982).

[4] P.P. Martin, *Potts Models and Related Problems in Statistical Mechanics*. (World Scientific, Singapore, 1991).

[5] R.J. Baxter, J. Math. Phys. **11**, 784 (1970).

[6] R.J. Baxter, Proc. Roy. Soc. London A **383**, 43 (1982).

[7] J.-S. Wang, R.H. Swendsen and R. Kotecký, Phys. Rev. B **42**, 2465 (1990).

[8] H. Saleur, Commun. Math. Phys. **132**, 657 (1990).

[9] H. Saleur, Nucl. Phys. B **360**, 219 (1991).

[10] J. Adler, A. Brandt, W. Janke and S. Shmulyan, J. Phys. A **28**, 5117 (1995).

[11] J. Salas and A.D. Sokal, J. Stat. Phys. **86**, 551 (1997), cond-mat/9603068.

[12] J. Salas and A.D. Sokal, J. Stat. Phys. **92**, 729 (1998), cond-mat/9801079.

[13] S.J. Ferreira and A.D. Sokal, J. Stat. Phys. **96**, 461 (1999), cond-mat/9811345.

[14] J. Cardy, J.L. Jacobsen and A.D. Sokal, J. Stat. Phys. **105**, 25 (2001), cond-mat/0101197.

[15] R.C. Read and W.T. Tutte, in *Selected Topics in Graph Theory 3*, ed. L.W. Beineke and R.J. Wilson (Academic Press, London, 1988).

[16] J. Salas and A.D. Sokal, J. Stat. Phys. **104**, 609 (2001), cond-mat/0004330.

[17] J.L. Jacobsen and J. Salas, J. Stat. Phys. **104**, 701 (2001), cond-mat/0011456.

[18] R.J. Baxter, J. Phys. A **19**, 2821 (1986).

[19] R.J. Baxter, J. Phys. A **20**, 5241 (1987).

[20] C.N. Yang and T.D. Lee, Phys. Rev. **87**, 404 (1952).

[21] S. Beraha and J. Kahane, J. Combin. Theory B **27**, 1 (1979).

[22] S. Beraha, J. Kahane and N.J. Weiss, J. Combin. Theory B **28**, 52 (1980).

[23] R. Shrock and S.-H. Tsai, Phys. Rev. E **55**, 5165 (1997), cond-mat/9612249.

[24] M. Roček, R. Shrock and S.-H. Tsai, Physica A **252**, 505 (1998), cond-mat/9712148.

[25] S. Beraha, J. Kahane and N.J. Weiss, Proc. Nat. Acad. Sci. USA **72**, 4209 (1975).

[26] S. Beraha, J. Kahane and N.J. Weiss, in *Studies in Foundations and Combinatorics* (Advances in Mathematics Supplementary Studies, Vol. 1), ed. G.-C. Rota (Academic Press, New York, 1978).

[27] A.D. Sokal, Chromatic roots are dense in the whole complex plane, Combin. Probab. Comput. (to appear), cond-mat/0101197.

[28] R. Shrock and S.-H. Tsai, Phys. Rev. E **56**, 1342 (1997), cond-mat/9703249.

[29] S. Beraha, unpublished, circa 1974.

[30] R.J. Baxter, H.N.V. Temperley and S.E. Ashley, Proc. Roy. Soc. London A **358**, 535 (1978).

[31] B. Nienhuis, Phys. Rev. Lett. **49**, 1062 (1982).

[32] J. Stephenson, J. Math. Phys. **5**, 1009 (1964).

[33] H.W.J. Blöte and H.J. Hilhorst, J. Phys. A **15**, L631 (1982).

[34] B. Nienhuis, H.J. Hilhorst and H.W.J. Blöte, J. Phys. A **17**, 3559 (1984).

[35] C.L. Henley, private communications.

[36] J. Salas and A.D. Sokal, unpublished.

[37] A.C.D. van Enter, R. Fernández and A.D. Sokal, unpublished (1996).

[38] J. Salas and A.D. Sokal, in preparation.

[39] P.W. Kasteleyn and C.M. Fortuin, J. Phys. Soc. Japan **26** (Suppl.), 11 (1969).

[40] C.M. Fortuin and P.W. Kasteleyn, Physica **57**, 536 (1972).

[41] M. Roček, R. Shrock and S.-H. Tsai, Physica A **259**, 367 (1998), cond-mat/9807106.

[42] R. Shrock and S.-H. Tsai, Phys. Rev. E **58**, 4332 (1998), cond-mat/9808057.

[43] R. Shrock, Discrete Math. **231**, 421 (2001), cond-mat/9908307.

[44] S.-C. Chang and R. Shrock, Annals Phys. **290**, 124 (2001), cond-mat/0004129.

[45] R. Shrock and S.-H. Tsai, Physica A **275**, 429 (2000), cond-mat/9907403.

[46] S.-C. Chang and R. Shrock, Physica A **292**, 307 (2001), cond-mat/0007491.

[47] S.-C. Chang and R. Shrock, Physica A **296**, 131 (2001), cond-mat/0005232.

[48] S.-C. Chang and R. Shrock, Physica A **286**, 189 (2000), cond-mat/0004181.

[49] S.-C. Chang, J.L. Jacobsen, J. Salas and R. Shrock, Exact Potts model partition functions for strips of the triangular lattice, cond-mat/0211623.

[50] S.-C. Chang and R. Shrock, Physica A **316**, 335 (2002), cond-mat/0201223.

[51] D.A. Bini and G. Fiorentino, Numerical computation of polynomial roots using MPSolve version 2.2 (January 2000). Software package and documentation available for download at `ftp://ftp.dm.unipi.it/pub/mpsolve/`.

[52] D.A. Bini and G. Fiorentino, Numer. Algorithms **23**, 127 (2000).

[53] S.-C. Chang, J. Salas and R. Shrock, J. Stat. Phys. **107**, 1207 (2002), cond-mat/0108144.

[54] I. Niven, *Diophantine Approximation* (Wiley–Interscience, New York, 1963).

[55] H. Rademacher, *Lectures on Elementary Number Theory* (Robert E. Krieger, Huntington NY, 1977).

[56] J.W.S. Cassels, *An Introduction to Diophantine Approximation* (Cambridge University Press, Cambridge, 1957).

[57] R.L. Graham, D.E. Knuth and O. Patashnik, *Concrete Mathematics: A Foundation for Computer Science*, 2nd ed. (Addison-Wesley, Reading, Mass., 1994).

[58] R.J. Baxter, S.B. Kelland and F.Y. Wu, J. Phys. A **9**, 397 (1976).

[59] R.J. Baxter, J. Stat. Phys. **28**, 1 (1982).

[60] L. Euler, *Introduction to Analysis of the Infinite* [*Introductio in Analysin Infinitorum*, 1748], 2 vols., translated by John D. Blanton (Springer-Verlag, New York, 1988/1990).

[61] A.D. Sokal, Numerical computation of $\prod\limits_{n=1}^{\infty}(1 - tx^n)$, preprint (December 2002), math.NA/0212035.

[62] G.E. Andrews, *The Theory of Partitions* (Cambridge University Press, Cambridge, 1998).

[63] M.I. Knopp, *Modular Functions in Analytic Number Theory* (Markham, Chicago, 1970).

[64] R. Remmert, *Classical Topics in Complex Function Theory* (Springer-Verlag, New York–Berlin–Heidelberg, 1998).

| Lattice | 4th Zero | 5th Zero | 6th Zero |
|---|---|---|---|
| $3_F \times 3_F$ | | | |
| $3_F \times 6_F$ | 2.552816126636 | | |
| $3_F \times 9_F$ | | | |
| $3_F \times 12_F$ | 2.562658027317 | | |
| $3_F \times 15_F$ | | | |
| $3_F \times 18_F$ | 2.565287184975 | | |
| $3_F \times 21_F$ | | | |
| $3_F \times 24_F$ | 2.566507072062 | | |
| $3_F \times 27_F$ | | | |
| $3_F \times 30_F$ | 2.567211365497 | | |
| $4_F \times 4_F$ | 2.604661945742 | | |
| $4_F \times 8_F$ | 2.618028652707 | | |
| $4_F \times 12_F$ | 2.618033986251 | | |
| $4_F \times 16_F$ | 2.618033988749 | | |
| $4_F \times 20_F$ | 2.618033988750 | | |
| $4_F \times 24_F$ | 2.618033988750 | | |
| $4_F \times 28_F$ | 2.618033988750 | | |
| $4_F \times 32_F$ | 2.618033988750 | | |
| $4_F \times 36_F$ | 2.618033988750 | | |
| $4_F \times 40_F$ | 2.618033988750 | | |
| $5_F \times 5_F$ | 2.618161303055 | 2.795370504128 | |
| $5_F \times 10_F$ | 2.618033988749 | | |
| $5_F \times 15_F$ | 2.618033988750 | 2.947523648832 | |
| $5_F \times 20_F$ | 2.618033988750 | | |
| $5_F \times 25_F$ | 2.618033988750 | 2.968180058756 | |
| $5_F \times 30_F$ | 2.618033988750 | | |
| $5_F \times 35_F$ | 2.618033988750 | 2.976760450197 | |
| $5_F \times 40_F$ | 2.618033988750 | | |
| $5_F \times 45_F$ | 2.618033988750 | 2.981534673779 | |
| $5_F \times 50_F$ | 2.618033988750 | | |
| $6_F \times 6_F$ | 2.618033979731 | | |
| $6_F \times 12_F$ | 2.618033988750 | 3.001429148693 | 3.054848659601 |
| $6_F \times 18_F$ | 2.618033988750 | 3.000001523178 | 3.100527321592 |
| $6_F \times 24_F$ | 2.618033988750 | 3.000000001785 | 3.118151997375 |
| $6_F \times 30_F$ | 2.618033988750 | 3.000000000002 | 3.127749140385 |
| $6_F \times 36_F$ | 2.618033988750 | 3.000000000000 | 3.133811079422 |
| $6_F \times 42_F$ | 2.618033988750 | 3.000000000000 | 3.137993327670 |
| $6_F \times 48_F$ | 2.618033988750 | 3.000000000000 | 3.141054810628 |
| $6_F \times 54_F$ | 2.618033988750 | 3.000000000000 | 3.143393623378 |
| $6_F \times 60_F$ | 2.618033988750 | 3.000000000000 | 3.145239011028 |
| Beraha | 2.618033988750 | 3 | 3.246979603717 |

Table 1: Real zeros of the chromatic polynomials of finite triangular-lattice strips with free boundary conditions in both directions, to 12 decimal places. A blank means that the zero in question is absent. The first three real zeros $q = 0, 1, 2$ are exact on all lattices. "Beraha" indicates the Beraha numbers $B_5 = (3 + \sqrt{5})/2$, $B_6 = 3$, and $B_7$.

| Lattice | 4th Zero | 5th Zero | 6th Zero | 7th Zero |
|---|---|---|---|---|
| $7_F \times 7_F$ | 2.618033988750 | 2.978584823651 | | |
| $7_F \times 14_F$ | 2.618033988750 | 3.000000029690 | 3.160410975706 | |
| $7_F \times 21_F$ | 2.618033988750 | 3.000000000000 | | |
| $7_F \times 28_F$ | 2.618033988750 | 3.000000000000 | 3.218685236695 | |
| $7_F \times 35_F$ | 2.618033988750 | 3.000000000000 | | |
| $7_F \times 42_F$ | 2.618033988750 | 3.000000000000 | 3.236121891966 | |
| $7_F \times 49_F$ | 2.618033988750 | 3.000000000000 | | |
| $7_F \times 56_F$ | 2.618033988750 | 3.000000000000 | 3.243833695579 | |
| $7_F \times 63_F$ | 2.618033988750 | 3.000000000000 | | |
| $7_F \times 70_F$ | 2.618033988750 | 3.000000000000 | 3.246633282347 | |
| $7_F \times 77_F$ | 2.618033988750 | 3.000000000000 | 3.247059872523 | 3.254369173708 |
| $7_F \times 84_F$ | 2.618033988750 | 3.000000000000 | 3.246965843358 | |
| $7_F \times 91_F$ | 2.618033988750 | 3.000000000000 | 3.246982133140 | 3.258435734303 |
| $8_F \times 8_F$ | 2.618033988750 | 3.000359693703 | 3.095706393163 | |
| $8_F \times 16_F$ | 2.618033988750 | 3.000000000000 | 3.229632685380 | |
| $8_F \times 24_F$ | 2.618033988750 | 3.000000000000 | 3.246928323759 | |
| $8_F \times 32_F$ | 2.618033988750 | 3.000000000000 | 3.246979586275 | |
| $8_F \times 40_F$ | 2.618033988750 | 3.000000000000 | 3.246979603712 | |
| $8_F \times 48_F$ | 2.618033988750 | 3.000000000000 | 3.246979603717 | |
| $8_F \times 56_F$ | 2.618033988750 | 3.000000000000 | 3.246979603717 | |
| $8_F \times 64_F$ | 2.618033988750 | 3.000000000000 | 3.246979603717 | |
| $8_F \times 72_F$ | 2.618033988750 | 3.000000000000 | 3.246979603717 | |
| $8_F \times 80_F$ | 2.618033988750 | 3.000000000000 | 3.246979603717 | |
| $8_F \times 88_F$ | 2.618033988750 | 3.000000000000 | 3.246979603717 | |
| $8_F \times 96_F$ | 2.618033988750 | 3.000000000000 | 3.246979603717 | |
| $9_F \times 9_F$ | 2.618033988750 | 2.999999518372 | | |
| $9_F \times 18_F$ | 2.618033988750 | 3.000000000000 | 3.246969773686 | |
| $9_F \times 27_F$ | 2.618033988750 | 3.000000000000 | 3.246979603720 | 3.342943823308 |
| $9_F \times 36_F$ | 2.618033988750 | 3.000000000000 | 3.246979603717 | |
| $9_F \times 45_F$ | 2.618033988750 | 3.000000000000 | 3.246979603717 | 3.374646284957 |
| $9_F \times 54_F$ | 2.618033988750 | 3.000000000000 | 3.246979603717 | |
| $9_F \times 63_F$ | 2.618033988750 | 3.000000000000 | 3.246979603717 | 3.387946181123 |
| $9_F \times 72_F$ | 2.618033988750 | 3.000000000000 | 3.246979603717 | |
| $9_F \times 81_F$ | 2.618033988750 | 3.000000000000 | 3.246979603717 | 3.395349738491 |
| $9_F \times 90_F$ | 2.618033988750 | 3.000000000000 | 3.246979603717 | |
| Beraha | 2.618033988750 | 3 | 3.246979603717 | 3.414213562373 |

Table 2: Real zeros of the chromatic polynomials of finite triangular-lattice strips with free boundary conditions in both directions, to 12 decimal places. We use the same notation as in Table 1.

| Lattice | 4th Zero | 5th Zero | 6th Zero | 7th Zero | 8th Zero |
|---|---|---|---|---|---|
| $4_P \times 4_F$ | 2.617986010522 | 3 | 3.465246100723 | | |
| $4_P \times 8_F$ | 2.618033988740 | 3 | 3.475055224065 | | |
| $4_P \times 12_F$ | 2.618033988750 | 3 | 3.477452996799 | | |
| $4_P \times 16_F$ | 2.618033988750 | 3 | 3.478536268722 | | |
| $4_P \times 20_F$ | 2.618033988750 | 3 | 3.479153472532 | | |
| $4_P \times 24_F$ | 2.618033988750 | 3 | 3.479552148708 | | |
| $4_P \times 28_F$ | 2.618033988750 | 3 | 3.479830901859 | | |
| $4_P \times 32_F$ | 2.618033988750 | 3 | 3.480036768366 | | |
| $4_P \times 36_F$ | 2.618033988750 | 3 | 3.480195030232 | | |
| $4_P \times 40_F$ | 2.618033988750 | 3 | 3.480320488501 | | |
| $5_P \times 5_F$ | 2.618033990394 | 3 | | | |
| $5_P \times 10_F$ | 2.618033988750 | 3 | 3.196843987850 | | |
| $5_P \times 15_F$ | 2.618033988750 | 3 | | | |
| $5_P \times 20_F$ | 2.618033988750 | 3 | 3.202699178454 | | |
| $5_P \times 25_F$ | 2.618033988750 | 3 | | | |
| $5_P \times 30_F$ | 2.618033988750 | 3 | 3.204333275156 | | |
| $5_P \times 35_F$ | 2.618033988750 | 3 | | | |
| $5_P \times 40_F$ | 2.618033988750 | 3 | 3.205100311429 | | |
| $5_P \times 45_F$ | 2.618033988750 | 3 | | | |
| $5_P \times 50_F$ | 2.618033988750 | 3 | 3.205545558020 | | |
| $6_P \times 6_F$ | 2.618033988750 | 3.001033705947 | 3.125892136302 | | |
| $6_P \times 12_F$ | 2.618033988750 | 3.000000003803 | 3.198900652620 | | |
| $6_P \times 18_F$ | 2.618033988750 | 3.000000000000 | 3.217111179820 | | |
| $6_P \times 24_F$ | 2.618033988750 | 3.000000000000 | 3.225649637432 | | |
| $6_P \times 30_F$ | 2.618033988750 | 3.000000000000 | 3.230657835149 | | |
| $6_P \times 36_F$ | 2.618033988750 | 3.000000000000 | 3.233968503481 | | |
| $6_P \times 42_F$ | 2.618033988750 | 3.000000000000 | 3.236327213212 | | |
| $6_P \times 48_F$ | 2.618033988750 | 3.000000000000 | 3.238096251767 | | |
| $6_P \times 54_F$ | 2.618033988750 | 3.000000000000 | 3.239473538415 | | |
| $6_P \times 60_F$ | 2.618033988750 | 3.000000000000 | 3.240576619481 | | |
| $6_P \times 66_F$ | 2.618033988750 | 3.000000000000 | 3.241479828709 | | |
| $6_P \times 72_F$ | 2.618033988750 | 3.000000000000 | 3.242232528364 | | |
| $6_P \times 78_F$ | 2.618033988750 | 3.000000000000 | 3.242868805497 | | |
| $6_P \times 84_F$ | 2.618033988750 | 3.000000000000 | 3.243412961909 | | |
| $6_P \times 90_F$ | 2.618033988750 | 3.000000000000 | 3.243882786313 | | |
| $7_P \times 7_F$ | 2.618033988750 | 3 | 3.247001348628 | 3.404690481534 | |
| $7_P \times 14_F$ | 2.618033988750 | 3 | 3.246979603718 | 3.414217072295 | 3.458917430738 |
| $7_P \times 21_F$ | 2.618033988750 | 3 | 3.246979603717 | 3.414213561735 | |
| $7_P \times 28_F$ | 2.618033988750 | 3 | 3.246979603717 | 3.414213562373 | 3.470544903913 |
| $7_P \times 35_F$ | 2.618033988750 | 3 | 3.246979603717 | 3.414213562373 | |
| $7_P \times 42_F$ | 2.618033988750 | 3 | 3.246979603717 | 3.414213562373 | 3.473634831556 |
| $7_P \times 49_F$ | 2.618033988750 | 3 | 3.246979603717 | 3.414213562373 | |
| $7_P \times 56_F$ | 2.618033988750 | 3 | 3.246979603717 | 3.414213562373 | 3.475070205361 |
| $7_P \times 63_F$ | 2.618033988750 | 3 | 3.246979603717 | 3.414213562373 | |
| $7_P \times 70_F$ | 2.618033988750 | 3 | 3.246979603717 | 3.414213562373 | 3.475899672990 |
| $8_P \times 8_F$ | 2.618033988750 | 3 | 3.246979601854 | | |
| $8_P \times 16_F$ | 2.618033988750 | 3 | 3.246979603717 | 3.414214415195 | 3.472683999084 |
| $8_P \times 24_F$ | 2.618033988750 | 3 | 3.246979603717 | 3.414213562387 | 3.488644630018 |
| $8_P \times 32_F$ | 2.618033988750 | 3 | 3.246979603717 | 3.414213562373 | 3.495735217349 |
| $8_P \times 40_F$ | 2.618033988750 | 3 | 3.246979603717 | 3.414213562373 | 3.499773262291 |
| $8_P \times 48_F$ | 2.618033988750 | 3 | 3.246979603717 | 3.414213562373 | 3.502387969424 |
| $8_P \times 56_F$ | 2.618033988750 | 3 | 3.246979603717 | 3.414213562373 | 3.504221641913 |
| $8_P \times 64_F$ | 2.618033988750 | 3 | 3.246979603717 | 3.414213562373 | 3.505579831565 |
| $8_P \times 72_F$ | 2.618033988750 | 3 | 3.246979603717 | 3.414213562373 | 3.506626776159 |
| $8_P \times 80_F$ | 2.618033988750 | 3 | 3.246979603717 | 3.414213562373 | 3.507458740757 |
| Beraha | 2.618033988750 | 3 | 3.246979603717 | 3.414213562373 | 3.532088886238 |

Table 3: Real zeros of the chromatic polynomials of finite triangular-lattice strips with periodic boundary conditions in the transverse direction and free boundary conditions in the longitudinal direction, to 12 decimal places. A blank means that the zero in question is absent. The first three real zeros $q = 0, 1, 2$ are exact on all lattices. "Beraha" indicates the Beraha numbers $B_5 = (3 + \sqrt{5})/2$, $B_6 = 3$, $B_7$, $B_8 = 2 + \sqrt{2}$, and $B_9$.

| Lattice | 4th Zero | 5th Zero | 6th Zero | 7th Zero | 8th Zero | 9th Zero | 10th Zero |
|---|---|---|---|---|---|---|---|
| $9_P \times 9_F$ | 2.618033988750 | 3.000000000000 | 3.246980644227 | 3.382733076359 | | | |
| $9_P \times 18_F$ | 2.618033988750 | 3.000000000000 | 3.246979603717 | 3.414215827400 | 3.467483864312 | | |
| $9_P \times 27_F$ | 2.618033988750 | 3.000000000000 | 3.246979603717 | 3.414213562359 | | | |
| $9_P \times 36_F$ | 2.618033988750 | 3.000000000000 | 3.246979603717 | 3.414213562373 | 3.499429426359 | | |
| $9_P \times 45_F$ | 2.618033988750 | 3.000000000000 | 3.246979603717 | 3.414213562373 | | | |
| $9_P \times 54_F$ | 2.618033988750 | 3.000000000000 | 3.246979603717 | 3.414213562373 | 3.508825024982 | | |
| $9_P \times 63_F$ | 2.618033988750 | 3.000000000000 | 3.246979603717 | 3.414213562373 | | | |
| $9_P \times 72_F$ | 2.618033988750 | 3.000000000000 | 3.246979603717 | 3.414213562373 | 3.513393802382 | | |
| $9_P \times 81_F$ | 2.618033988750 | 3.000000000000 | 3.246979603717 | 3.414213562373 | | | |
| $9_P \times 90_F$ | 2.618033988750 | 3.000000000000 | 3.246979603717 | 3.414213562373 | 3.516109505154 | | |
| $10_P \times 10_F$ | 2.618033988750 | 3 | 3.246979603717 | 3.414213601215 | 3.522072913706 | | |
| $10_P \times 20_F$ | 2.618033988750 | 3 | 3.246979603717 | 3.414213562373 | 3.532088885496 | | |
| $10_P \times 30_F$ | 2.618033988750 | 3 | 3.246979603717 | 3.414213562373 | 3.532088886238 | | |
| $10_P \times 40_F$ | 2.618033988750 | 3 | 3.246979603717 | 3.414213562373 | 3.532088886238 | | |
| $10_P \times 50_F$ | 2.618033988750 | 3 | 3.246979603717 | 3.414213562373 | 3.532088886238 | | |
| $10_P \times 60_F$ | 2.618033988750 | 3 | 3.246979603717 | 3.414213562373 | 3.532088886238 | 3.618274945403 | 3.620352727045 |
| $10_P \times 70_F$ | 2.618033988750 | 3 | 3.246979603717 | 3.414213562373 | 3.532088886238 | 3.618041117772 | 3.623157797032 |
| $10_P \times 80_F$ | 2.618033988750 | 3 | 3.246979603717 | 3.414213562373 | 3.532088886238 | 3.618034257877 | 3.624885448640 |
| $10_P \times 90_F$ | 2.618033988750 | 3 | 3.246979603717 | 3.414213562373 | 3.532088886238 | 3.618033998995 | 3.626138707957 |
| $10_P \times 100_F$ | 2.618033988750 | 3 | 3.246979603717 | 3.414213562373 | 3.532088886238 | 3.618033989140 | 3.627101535574 |
| $11_P \times 11_F$ | 2.618033988750 | 3 | 3.246979603717 | 3.414213539527 | | | |
| $11_P \times 22_F$ | 2.618033988750 | 3 | 3.246979603717 | 3.414213562373 | 3.532088885575 | | |
| $11_P \times 33_F$ | 2.618033988750 | 3 | 3.246979603717 | 3.414213562373 | 3.532088886238 | 3.608601511861 | |
| $11_P \times 44_F$ | 2.618033988750 | 3 | 3.246979603717 | 3.414213562373 | 3.532088886238 | | |
| $11_P \times 55_F$ | 2.618033988750 | 3 | 3.246979603717 | 3.414213562373 | 3.532088886238 | 3.617975980728 | |
| $11_P \times 66_F$ | 2.618033988750 | 3 | 3.246979603717 | 3.414213562373 | 3.532088886238 | 3.618034451624 | 3.627344614702 |
| $11_P \times 77_F$ | 2.618033988750 | 3 | 3.246979603717 | 3.414213562373 | 3.532088886238 | 3.618033985241 | |
| $11_P \times 88_F$ | 2.618033988750 | 3 | 3.246979603717 | 3.414213562373 | 3.532088886238 | 3.618033988777 | 3.631979435582 |
| $11_P \times 99_F$ | 2.618033988750 | 3 | 3.246979603717 | 3.414213562373 | 3.532088886238 | 3.618033988750 | |
| $11_P \times 110_F$ | 2.618033988750 | 3 | 3.246979603717 | 3.414213562373 | 3.532088886238 | 3.618033988750 | 3.634574709990 |
| $12_P \times 12_F$ | 2.618033988750 | 3.000000000000 | 3.246979603717 | 3.414213593041 | 3.511032635472 | | |
| $12_P \times 24_F$ | 2.618033988750 | 3.000000000000 | 3.246979603717 | 3.414213562373 | 3.532088885001 | | |
| $12_P \times 36_F$ | 2.618033988750 | 3.000000000000 | 3.246979603717 | 3.414213562373 | 3.532088886238 | | |
| $12_P \times 48_F$ | 2.618033988750 | 3.000000000000 | 3.246979603717 | 3.414213562373 | 3.532088886238 | | |
| $12_P \times 60_F$ | 2.618033988750 | 3.000000000000 | 3.246979603717 | 3.414213562373 | 3.532088886238 | | |
| $12_P \times 72_F$ | 2.618033988750 | 3.000000000000 | 3.246979603717 | 3.414213562373 | 3.532088886238 | 3.618040035384 | 3.624320958404 |
| $12_P \times 84_F$ | 2.618033988750 | 3.000000000000 | 3.246979603717 | 3.414213562373 | 3.532088886238 | 3.618034035926 | 3.627419917635 |
| $12_P \times 96_F$ | 2.618033988750 | 3.000000000000 | 3.246979603717 | 3.414213562373 | 3.532088886238 | 3.618033989120 | 3.629588218978 |
| $12_P \times 108_F$ | 2.618033988750 | 3.000000000000 | 3.246979603717 | 3.414213562373 | 3.532088886238 | 3.618033988753 | 3.631215401061 |
| $12_P \times 120_F$ | 2.618033988750 | 3.000000000000 | 3.246979603717 | 3.414213562373 | 3.532088886238 | 3.618033988750 | 3.632487726562 |
| Beraha | 2.618033988750 | 3 | 3.246979603717 | 3.414213562373 | 3.532088886238 | 3.618033988750 | 3.682507065662 |

Table 4: Real zeros of the chromatic polynomials of finite triangular-lattice strips with periodic boundary conditions in the transverse direction and free boundary conditions in the longitudinal direction, to 12 decimal places. We use the same notation as in Table 3.

| Lattice | 4th Zero | 5th Zero | 6th Zero | 7th Zero | 8th Zero | 9th Zero | 10th Zero |
|---|---|---|---|---|---|---|---|
| $4_Z \times 4_F$ | 2.485072022789 | 2.527537649962 | 2.596617094656 | | | | |
| $4_Z \times 8_F$ | 2.499965989337 | 2.500034085574 | 2.618031965217 | | | | |
| $4_Z \times 12_F$ | 2.499999937358 | 2.500000062643 | 2.618033988527 | | | | |
| $4_Z \times 16_F$ | 2.499999999885 | 2.500000000115 | 2.618033988750 | | | | |
| $4_Z \times 20_F$ | 2.500000000000 | 2.500000000000 | 2.618033988750 | | | | |
| $4_Z \times 24_F$ | 2.500000000000 | 2.500000000000 | 2.618033988750 | | | | |
| $4_Z \times 28_F$ | 2.500000000000 | 2.618033988750 | | | | | |
| $4_Z \times 32_F$ | 2.500000000000 | 2.618033988750 | | | | | |
| $4_Z \times 36_F$ | 2.500000000000 | 2.618033988750 | | | | | |
| $4_Z \times 40_F$ | 2.500000000000 | 2.618033988750 | | | | | |
| $6_Z \times 6_F$ | 2.618033988528 | | | | | | |
| $6_Z \times 12_F$ | 2.618033988750 | 3.000017186720 | 3.117917986708 | | | | |
| $6_Z \times 18_F$ | 2.618033988750 | 3.000000004191 | 3.141107899326 | | | | |
| $6_Z \times 24_F$ | 2.618033988750 | 3.000000000001 | 3.150834657646 | | | | |
| $6_Z \times 30_F$ | 2.618033988750 | 3.000000000000 | 3.156227017803 | | | | |
| $6_Z \times 36_F$ | 2.618033988750 | 2.722632835458 | 3.000000000000 | 3.159661924115 | | | |
| $6_Z \times 42_F$ | 2.618033988750 | 2.722632835458 | 3.000000000000 | 3.162043675850 | | | |
| $6_Z \times 48_F$ | 2.618033988750 | 2.722632835458 | 3.000000000000 | 3.163793040154 | | | |
| $6_Z \times 54_F$ | 2.618033988750 | 2.722632835458 | 3.000000000000 | 3.165132700997 | | | |
| $6_Z \times 60_F$ | 2.618033988750 | 2.722632835458 | 3.000000000000 | 3.166191662980 | | | |
| $8_Z \times 8_F$ | 2.618033988750 | 3.000000844168 | 3.203925019292 | | | | |
| $8_Z \times 16_F$ | 2.618033988750 | 3.000000000000 | 3.246976356780 | | | | |
| $8_Z \times 24_F$ | 2.618033988750 | 3.000000000000 | 3.246979603696 | | | | |
| $8_Z \times 32_F$ | 2.618033988750 | 2.821420495535 | 3.000000000000 | 3.246979603717 | | | |
| $8_Z \times 40_F$ | 2.618033988750 | 2.821420495535 | 3.000000000000 | 3.246979603717 | | | |
| $8_Z \times 48_F$ | 2.618033988750 | 2.821420495535 | 3.000000000000 | 3.246979603717 | | | |
| $8_Z \times 56_F$ | 2.618033988750 | 2.821420495535 | 3.000000000000 | 3.246979603717 | | | |
| $8_Z \times 64_F$ | 2.618033988750 | 2.821420495535 | 3.000000000000 | 3.246979603717 | | | |
| $8_Z \times 72_F$ | 2.618033988750 | 2.821420495535 | 3.000000000000 | 3.246979603717 | | | |
| $8_Z \times 80_F$ | 2.618033988750 | 2.821420495535 | 3.000000000000 | 3.246979603717 | | | |
| $10_Z \times 10_F$ | 2.618033988750 | 3.000000000000 | 3.246953122227 | | | | |
| $10_Z \times 20_F$ | 2.618033988750 | 3.000000000000 | 3.246979603717 | 3.416320582746 | 3.428202969384 | | |
| $10_Z \times 30_F$ | 2.618033988750 | 3.000000000000 | 3.246979603717 | 3.414213564771 | 3.470075808656 | | |
| $10_Z \times 40_F$ | 2.618033988750 | 2.873731249334 | 3.000000000000 | 3.246979603717 | 3.414213562373 | 3.484585415185 | |
| $10_Z \times 50_F$ | 2.618033988750 | 2.873731249334 | 3.000000000000 | 3.246979603717 | 3.414213562373 | 3.492475877808 | |
| $10_Z \times 60_F$ | 2.618033988750 | 2.873731249334 | 3.000000000000 | 3.246979603717 | 3.414213562373 | 3.497477600415 | |
| $10_Z \times 70_F$ | 2.618033988750 | 2.873731249334 | 3.000000000000 | 3.246979603717 | 3.383128531235 | 3.414213562373 | 3.500942791087 |
| $10_Z \times 80_F$ | 2.618033988750 | 2.873731249334 | 3.000000000000 | 3.246979603717 | 3.383128531235 | 3.414213562373 | 3.503489509874 |
| $10_Z \times 90_F$ | 2.618033988750 | 2.873731249334 | 3.000000000000 | 3.246979603717 | 3.383128531235 | 3.414213562373 | 3.505442176204 |
| $10_Z \times 100_F$ | 2.618033988750 | 2.873731249334 | 3.000000000000 | 3.246979603717 | 3.383128531235 | 3.414213562373 | 3.506987965042 |
| Beraha | 2.618033988750 | 3 | 3.246979603717 | 3.414213562373 | 3.532088886238 | 3.618033988750 | 3.682507065662 |

Table 5: Real zeros of the chromatic polynomials of finite triangular-lattice strips with zig-zag boundary conditions, to 12 decimal places. We use the same notation as in Table 3.

| | Eigenvalue-Crossing Curves $\mathcal{B}$ | | | | | | | | Isolated Points | |
|---|---|---|---|---|---|---|---|---|---|---|
| Lattice | # C | # E | # T | # D | # ER | min Re $q$ | $q_0$ | max Re $q$ | # RI | # CI |
| $2_\mathrm{F}$ | | | | | | | | | 2 | 0 |
| $3_\mathrm{F}$ | 3 | 6 | 0 | 0 | 0 | 1.20474 | 2.56984 | 3.40223 | 3 | 0 |
| $4_\mathrm{F}$ | 2 | 6 | 2 | 0 | 0 | 0.81647 | $2.75925 \pm 0.15444\,i^*$ | 3.63983 | 4 | 0 |
| $5_\mathrm{F}$ | 1 | 6 | 12 | 0 | 4 | 0.55862 | 3 | 3.77830 | 4 | 0 |
| $6_\mathrm{F}$ | 1 | 6 | 4 | 0 | 0 | 0.37963 | 3.16093 | 3.86641 | 5 | 0 |
| $7_\mathrm{F}$ | $1^\dagger$ | $6^\dagger$ | $4^\dagger$ | 0 | $0^\dagger$ | 0.25054 | 3.27640 | 3.92580 | 6 | 0 |
| $8_\mathrm{F}$ | $1^\dagger$ | $6^\dagger$ | $4^\dagger$ | 0 | $0^\dagger$ | 0.13343 | 3.36106 | 3.96756 | 6 | 0 |
| $9_\mathrm{F}$ | | | | | | | 3.42513 | | 7 | 0 |
| $2_\mathrm{P}$ | | | | | | | | | 2 | 0 |
| $3_\mathrm{P}$ | | | | | | | | | 3 | 0 |
| $4_\mathrm{P}$ | 3 | 4 | 0 | 0 | 1 | 1.37053 | 3.48141 | 4 | 5 | 0 |
| $5_\mathrm{P}$ | 3 | 4 | 0 | 0 | 1 | 0.47725 | 3.20722 | 3.87699 | 5 | 0 |
| $6_\mathrm{P}$ | 1 | 4 | 2 | 0 | 0 | 0.02077 | 3.25242 | 4.28386 | 6 | 0 |
| $7_\mathrm{P}$ | 1 | 4 | 4 | 0 | 1 | $-0.22792$ | 3.47900 | 3.99964 | 7 | 0 |
| $8_\mathrm{P}$ | 1 | 4 | 2 | 0 | 0 | $-0.37137$ | 3.51477 | 4.04970 | 7 | 0 |
| $9_\mathrm{P}$ | 1 | 4 | 2 | 0 | 0 | $-0.45760$ | 3.52706 | 4.28286 | 7 | 0 |
| $10_\mathrm{P}$ | $1^\dagger$ | $4^\dagger$ | $2^\dagger$ | 0 | $0^\dagger$ | $-0.51081$ | 3.63483 | 4.12341 | 9 | 0 |
| $11_\mathrm{P}$ | $1^\dagger$ | $4^\dagger$ | $2^\dagger$ | 0 | $0^\dagger$ | $-0.54399$ | 3.64414 | 4.15609 | 9 | 0 |
| $12_\mathrm{P}$ | | | $2^\dagger$ | | | | 3.64317 | | 9 | 0 |
| $2_\mathrm{Z}$ | | | | | | | | | 2 | 0 |
| $4_\mathrm{Z}$ | 2 | 4 | 0 | 0 | 0 | 2.09914 | $2.73717 \pm 0.17233\,i^*$ | 4.00485 | 5 | 0 |
| $6_\mathrm{Z}$ | 1 | 4 | 2 | 0 | 0 | 0.36185 | 3.17526 | 4.25895 | 6 | 1 |
| $8_\mathrm{Z}$ | $1^\dagger$ | $4^\dagger$ | $2^\dagger$ | 0 | $0^\dagger$ | $-0.21435$ | 3.39410 | 4.28991 | 7 | $1^\dagger$ |
| $10_\mathrm{Z}$ | | | | | | | 3.52044 | | 9 | |

Table 6: Summary of qualitative results for the eigenvalue-crossing curves $\mathcal{B}$ and for the isolated limiting points of zeros. For each triangular-lattice strip considered in this paper, we give the number of connected components of $\mathcal{B}$ (# C), the number of endpoints (# E), the number of T points (# T), the number of double points (# D), and the number of enclosed regions (# ER); we also give the minimum value of Re $q$ on $\mathcal{B}$, the smallest value $q_0$ where $\mathcal{B}$ intersects the real axis (* denotes an almost-crossing), and the maximum value of Re $q$ on $\mathcal{B}$. We also report the number of real isolated limiting points of zeros (# RI) and the number of complex-conjugate pairs of isolated limiting points (# CI). The symbol $^\dagger$ indicates uncertain results.

| $m$ | TriCyl($m$) | # VA | TriCyl$'$($m$) | SqCyl($m$) |
|---|---|---|---|---|
| 1 | 1 | 0 | 1 | 1 |
| 2 | 1 | 0 | 1 | 1 |
| 3 | 1 | 0 | 1 | 1 |
| 4 | 2 | 0 | 2 | 2 |
| 5 | 2 | 0 | 2 | 2 |
| 6 | 5 | 0 | 5 | 5 |
| 7 | 6 | 0 | 6 | 6 |
| 8 | 15 | 2 | 13 | 14 |
| 9 | 28 | 12 | 16 | 22 |
| 10 | 67 | 32 | 35 | 51 |
| 11 | 145 | 100 | 45 | 95 |
| 12 | 368 | 272 | 96 | 232 |
| 13 | 870 | 742* | 126* | 498 |
| 14 | 2211 | 1940* | 267* | 1239 |

Table 7: Transfer-matrix dimensions for a triangular-lattice strip of width $m$ and cylindrical boundary conditions. For each value of the strip width $m$ we give the dimension of the transfer matrix [TriCyl($m$)], the number of vanishing amplitudes (# VA), and the *effective* dimension of the transfer matrix [TriCyl$'$($m$) = TriCyl($m$) − # VA]. For comparison, we also give the dimensionality of the transfer matrix for a square-lattice strip of width $m$ and cylindrical boundary conditions [SqCyl($m$)]. The values of TriCyl($m$) and SqCyl($m$) were obtained in [16, 53]. An asterisk denotes *conjectured* results.

| Curve | Point | $\mathrm{Arg}\, p_{\mathrm{Fit}}/\pi$ | $\mathrm{Arg}\, p/\pi$ | "discrepancy" | $\epsilon$ | $\theta/\pi$ |
|---|---|---|---|---|---|---|
| $C_1$ | G | 1.0000000(3) | 1 | 0.00000005 | 0.0000002 | 1/6 |
|  | H | −0.4999999(3) | −1/2 | 0.0000001 | 0.000001 | 2/3 |
| $C_2$ | I | 0.5000001(3) | 1/2 | 0.0000001 | 0.000001 | 2/9 |
|  | J | 0.4285703(3) | 3/7 | 0.000008 | 0.0006 | 7/30 |
| $C_3$ | L | −0.2500003(3) | −1/4 | 0.000001 | 0.00004 | 4/9 |
|  | K | −0.1999993(3) | −1/5 | 0.000004 | 0.0001 | 5/12 |
| $C_4$ | P | 0.2727311(7) | 3/11 | 0.00004 | 0.006 | 11/42 |
|  | O | 0.2499995(3) | 1/4 | 0.000002 | 0.00006 | 4/15 |
| $C_5$ | M | −0.1428584(3) | −1/7 | 0.000009 | 0.0006 | 7/18 |
|  | N | −0.1249980(3) | −1/8 | 0.00002 | 0.001 | 8/21 |
| $C_7$ | T | −0.3846221(7) | −5/13 | 0.00009 | 0.02 | 13/24 |
|  | S | −0.3749980(3) | −3/8 | 0.00002 | 0.001 | 8/15 |
| $C_8$ |  | 0.1250023(3) | 1/8 | 0.00002 | 0.002 | 8/27 |
|  |  | 0.1199957(7) | 3/25 | 0.0001 | 0.05 | 25/84 |
| $C_{17}$ |  | −0.4285727(3) | −3/7 | 0.000009 | 0.0006 | 7/12 |
|  |  | −0.4230929(3) | −11/26 | 0.0007 | 0.04 | 26/45 |
| $C_{18}$ |  | −0.1000025(3) | −1/10 | 0.00003 | 0.003 | 10/27 |
|  |  | −0.0909045(7) | −1/11 | 0.00005 | 0.007 | 11/30 |
| $C_{19}$ |  | −0.0769285(7) | −1/13 | 0.00007 | 0.01 | 13/36 |
|  |  | −0.0714257(7) | −1/14 | 0.00004 | 0.008 | 14/39 |
| Others |  | −0.5999993(3) | −3/5 | 0.000004 | 0.0002 | 5/6 |
|  |  | −0.7500002(3) | −3/4 | 0.00000009 | 0.00003 | 4/27 |
|  |  | 0.7499995(3) | 3/4 | 0.000002 | 0.00006 | 4/21 |
|  |  | 0.6000006(3) | 3/5 | 0.000003 | 0.0001 | 5/24 |
|  |  | 0.2999986(7) | 3/10 | 0.00001 | 0.002 | 10/39 |
|  | V | 0.2000006(3) | 1/5 | 0.000003 | 0.0001 | 5/18 |
|  |  | 0.1428558(3) | 1/7 | 0.00001 | 0.0007 | 7/24 |
|  |  | 0.0999991(7) | 1/10 | 0.000009 | 0.001 | 10/33 |

Table 8: Endpoints in the complex $p$-plane with $|p| = 1$ of the curves where $|g_2/g_1| = 1$. For each endpoint we show the "Curve" to which it belongs (see Figure 22), the estimated value of its phase $\mathrm{Arg}\, p_{\mathrm{Fit}}$ (see text), the conjectured exact value $\mathrm{Arg}\, p$, the "discrepancy" [cf. (6.10)], the "significance level" $\epsilon$ [cf. (6.14)], and the corresponding "primary" $\theta$ value. For some selected values we also include a label ("Point"). When we have a curve for which one endpoint is well-determined and the other is not, we include the former point in the category "Others" (see text).

| Curve | Point | $\mathrm{Arg}\, y_{\mathrm{Fit}}/\pi$ | $\mathrm{Arg}\, y/\pi$ | "discrepancy" | $\epsilon$ | $\theta/\pi$ |
|---|---|---|---|---|---|---|
| $D_1$ | G | $-0.8000002(3)$ | $-4/5$ | 0.000001 | 0.00004 | 1/6 |
|  | H | 0.0000000(6) | 0 | 0.00000002 | 0.00000006 | 2/3 |
| $D_2$ | K | 0.8571435(3) | 6/7 | 0.000005 | 0.0003 | 5/12 |
|  | L | 0.7999997(3) | 4/5 | 0.000002 | 0.00008 | 4/9 |
| $D_4$ |  | $-0.7692308(7)$ | $-10/13$ | 0.0000001 | 0.00003 | 2/15 |
|  |  | $-0.7272743(3)$ | $-8/11$ | 0.00002 | 0.002 | 1/12 |
| $D_6$ |  | $-0.4615359(7)$ | $-6/13$ | 0.00003 | 0.006 | 35/48 |
|  |  | $-0.4000003(3)$ | $-2/5$ | 0.000001 | 0.00006 | 13/18 |
| $D_7$ |  | $-0.5714279(3)$ | $-4/7$ | 0.000004 | 0.0003 | 20/27 |
|  |  | $-0.5454561(3)$ | $-6/11$ | 0.00002 | 0.002 | 31/42 |
| $D_9$ | N | 0.9230794(3) | 12/13 | 0.00003 | 0.006 | 8/21 |
|  | M | 0.9090890(3) | 10/11 | 0.00002 | 0.003 | 7/18 |
| Others |  | $-0.4705939(7)$ | $-8/17$ | 0.0001 | 0.03 | 46/63 |
|  |  | $-0.5263122(7)$ | $-10/19$ | 0.00007 | 0.02 | 53/72 |
|  |  | $-0.6153817(3)$ | $-8/13$ | 0.00004 | 0.007 | 38/51 |
|  |  | $-0.7058815(7)$ | $-12/17$ | 0.00001 | 0.004 | 1/18 |
|  | I | $-0.8571420(1)$ | $-6/7$ | 0.000006 | 0.0004 | 2/9 |
|  | O | $-0.9090929(3)$ | $-10/11$ | 0.00002 | 0.003 | 4/15 |
|  | V | $-0.9230785(7)$ | $-12/13$ | 0.00002 | 0.004 | 5/18 |
|  | S | 0.5714292(3) | 4/7 | 0.000004 | 0.0003 | 8/15 |
|  | T | 0.5454538(7) | 6/11 | 0.000008 | 0.001 | 13/24 |
|  |  | 0.3999997(3) | 2/5 | 0.000002 | 0.00007 | 7/12 |
|  |  | 0.2857149(7) | 2/7 | 0.000004 | 0.0003 | 11/18 |

Table 9: Endpoints in the complex $y$-plane with $|y| = 1$ of the curves where $|g_3/g_1| = 1$. For each endpoint we show the "Curve" to which it belongs (see Figure 23), the estimated value of its phase $\mathrm{Arg}\, y_{\mathrm{Fit}}$ (see text), the conjectured exact value $\mathrm{Arg}\, p$, the "discrepancy" [cf. (6.10)], the "significance level" $\epsilon$ [cf. (6.14)], and the corresponding "primary" $\theta$ value. For some selected values we also include a label ("Point"). When we have a curve for which one endpoint is well-determined and the other is not, we include the former point in the category "Others" (see text).

| $L$ | Beraha numbers |
|---|---|
| $2_\mathrm{F}$ | $\boldsymbol{B_2}\ \boldsymbol{B_3}$ |
| $3_\mathrm{F}$ | $\boldsymbol{B_2}\ \boldsymbol{B_3}\ \boldsymbol{B_4}$ |
| $4_\mathrm{F}$ | $\boldsymbol{B_2}\ \boldsymbol{B_3}\ \boldsymbol{B_4}\ \boldsymbol{B_5}\ B_6$ |
| $5_\mathrm{F}$ | $\boldsymbol{B_2}\ \boldsymbol{B_3}\ \boldsymbol{B_4}\ \boldsymbol{B_5}\ B_6$ |
| $6_\mathrm{F}$ | $\boldsymbol{B_2}\ \boldsymbol{B_3}\ \boldsymbol{B_4}\ \boldsymbol{B_5}\ \boldsymbol{B_6}\ B_7$ |
| $7_\mathrm{F}$ | $\boldsymbol{B_2}\ \boldsymbol{B_3}\ \boldsymbol{B_4}\ \boldsymbol{B_5}\ \boldsymbol{B_6}\ \boldsymbol{B_7}\ B_8$ |
| $8_\mathrm{F}$ | $\boldsymbol{B_2}\ \boldsymbol{B_3}\ \boldsymbol{B_4}\ \boldsymbol{B_5}\ \boldsymbol{B_6}\ \boldsymbol{B_7}\ B_8\ B_9$ |
| $9_\mathrm{F}$ | $\boldsymbol{B_2}\ \boldsymbol{B_3}\ \boldsymbol{B_4}\ \boldsymbol{B_5}\ \boldsymbol{B_6}\ \boldsymbol{B_7}\ \boldsymbol{B_8}\ B_9\ B_{10}$ |
| $2_\mathrm{P}$ | $\boldsymbol{B_2}\ \boldsymbol{B_3}$ |
| $3_\mathrm{P}$ | $\boldsymbol{B_2}\ \boldsymbol{B_3}\ \boldsymbol{B_4}$ |
| $4_\mathrm{P}$ | $\boldsymbol{B_2}\ \boldsymbol{B_3}\ \boldsymbol{B_4}\ \boldsymbol{B_5}\ B_6$ |
| $5_\mathrm{P}$ | $\boldsymbol{B_2}\ \boldsymbol{B_3}\ \boldsymbol{B_4}\ \boldsymbol{B_5}\ \boldsymbol{B_6}$ |
| $6_\mathrm{P}$ | $\boldsymbol{B_2}\ \boldsymbol{B_3}\ \boldsymbol{B_4}\ \boldsymbol{B_5}\ \boldsymbol{B_6}\ \boldsymbol{B_7}\ B_{10}$ |
| $7_\mathrm{P}$ | $\boldsymbol{B_2}\ \boldsymbol{B_3}\ \boldsymbol{B_4}\ \boldsymbol{B_5}\ \boldsymbol{B_6}\ \boldsymbol{B_7}\ \boldsymbol{B_8}\ B_{10}$ |
| $8_\mathrm{P}$ | $\boldsymbol{B_2}\ \boldsymbol{B_3}\ \boldsymbol{B_4}\ \boldsymbol{B_5}\ \boldsymbol{B_6}\ \boldsymbol{B_7}\ \boldsymbol{B_8}\ B_9\ B_{10}\ B_{14}$ |
| $9_\mathrm{P}$ | $\boldsymbol{B_2}\ \boldsymbol{B_3}\ \boldsymbol{B_4}\ \boldsymbol{B_5}\ \boldsymbol{B_6}\ \boldsymbol{B_7}\ \boldsymbol{B_8}\ B_9\ B_{10}\ B_{14}$ |
| $10_\mathrm{P}$ | $\boldsymbol{B_2}\ \boldsymbol{B_3}\ \boldsymbol{B_4}\ \boldsymbol{B_5}\ \boldsymbol{B_6}\ \boldsymbol{B_7}\ \boldsymbol{B_8}\ \boldsymbol{B_9}\ \boldsymbol{B_{10}}\ B_{11}\ B_{14}\ B_{18}$ |
| $11_\mathrm{P}$ | $\boldsymbol{B_2}\ \boldsymbol{B_3}\ \boldsymbol{B_4}\ \boldsymbol{B_5}\ \boldsymbol{B_6}\ \boldsymbol{B_7}\ \boldsymbol{B_8}\ \boldsymbol{B_9}\ \boldsymbol{B_{10}}\ B_{11}\ B_{12}\ B_{14}\ B_{18}$ |
| $12_\mathrm{P}$ | $\boldsymbol{B_2}\ \boldsymbol{B_3}\ \boldsymbol{B_4}\ \boldsymbol{B_5}\ \boldsymbol{B_6}\ \boldsymbol{B_7}\ \boldsymbol{B_8}\ \boldsymbol{B_9}\ \boldsymbol{B_{10}}\ B_{11}\ B_{12}\ B_{13}\ B_{14}\ B_{18}\ B_{22}$ |
| $2_\mathrm{Z}$ | $\boldsymbol{B_2}\ \boldsymbol{B_3}$ |
| $4_\mathrm{Z}$ | $\boldsymbol{B_2}\ \boldsymbol{B_3}\ \boldsymbol{B_4}\ \boldsymbol{B_5}\ B_6$ |
| $6_\mathrm{Z}$ | $\boldsymbol{B_2}\ \boldsymbol{B_3}\ \boldsymbol{B_4}\ \boldsymbol{B_5}\ \boldsymbol{B_6}\ B_7$ |
| $8_\mathrm{Z}$ | $\boldsymbol{B_2}\ \boldsymbol{B_3}\ \boldsymbol{B_4}\ \boldsymbol{B_5}\ \boldsymbol{B_6}\ \boldsymbol{B_7}\ B_8\ B_9$ |
| $10_\mathrm{Z}$ | $\boldsymbol{B_2}\ \boldsymbol{B_3}\ \boldsymbol{B_4}\ \boldsymbol{B_5}\ \boldsymbol{B_6}\ \boldsymbol{B_7}\ \boldsymbol{B_8}\ B_9\ B_{10}\ B_{11}$ |

Table 10: Beraha numbers $B_n$ that are zeros of det $D(q)$. Those shown in boldface (resp. normal face) correspond to the vanishing of a dominant (resp. subdominant) amplitude.
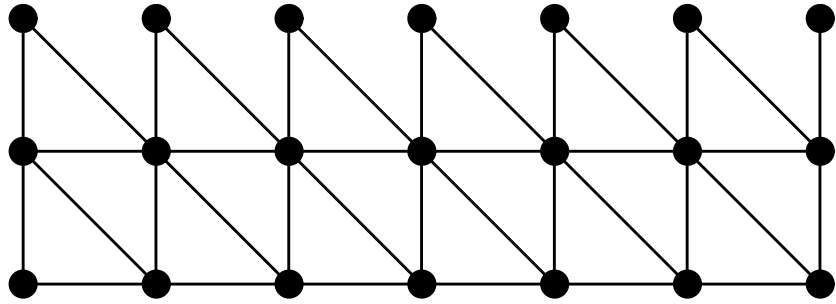
(a)
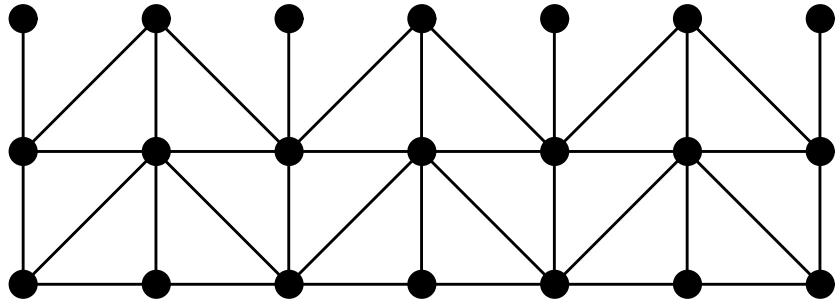


(b)

Figure 1: Two ways of building a triangular-lattice strip using a transfer-matrix approach. (a) Standard method (see e.g. Ref. [16]). (b) Alternative method (called "zig-zag" boundary conditions).
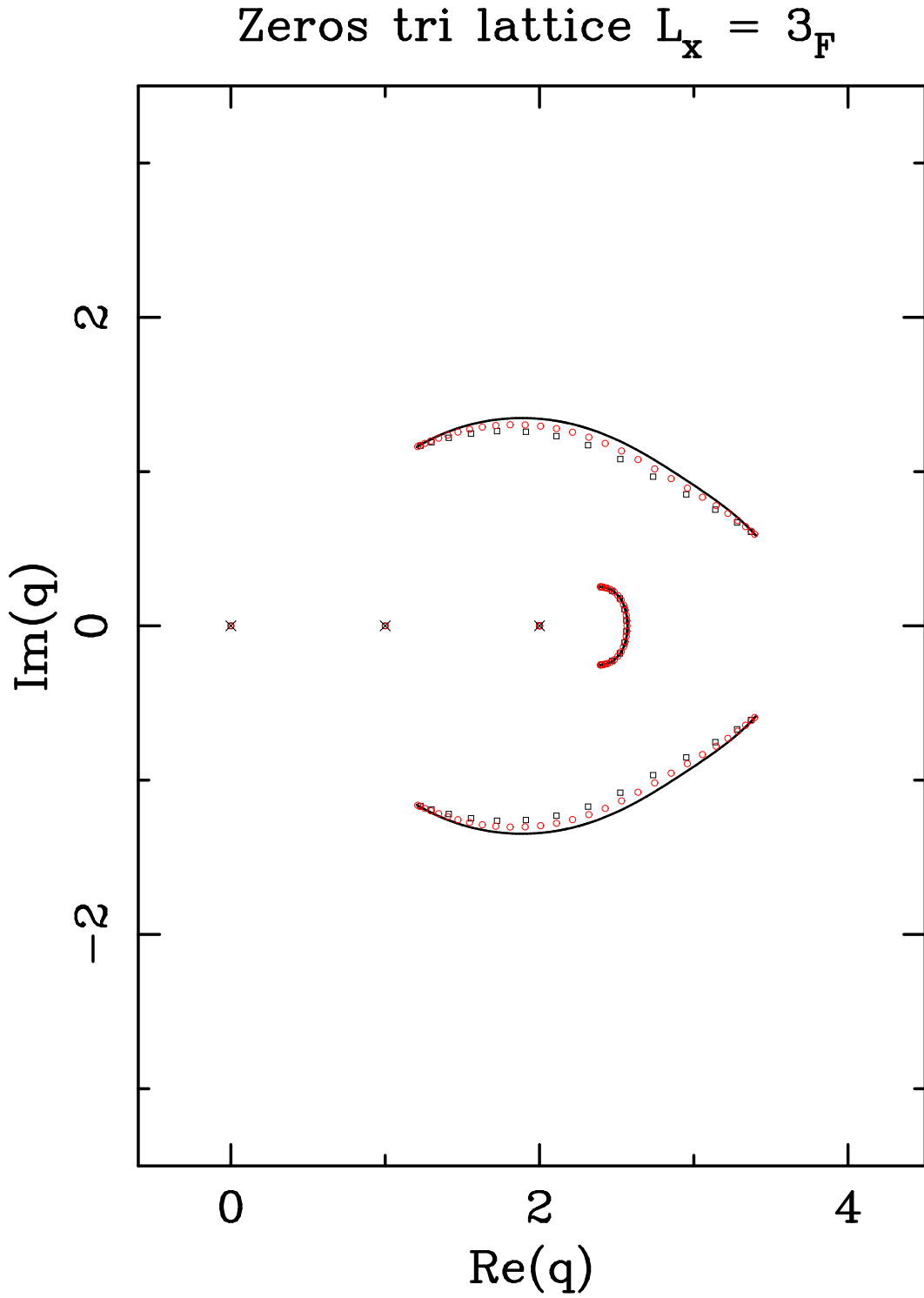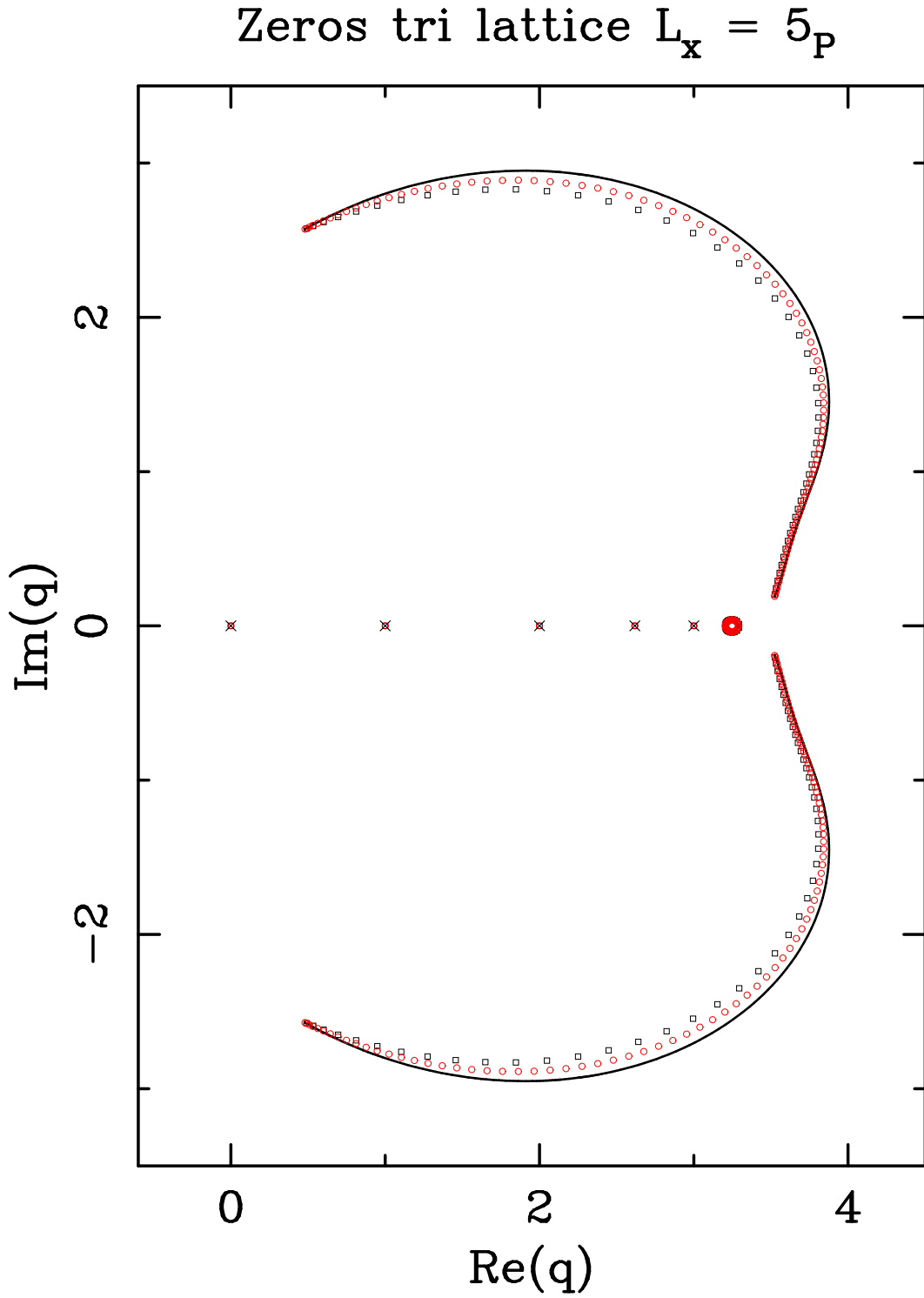
Figure 2: Zeros of the partition function of the $q$-state Potts antiferromagnet on the triangular lattices $3_F \times 15_F$ (squares), $3_F \times 30_F$ (circles) and $3_F \times \infty_F$ (solid line). The isolated limiting points are denoted by a $\times$.
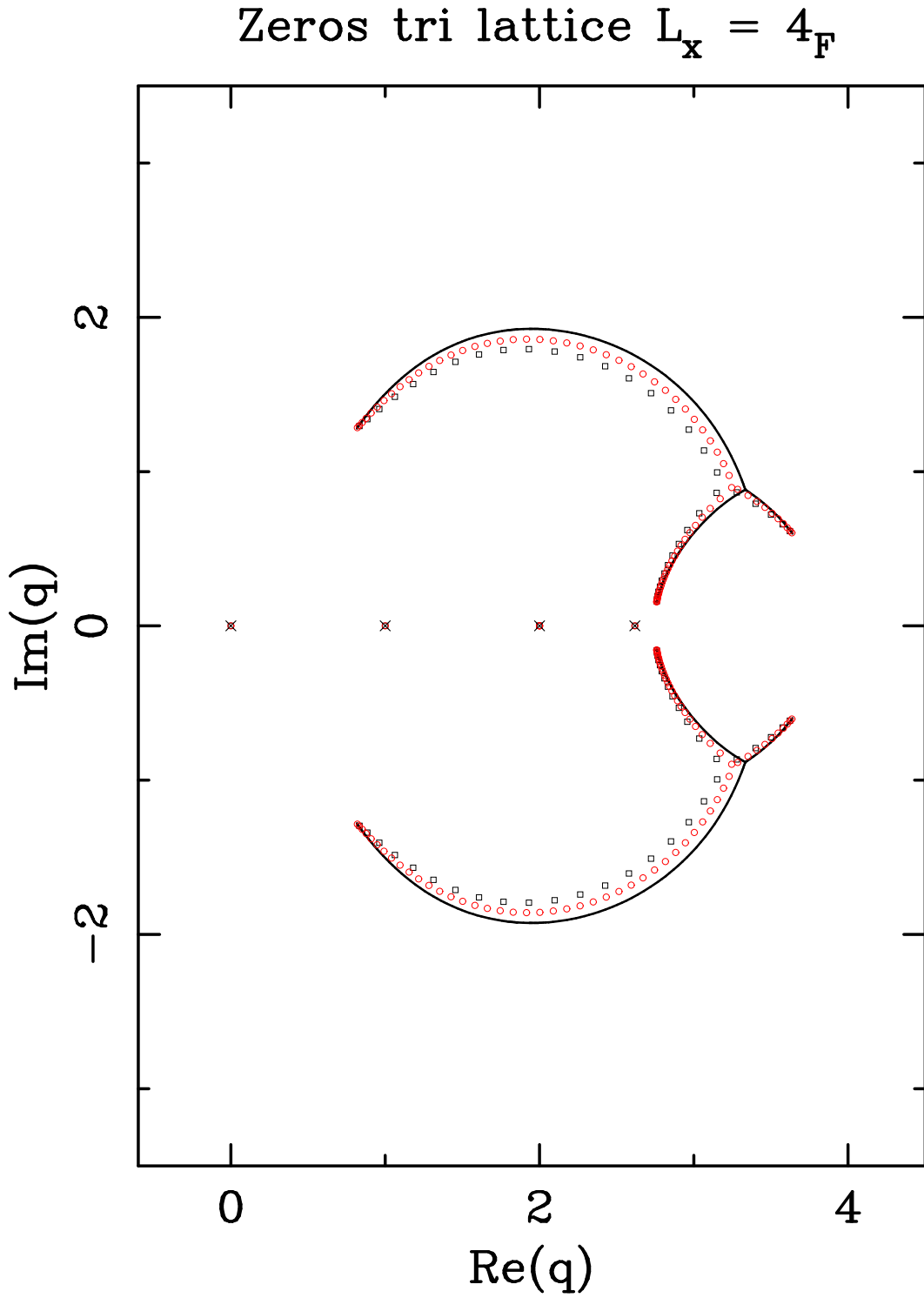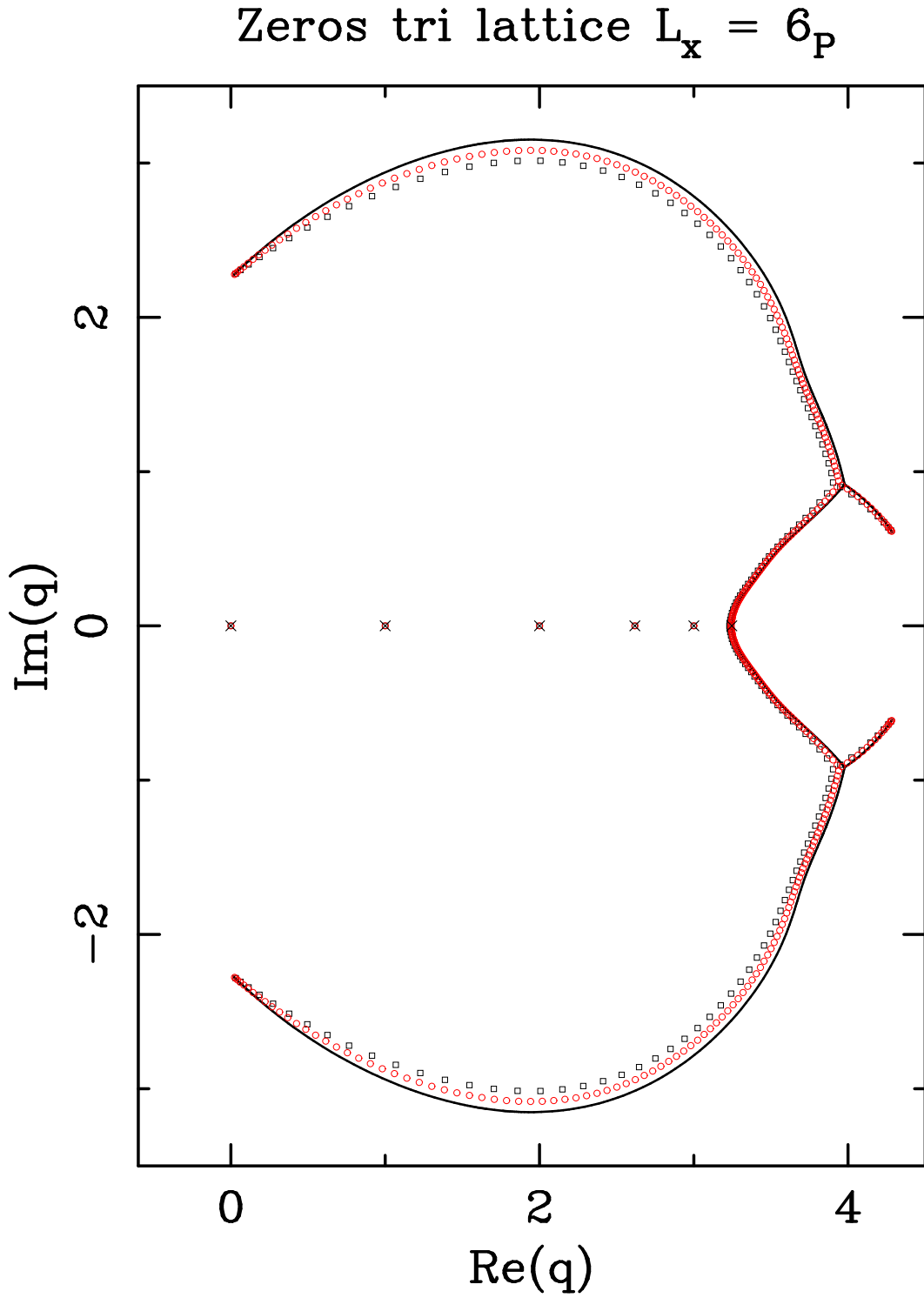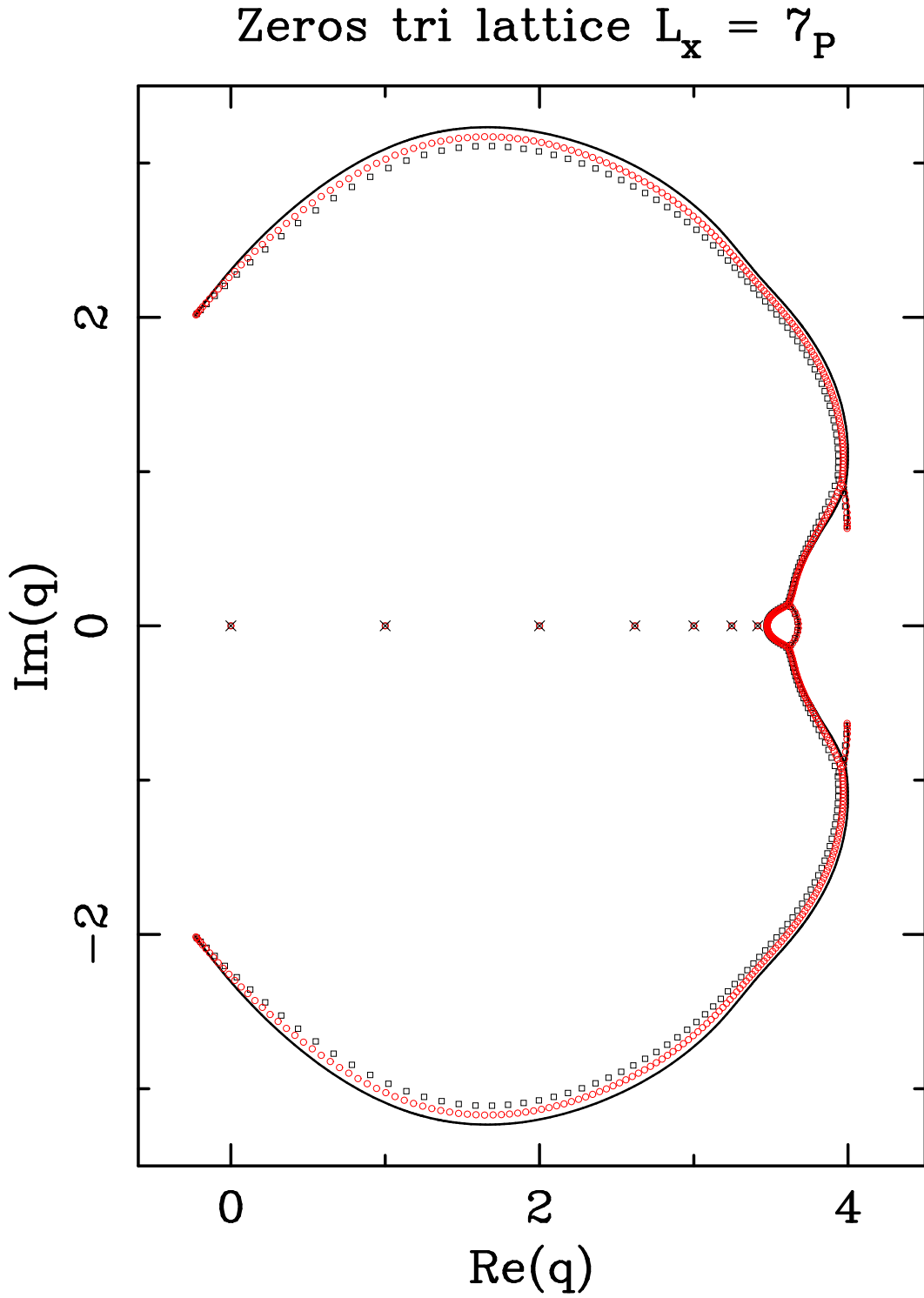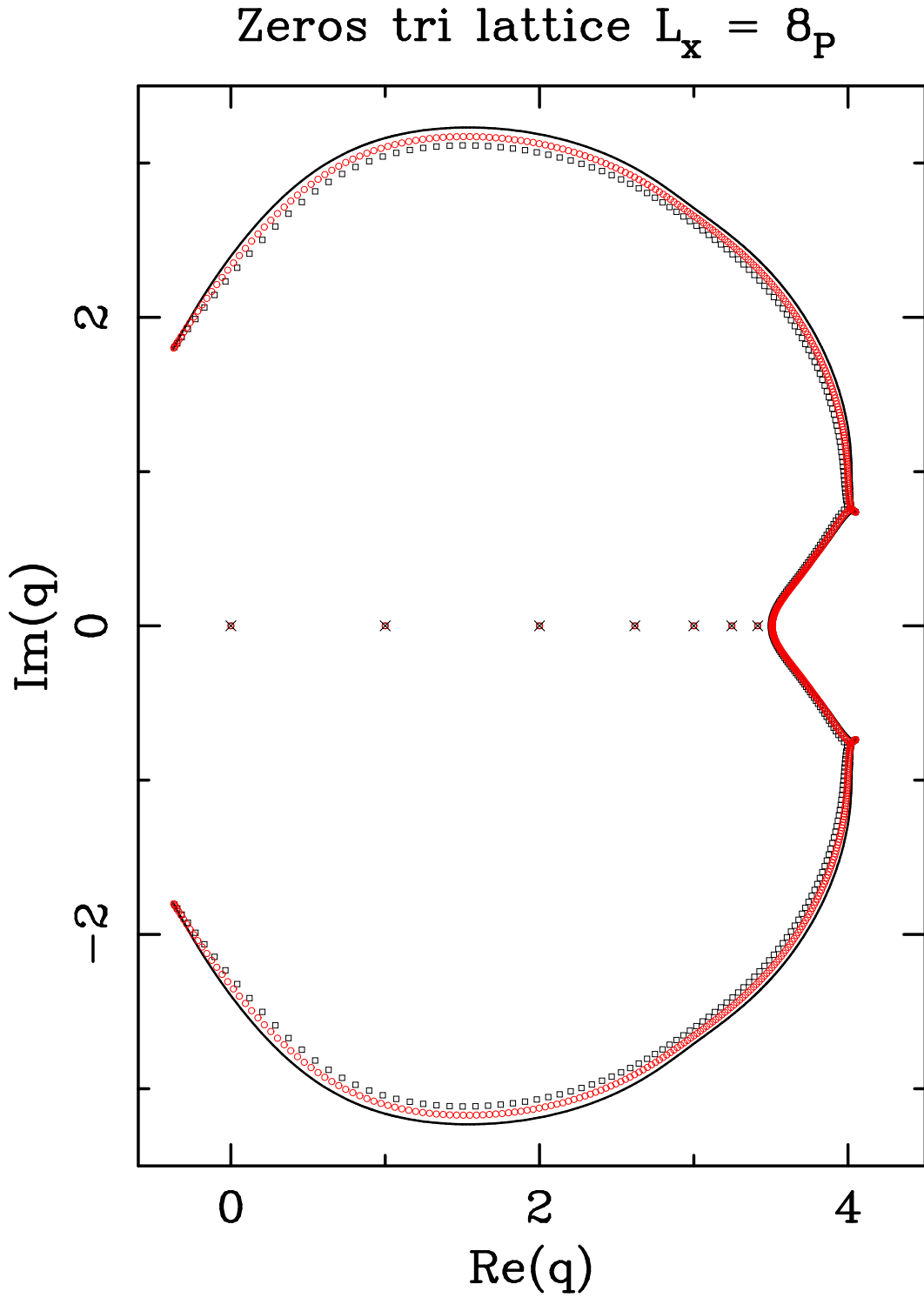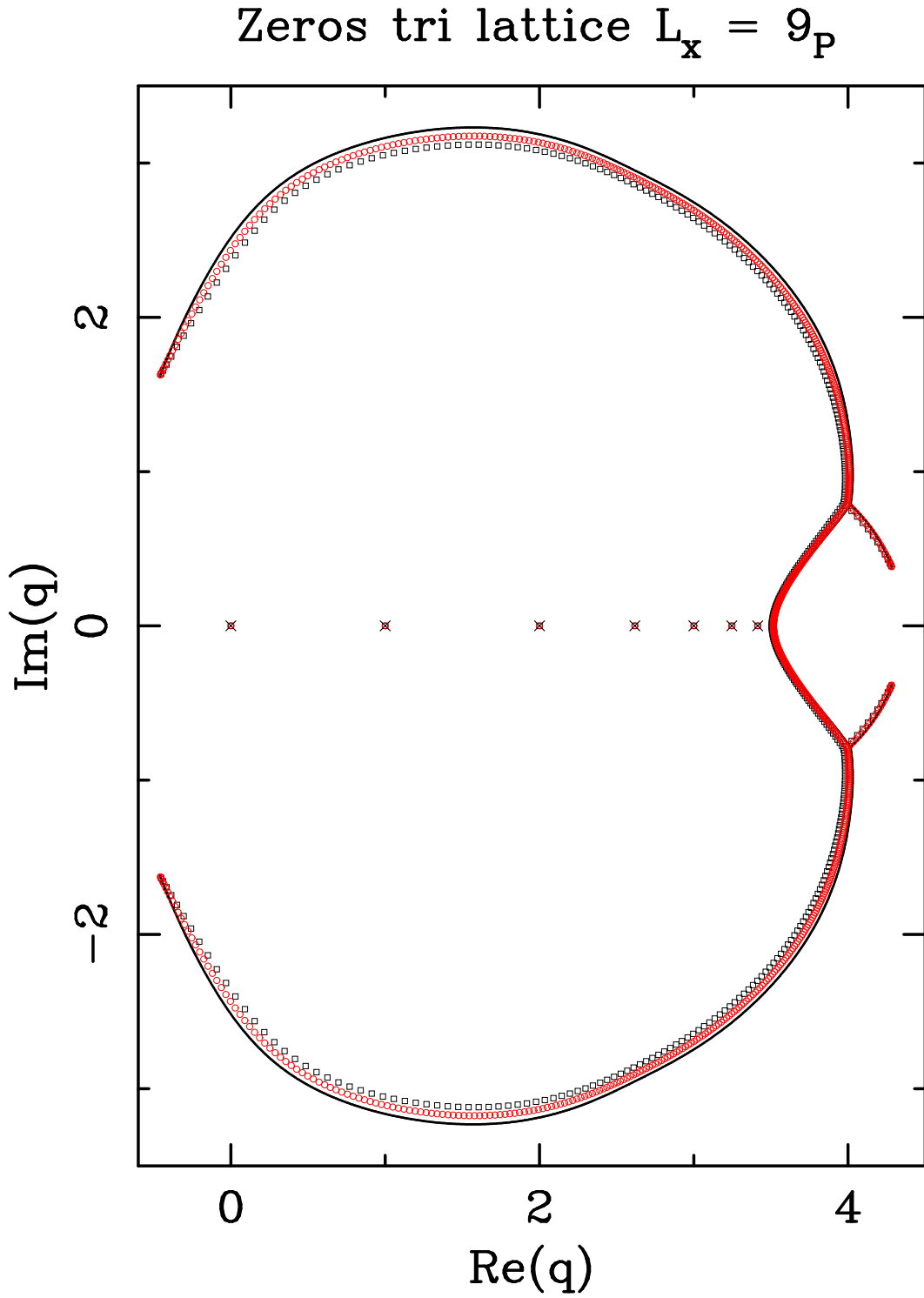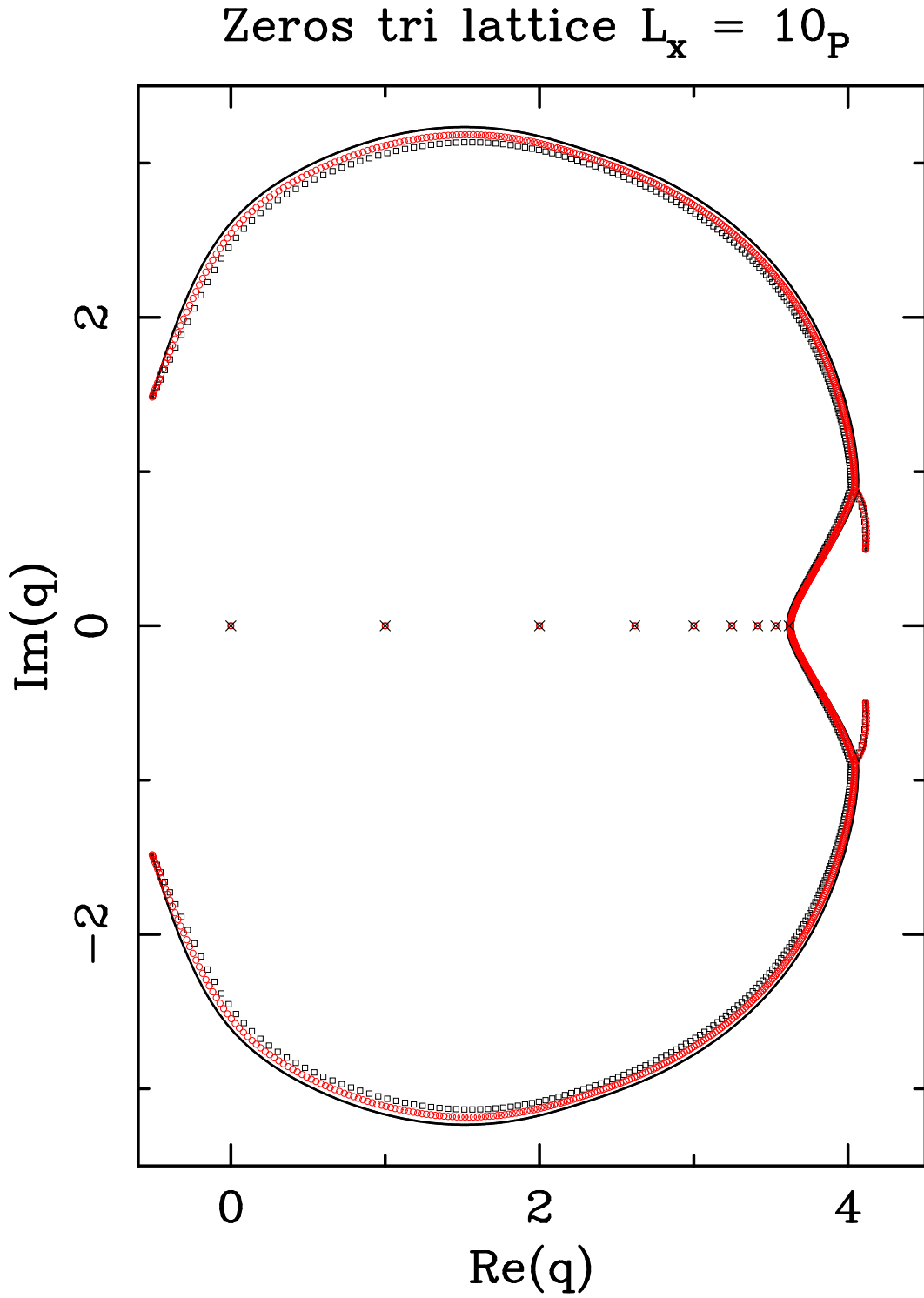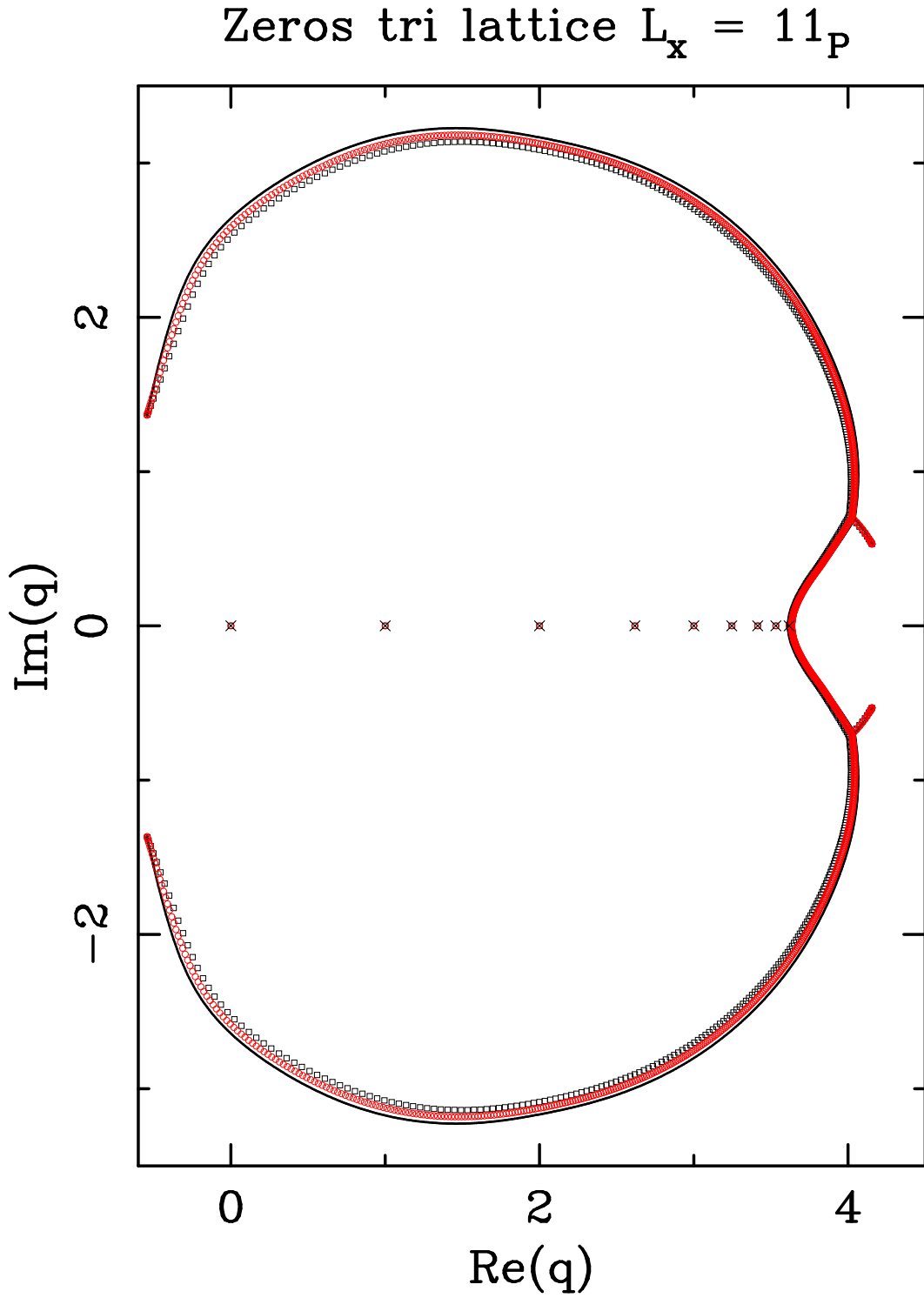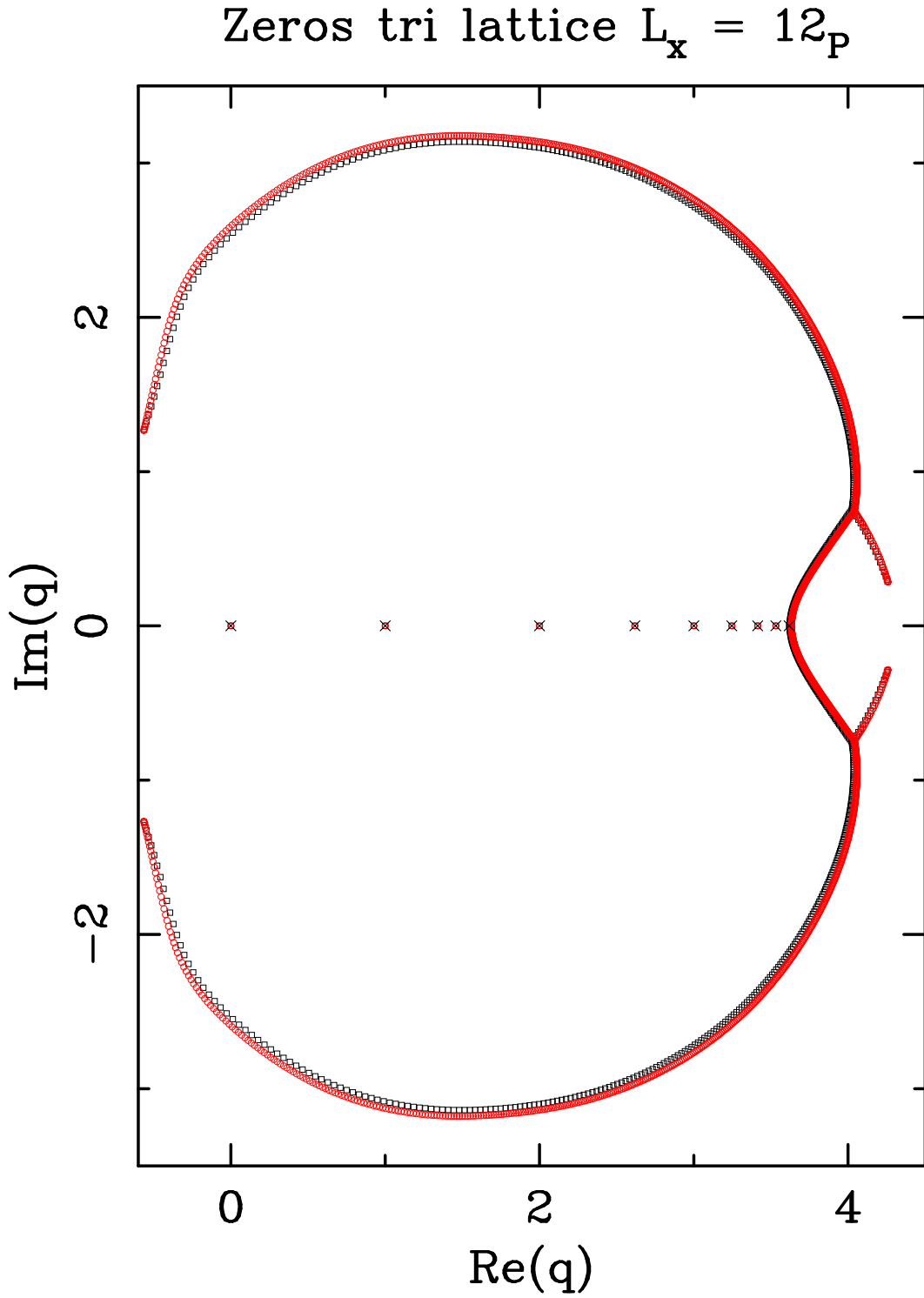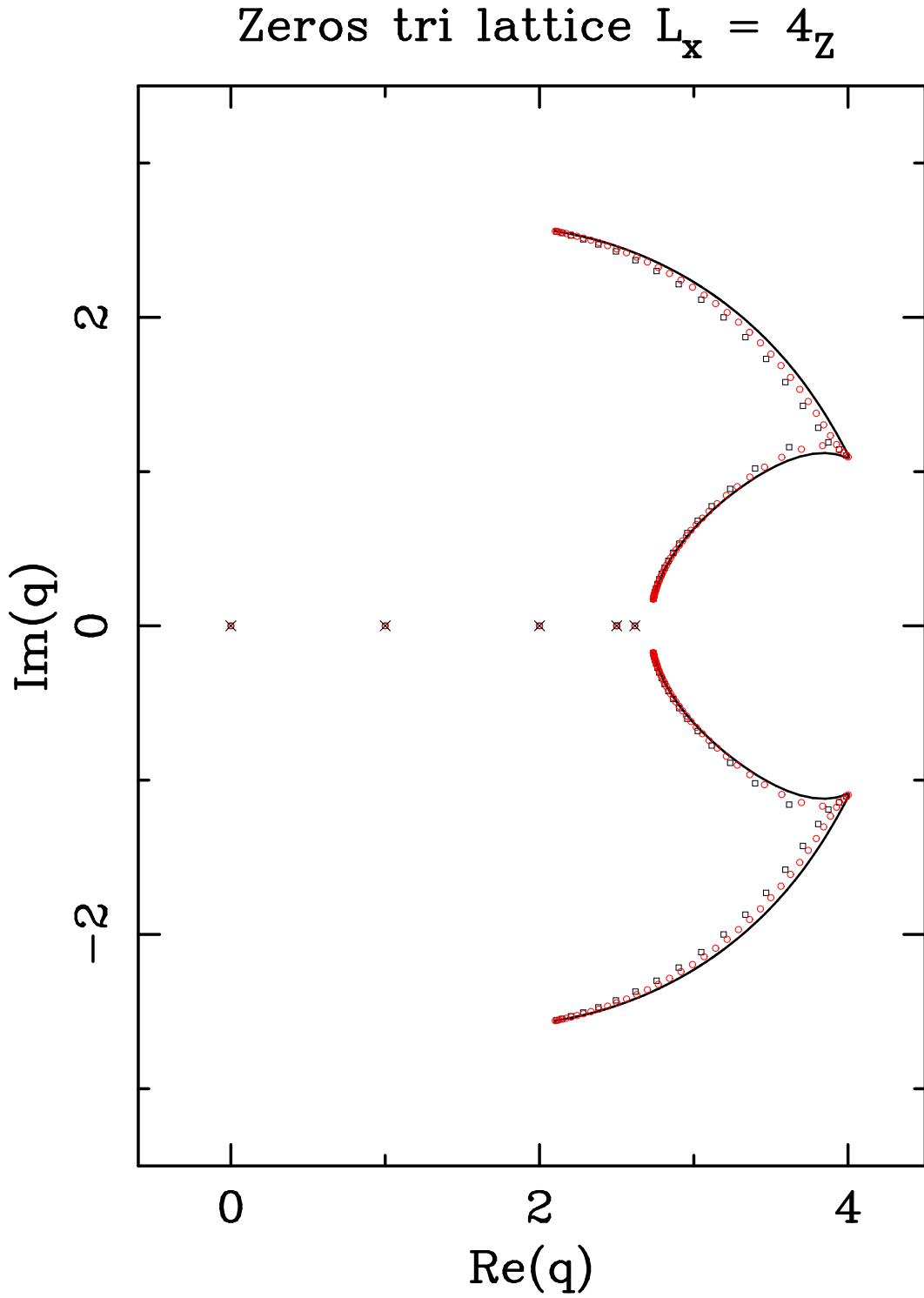
Figure 3: Zeros of the partition function of the $q$-state Potts antiferromagnet on the triangular lattices $4_F \times 20_F$ (squares), $4_F \times 40_F$ (circles) and $4_F \times \infty_F$ (solid line). The isolated limiting points are denoted by a $\times$.

71
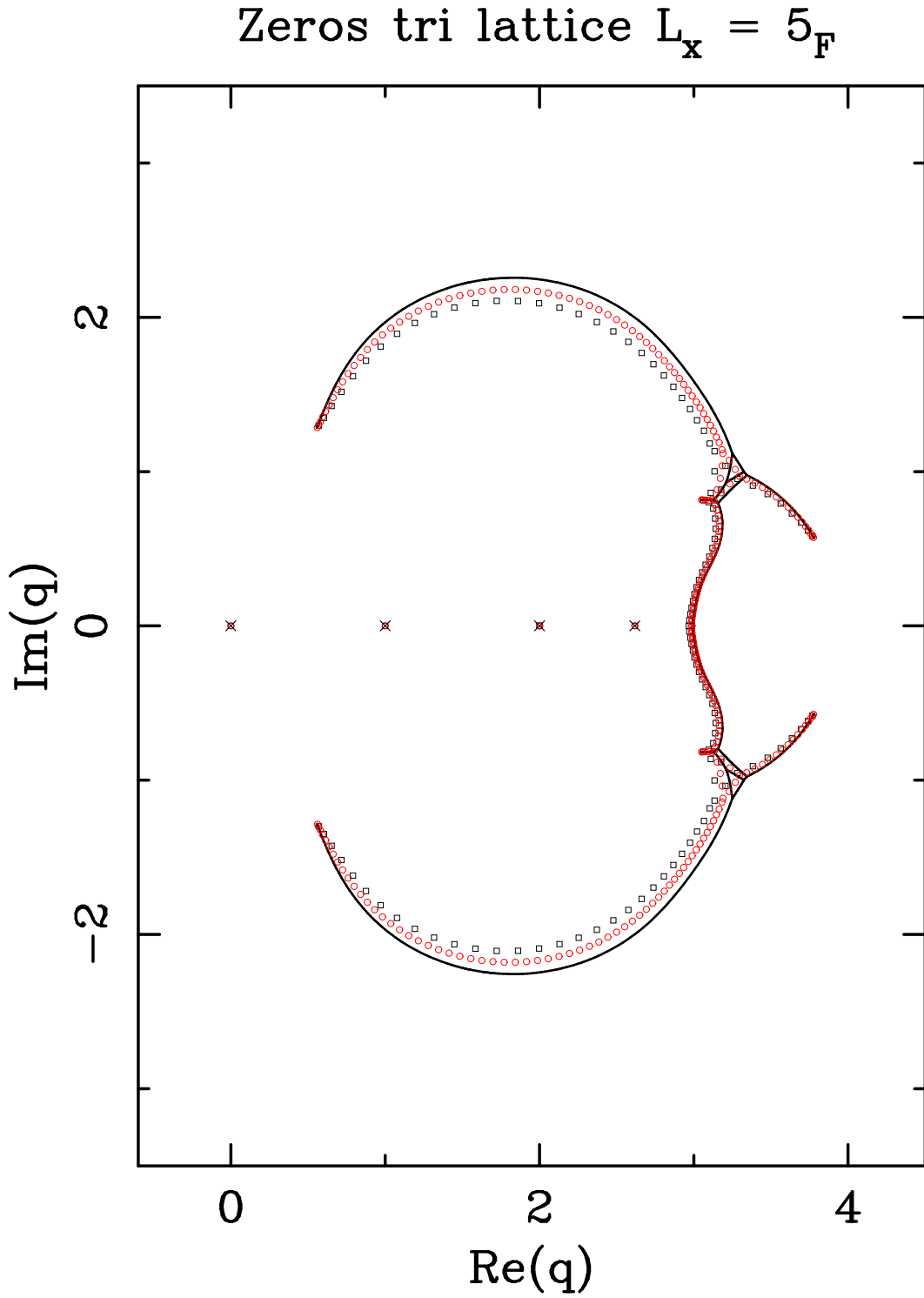
Figure 4: Zeros of the partition function of the $q$-state Potts antiferromagnet on the triangular lattices $5_F \times 25_F$ (squares), $5_F \times 50_F$ (circles) and $5_F \times \infty_F$ (solid line). The isolated limiting points are denoted by a $\times$.
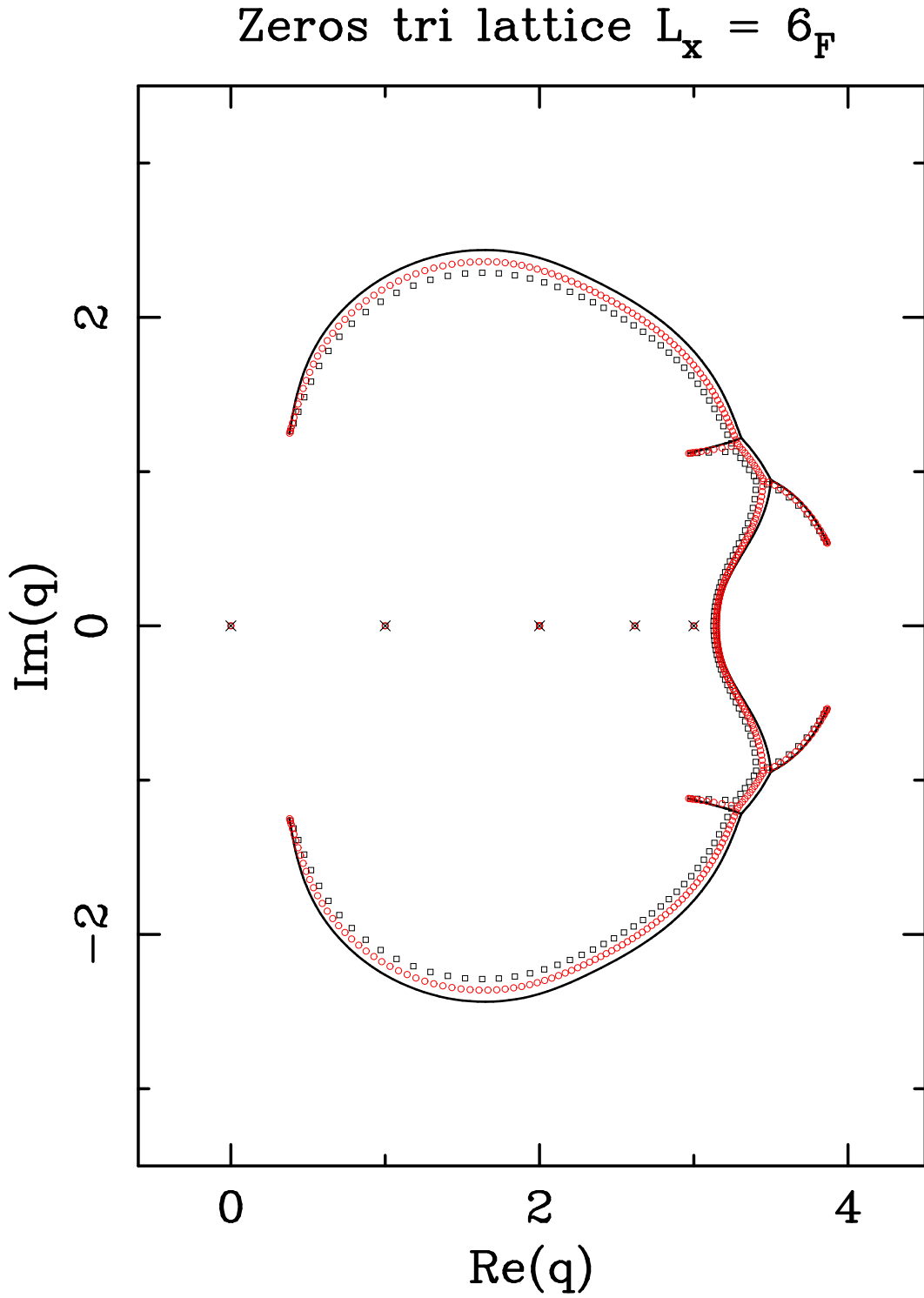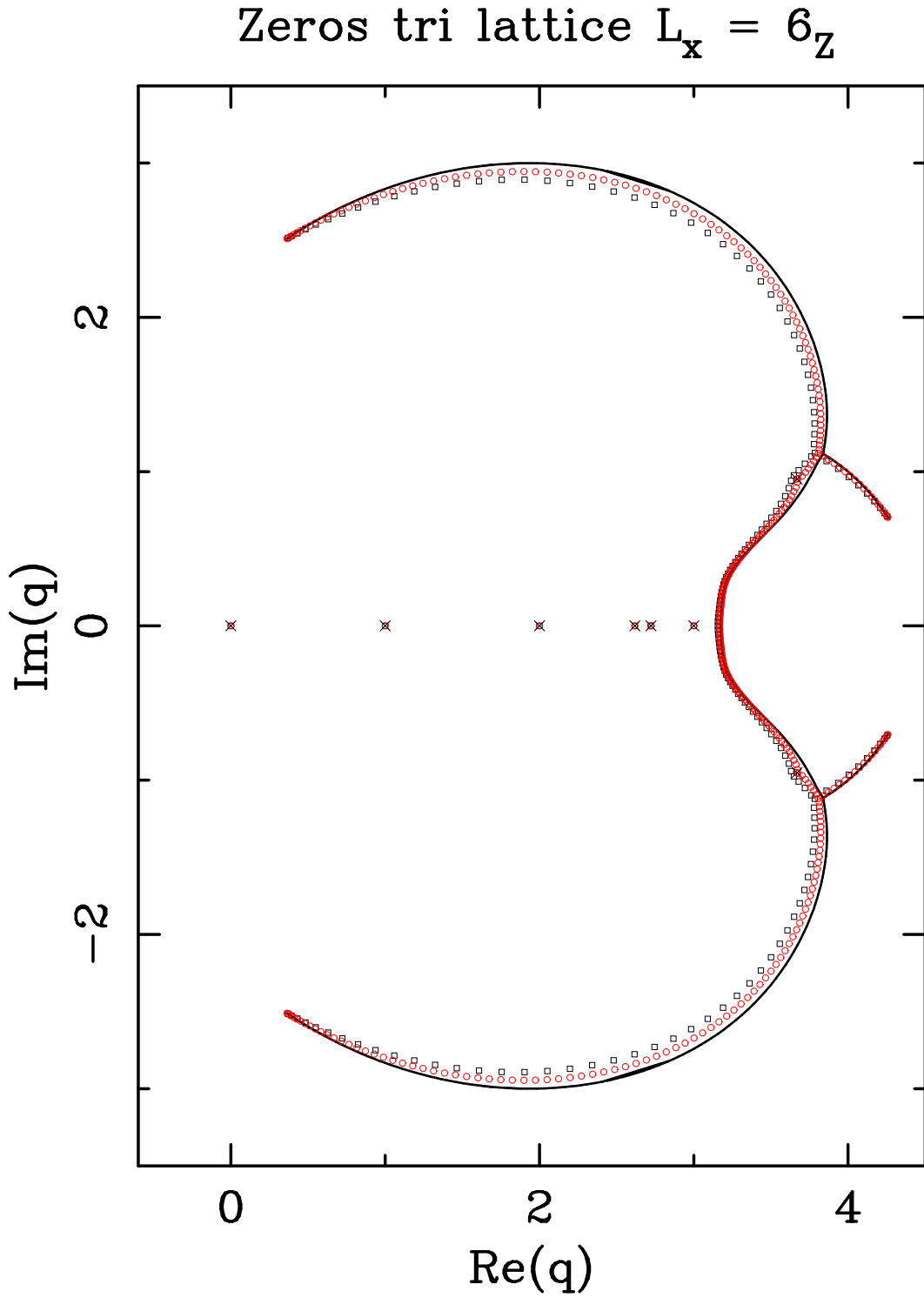
Figure 5: Zeros of the partition function of the $q$-state Potts antiferromagnet on the triangular lattices $6_F \times 30_F$ (squares), $6_F \times 60_F$ (circles) and $6_F \times \infty_F$ (solid line). The isolated limiting points are denoted by a $\times$.
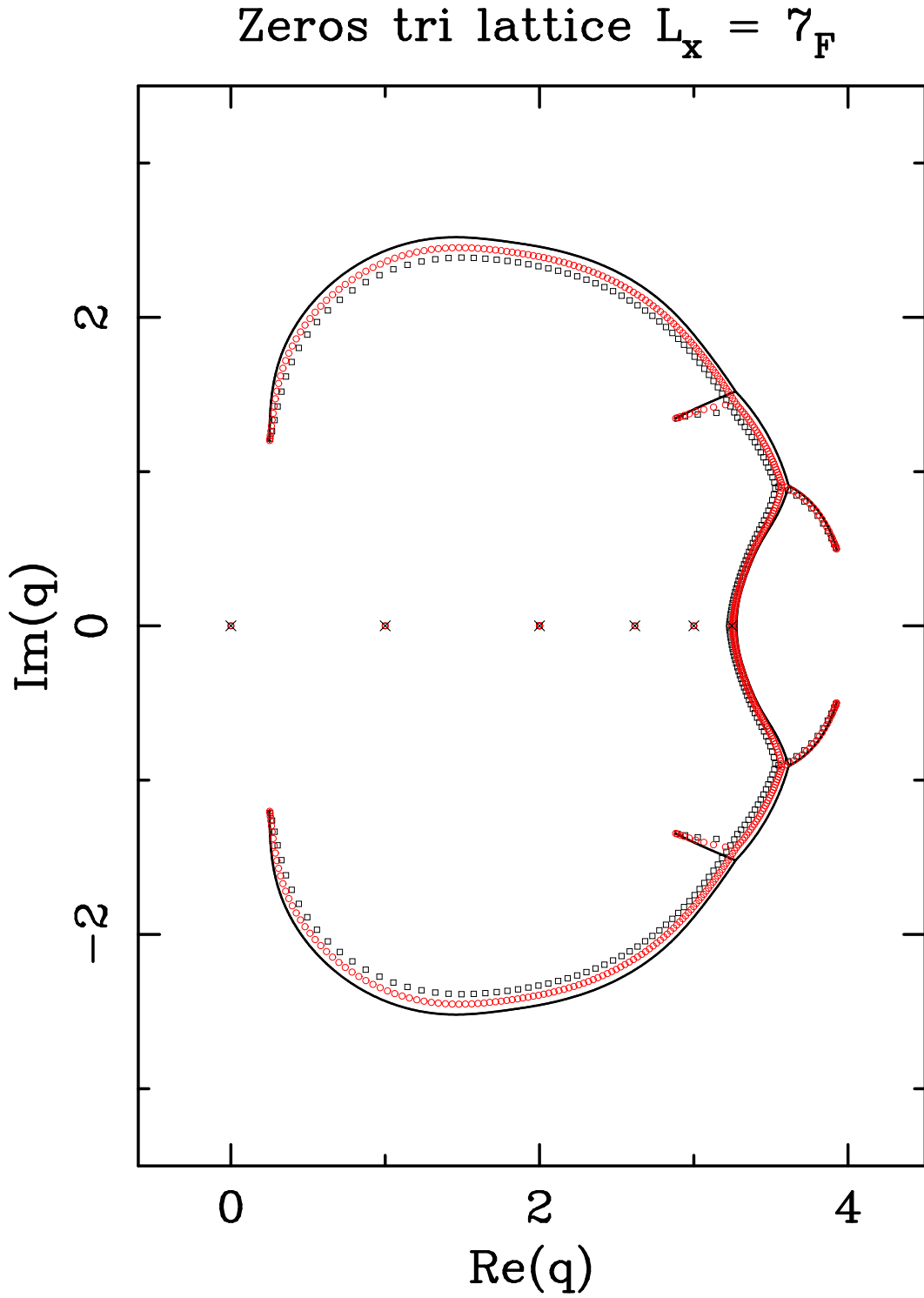
Figure 6: Zeros of the partition function of the $q$-state Potts antiferromagnet on the triangular lattices $7_F \times 35_F$ (squares), $7_F \times 70_F$ (circles) and $7_F \times \infty_F$ (solid line). The isolated limiting points are denoted by a $\times$.
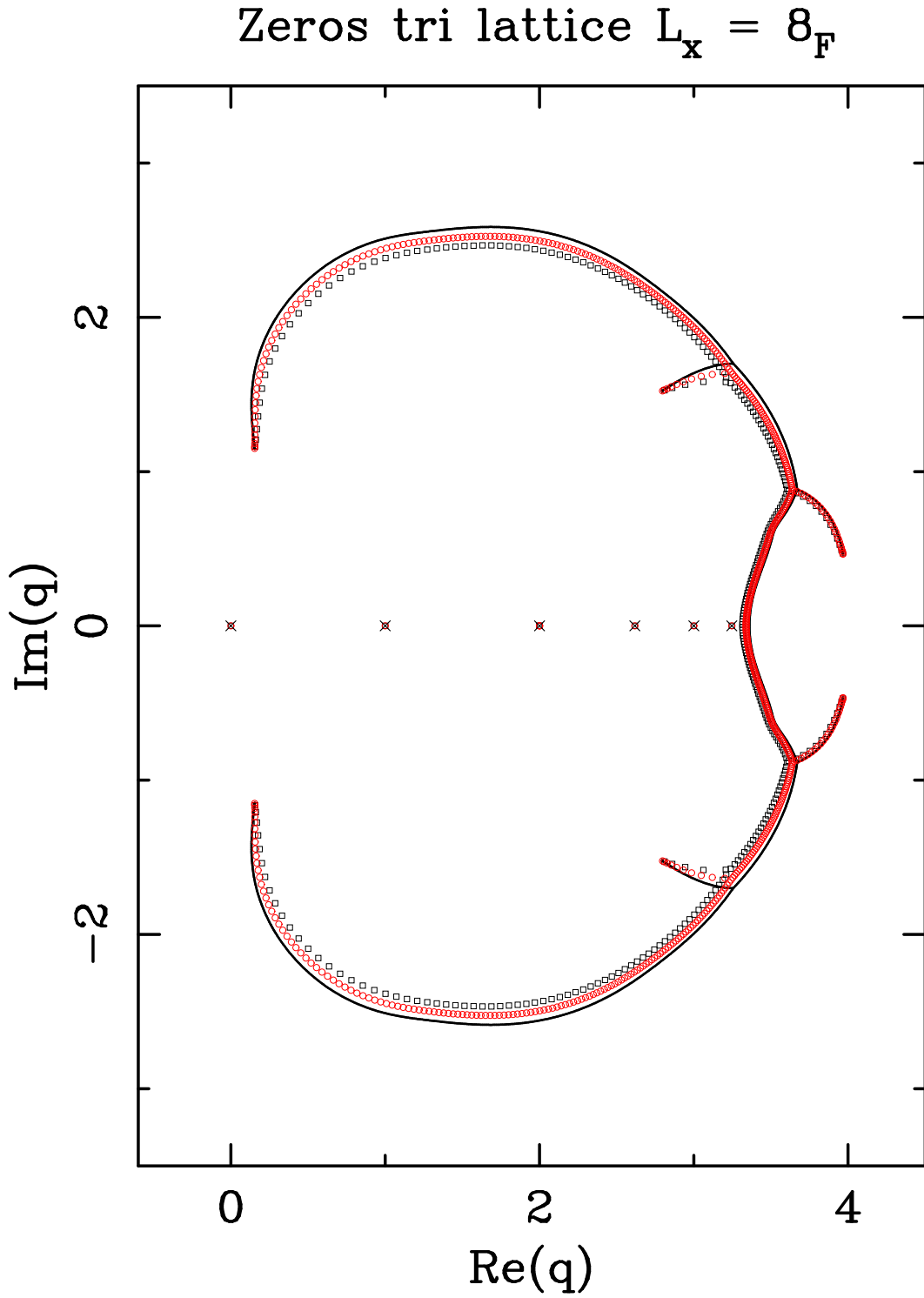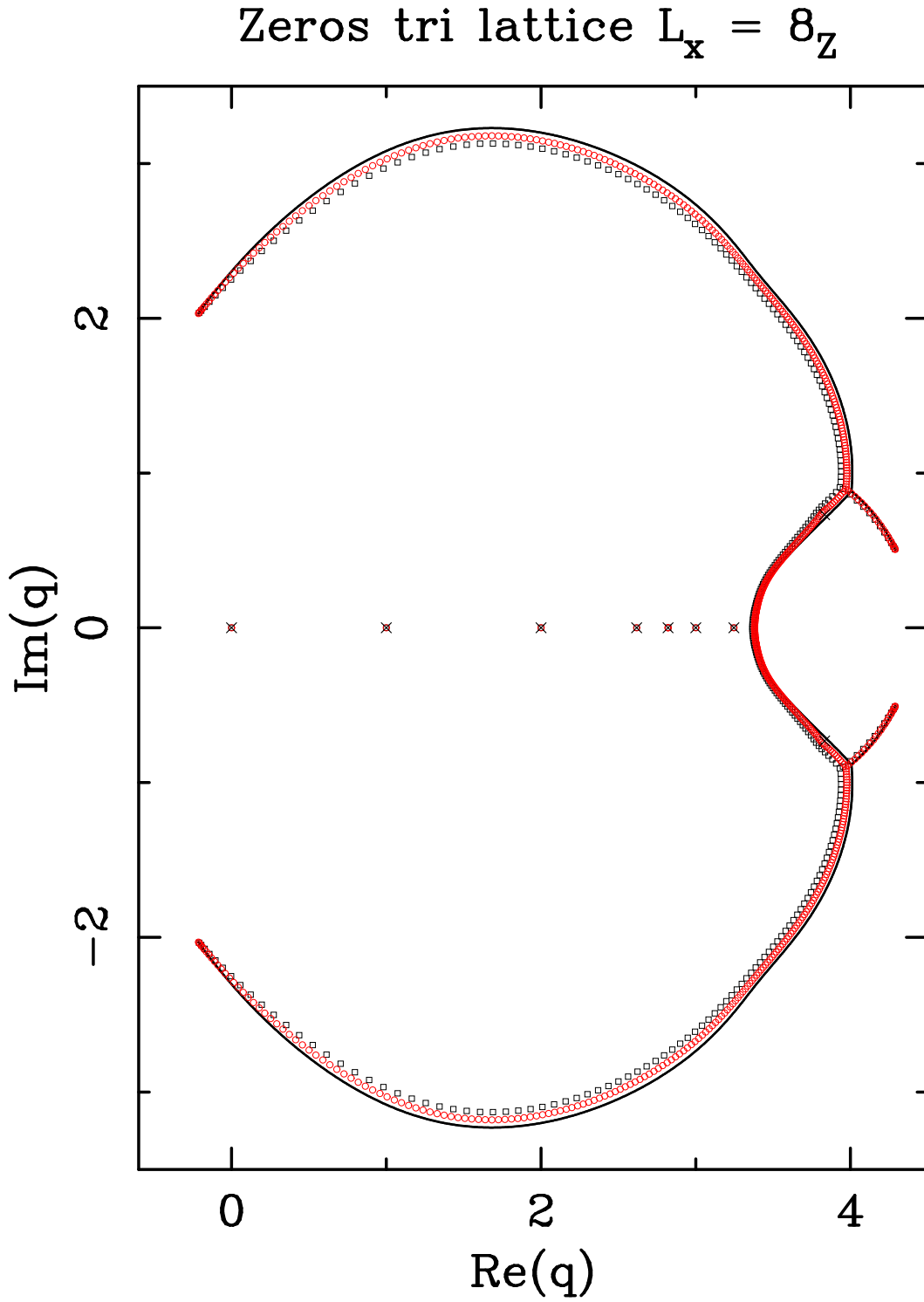
Figure 7: Zeros of the partition function of the $q$-state Potts antiferromagnet on the triangular lattices $8_F \times 40_F$ (squares), $8_F \times 80_F$ (circles) and $8_F \times \infty_F$ (solid line). The isolated limiting points are denoted by a $\times$.
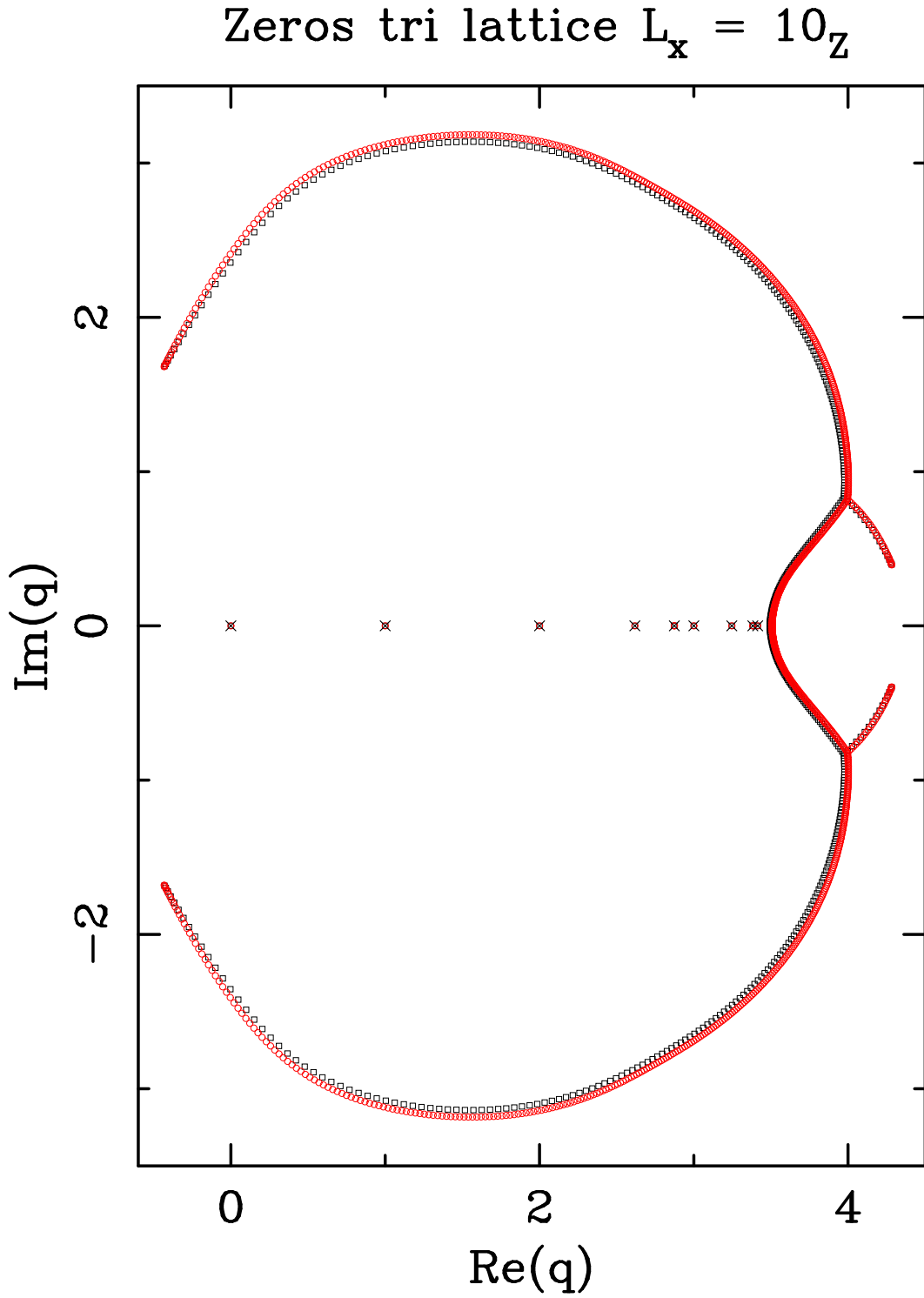
## Zeros tri lattice $L_x = 9_F$
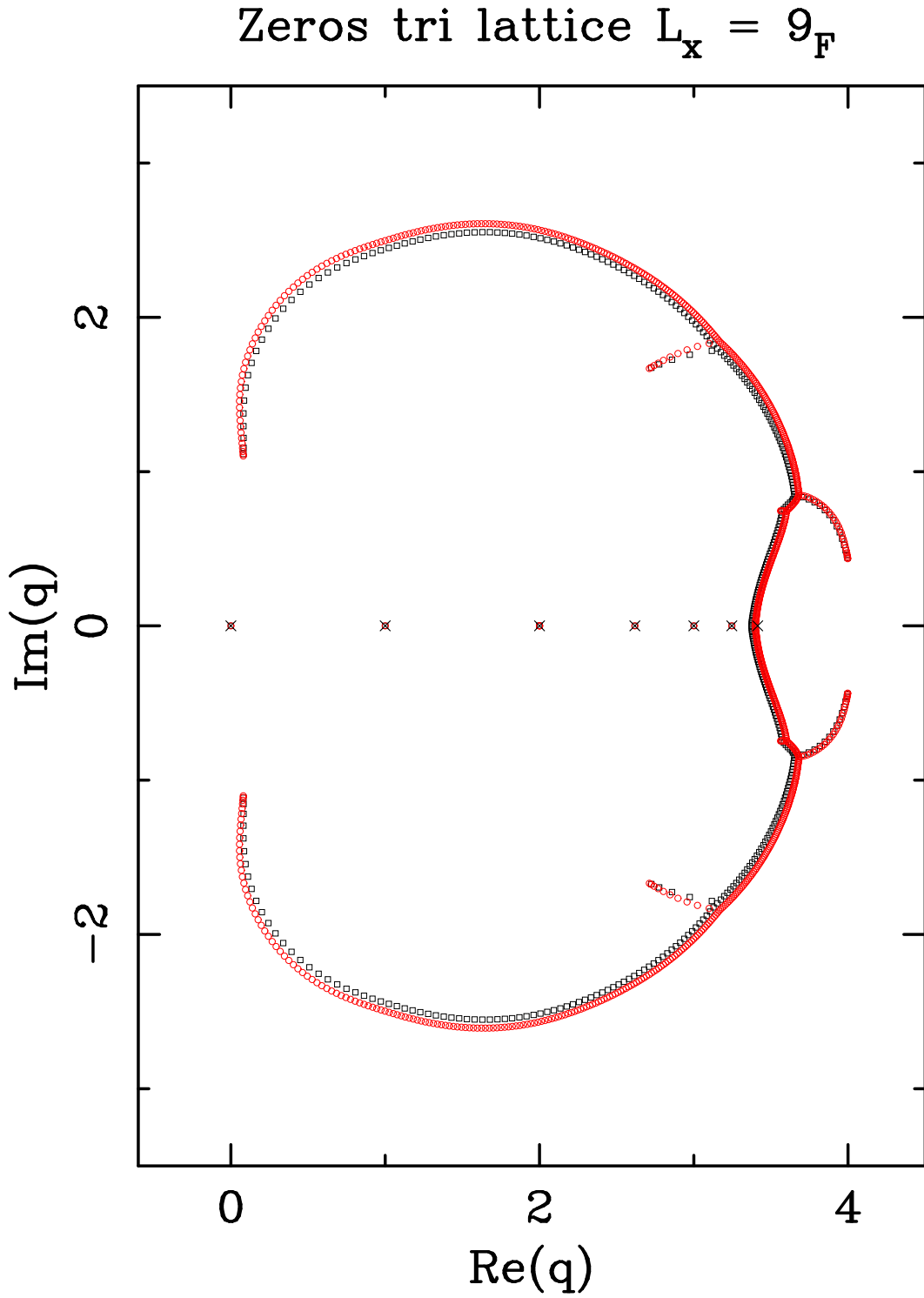


Figure 8: Zeros of the partition function of the $q$-state Potts antiferromagnet on the triangular lattices $9_F \times 45_F$ (squares) and $9_F \times 90_F$ (circles). The isolated limiting points are denoted by a $\times$.
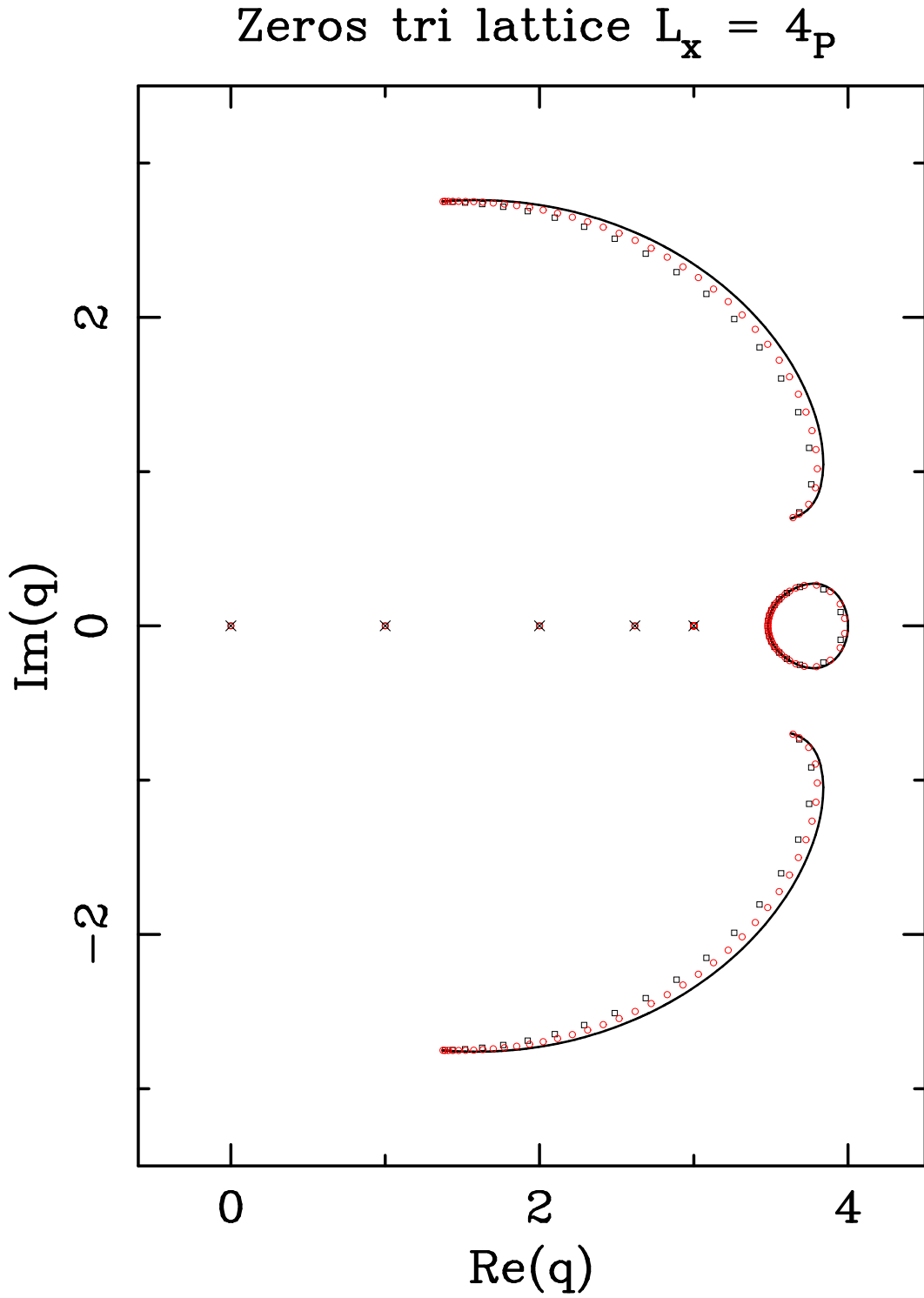
Figure 9: Zeros of the partition function of the $q$-state Potts antiferromagnet on the triangular lattices $4_P \times 20_F$ (squares), $4_P \times 40_F$ (circles) and $4_P \times \infty_F$ (solid line). The isolated limiting points are denoted by a $\times$.

Figure 10: Zeros of the partition function of the $q$-state Potts antiferromagnet on the triangular lattices $5_P \times 25_F$ (squares), $5_P \times 50_F$ (circles) and $5_P \times \infty_F$ (solid line). The isolated limiting points are denoted by a $\times$.

Figure 11: Zeros of the partition function of the $q$-state Potts antiferromagnet on the triangular lattices $6_P \times 30_F$ (squares), $6_P \times 60_F$ (circles) and $6_P \times \infty_F$ (solid line). The isolated limiting points are denoted by a $\times$.

Figure 12: Zeros of the partition function of the $q$-state Potts antiferromagnet on the triangular lattices $7_P \times 35_F$ (squares), $7_P \times 70_F$ (circles) and $7_P \times \infty_F$ (solid line). The isolated limiting points are denoted by a $\times$.

Figure 13: Zeros of the partition function of the $q$-state Potts antiferromagnet on the triangular lattices $8_P \times 40_F$ (squares), $8_P \times 80_F$ (circles) and $8_P \times \infty_F$ (solid line). The isolated limiting points are denoted by a $\times$.

Figure 14: Zeros of the partition function of the $q$-state Potts antiferromagnet on the triangular lattices $9_P \times 45_F$ (squares), $9_P \times 90_F$ (circles) and $9_P \times \infty_F$ (solid line). The isolated limiting points are denoted by a $\times$.

Figure 15: Zeros of the partition function of the $q$-state Potts antiferromagnet on the triangular lattices $10_P \times 50_F$ (squares), $10_P \times 100_F$ (circles) and $10_P \times \infty_F$ (solid line). The isolated limiting points are denoted by a $\times$.

Figure 16: Zeros of the partition function of the $q$-state Potts antiferromagnet on the triangular lattices $11_P \times 55_F$ (squares), $11_P \times 110_F$ (circles) and $11_P \times \infty_F$ (solid line). The isolated limiting points are denoted by a $\times$.

Figure 17: Zeros of the partition function of the $q$-state Potts antiferromagnet on the triangular lattices $12_P \times 60_F$ (squares) and $12_P \times 120_F$ (circles). The isolated limiting points are denoted by a $\times$.

Figure 18: Zeros of the partition function of the $q$-state Potts antiferromagnet on the triangular lattices $4_P \times 20_Z$ (squares), $4_P \times 40_Z$ (circles) and $4_P \times \infty_Z$ (solid line). The isolated limiting points are denoted by a $\times$.

Figure 19: Zeros of the partition function of the $q$-state Potts antiferromagnet on the triangular lattices $6_P \times 30_Z$ (squares), $6_P \times 60_Z$ (circles) and $6_P \times \infty_Z$ (solid line). The isolated limiting points are denoted by a $\times$.

Figure 20: Zeros of the partition function of the $q$-state Potts antiferromagnet on the triangular lattices $8_P \times 40_Z$ (squares), $8_P \times 80_Z$ (circles) and $8_P \times \infty_Z$ (solid line). The isolated limiting points are denoted by a $\times$.

Figure 21: Zeros of the partition function of the $q$-state Potts antiferromagnet on the triangular lattices $10_P \times 50_Z$ (squares) and $10_P \times 80_Z$ (circles). The isolated limiting points are denoted by a $\times$.

# $|g_2/g_1| = 1$ in complex p−plane
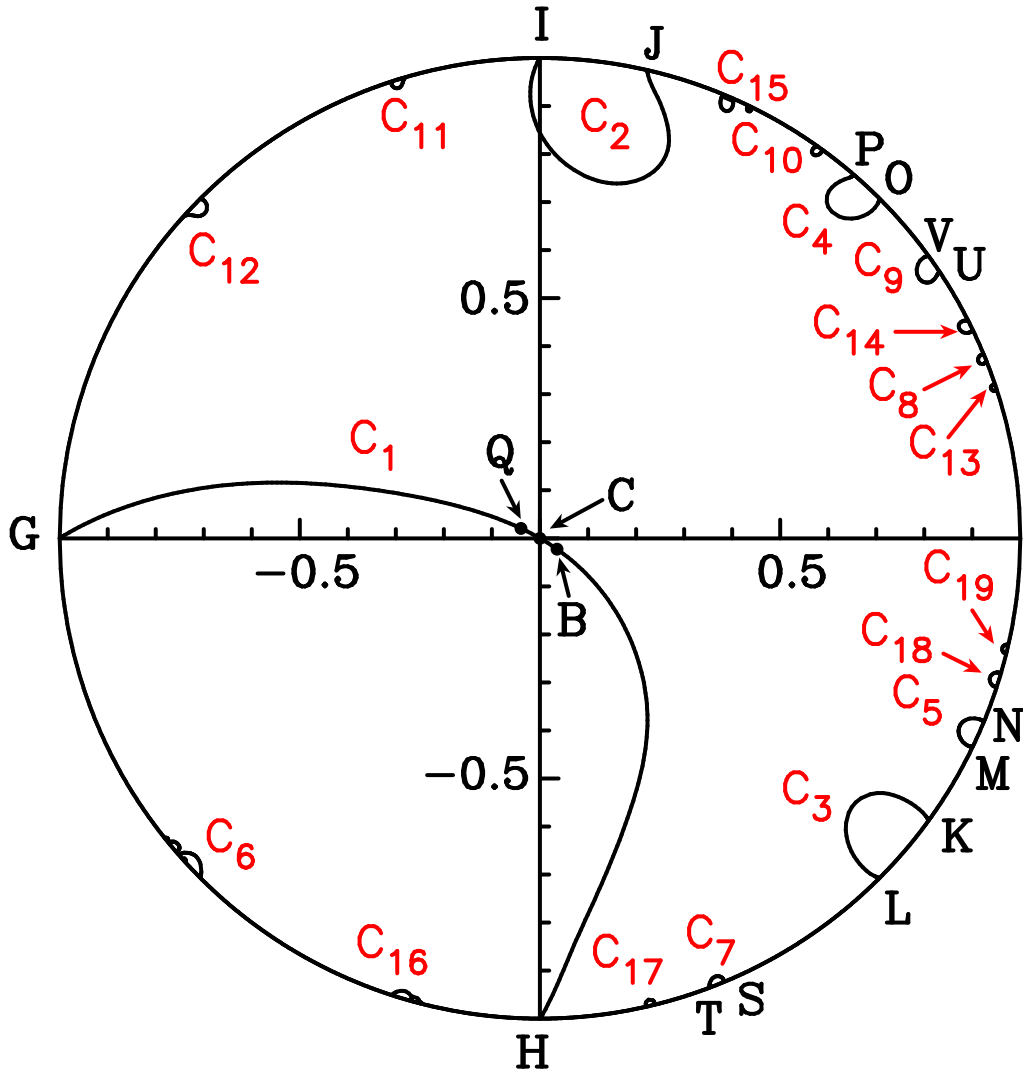


Figure 22: Equimodular curves $|g_2/g_1| = 1$ in the complex $p$-plane. Several important points are labelled G, H, I, J, . . .  (see text).
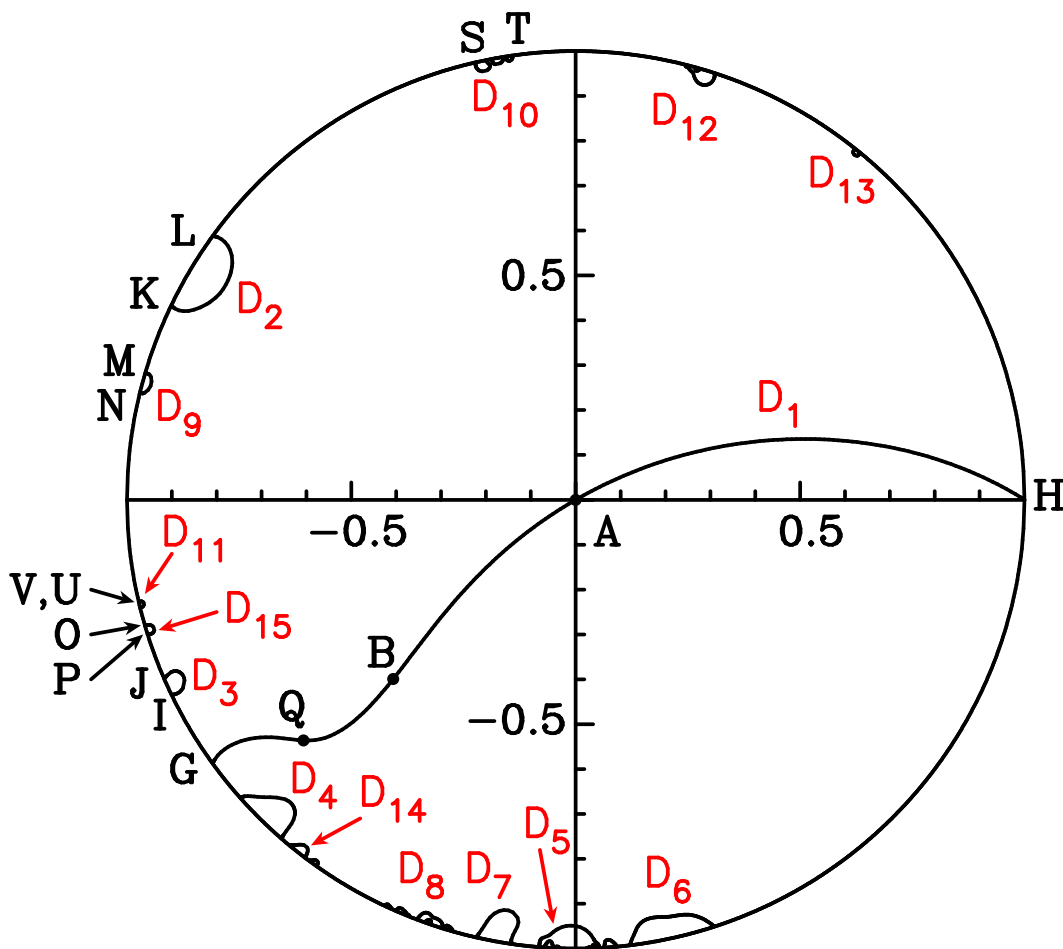
Figure 23: Equimodular curves $|g_3/g_1| = 1$ in the complex $y$-plane. Several important points are labelled G, H, I, J, ... (see text).
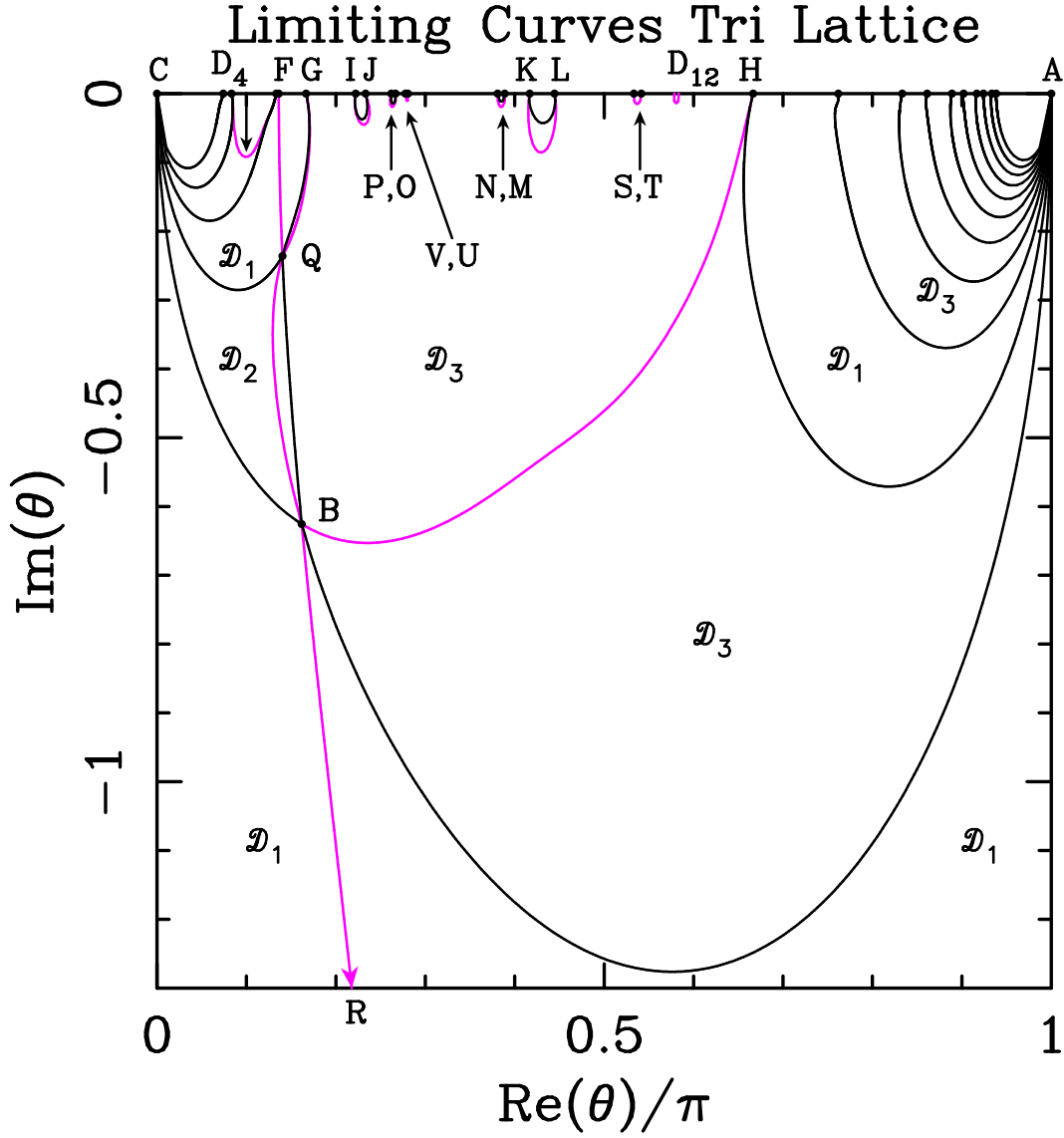
Figure 24: Equimodular curves for the eigenvalues $g_i$ in the complex $\theta$-plane. The portions of curves where the equimodular eigenvalues are dominant (resp. subdominant) are depicted in black (resp. pink). The eigenvalue $g_i$ is dominant in each region labelled $\mathcal{D}_i$. Several important points are labelled A, B, C, ... (see text). To facilitate comparison with Baxter's results [19, Fig. 5], we have used the same labelling of points wherever possible.
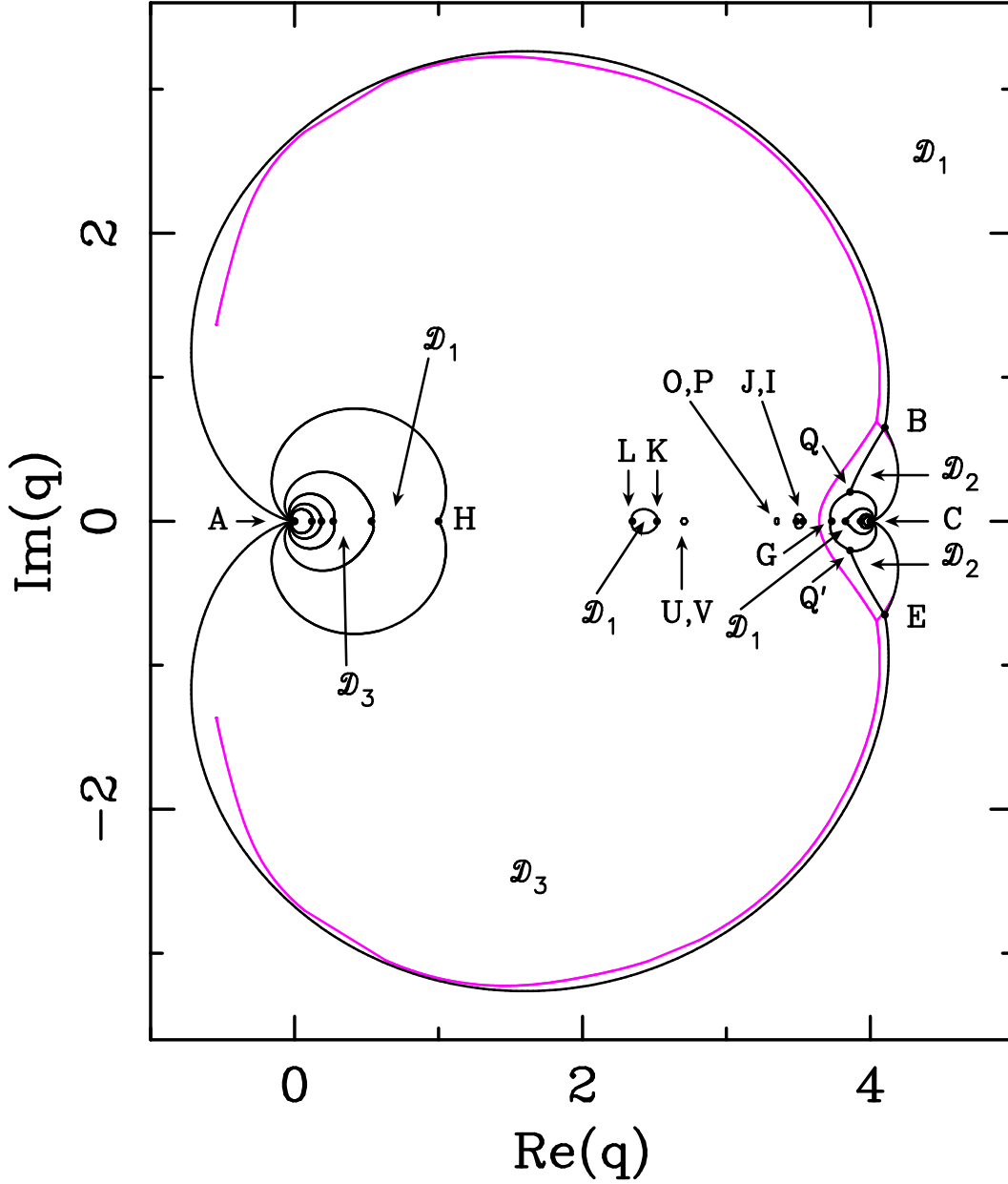
Figure 25: Dominant equimodular curves for the eigenvalues $g_i$ in the complex $q$-plane (in black). For comparison, we show (in pink) the limiting curve $\mathcal{B}$ for the strip $L_x = 11_{\mathrm{P}}$. To facilitate comparison with Baxter's results [19, Fig. 5], we have used the same labelling of points wherever possible. We warn the reader that the presence of the additional curves (AH, LK, etc.) to the right of $q = 0$ has not been definitively established; see Sections 6.3 and 6.4 for a detailed discussion.
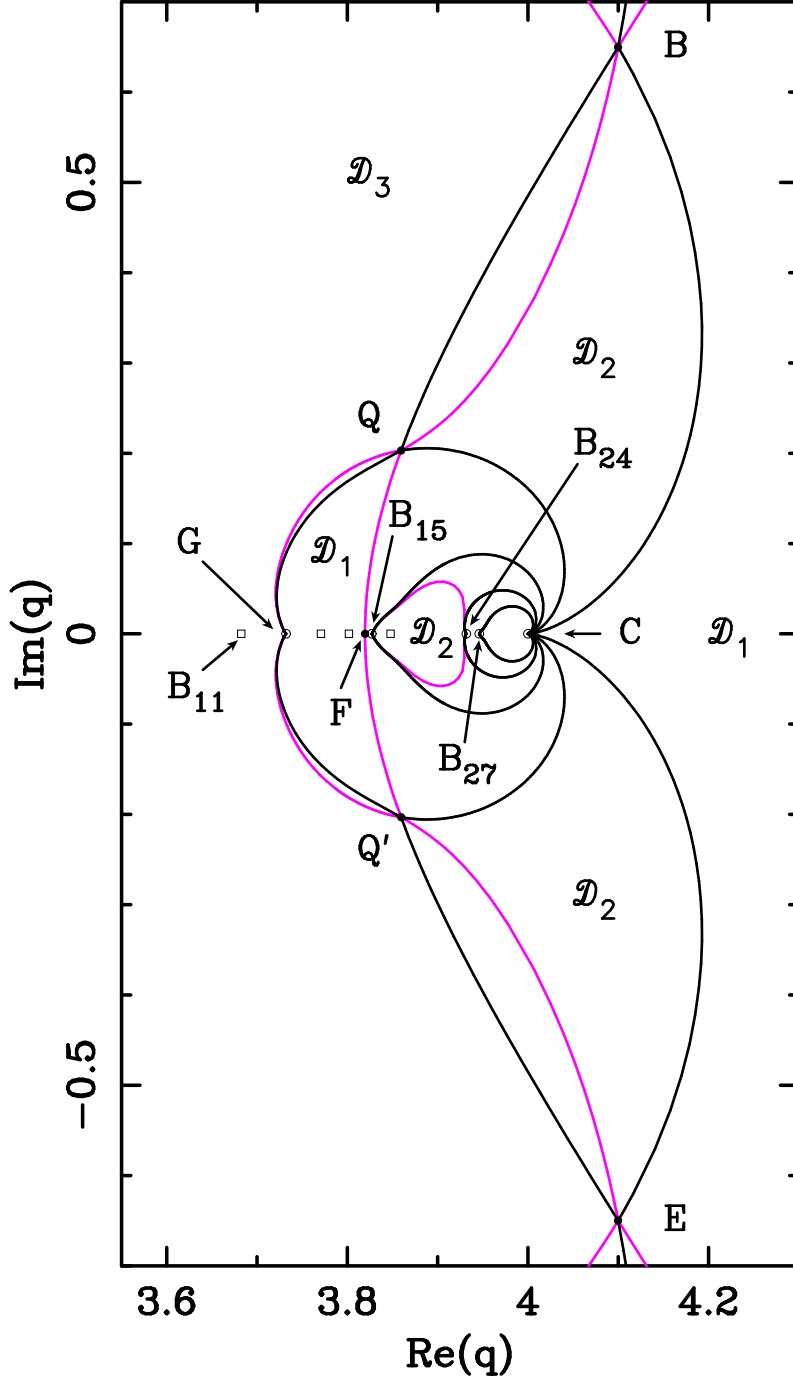
Figure 26: Detail of Figure 25 around the point $q = 4$. We depict the dominant (resp. subdominant) equimodular curves in black (resp. pink). The solid circles ($\bullet$) denote special points discussed in the text, while the squares ($\square$) and empty circles ($\circ$) denote the Beraha numbers $q = B_{11}, \ldots, B_{16}$, $B_{24}$, $B_{27}$ and $B_\infty = 4$ (point C). The empty circles denote those Beraha numbers which belong to any equimodular curve. We denote by $\mathcal{D}_i$ the regions where the eigenvalue $g_i$ is dominant.

# Limiting Curves Tri Lattice
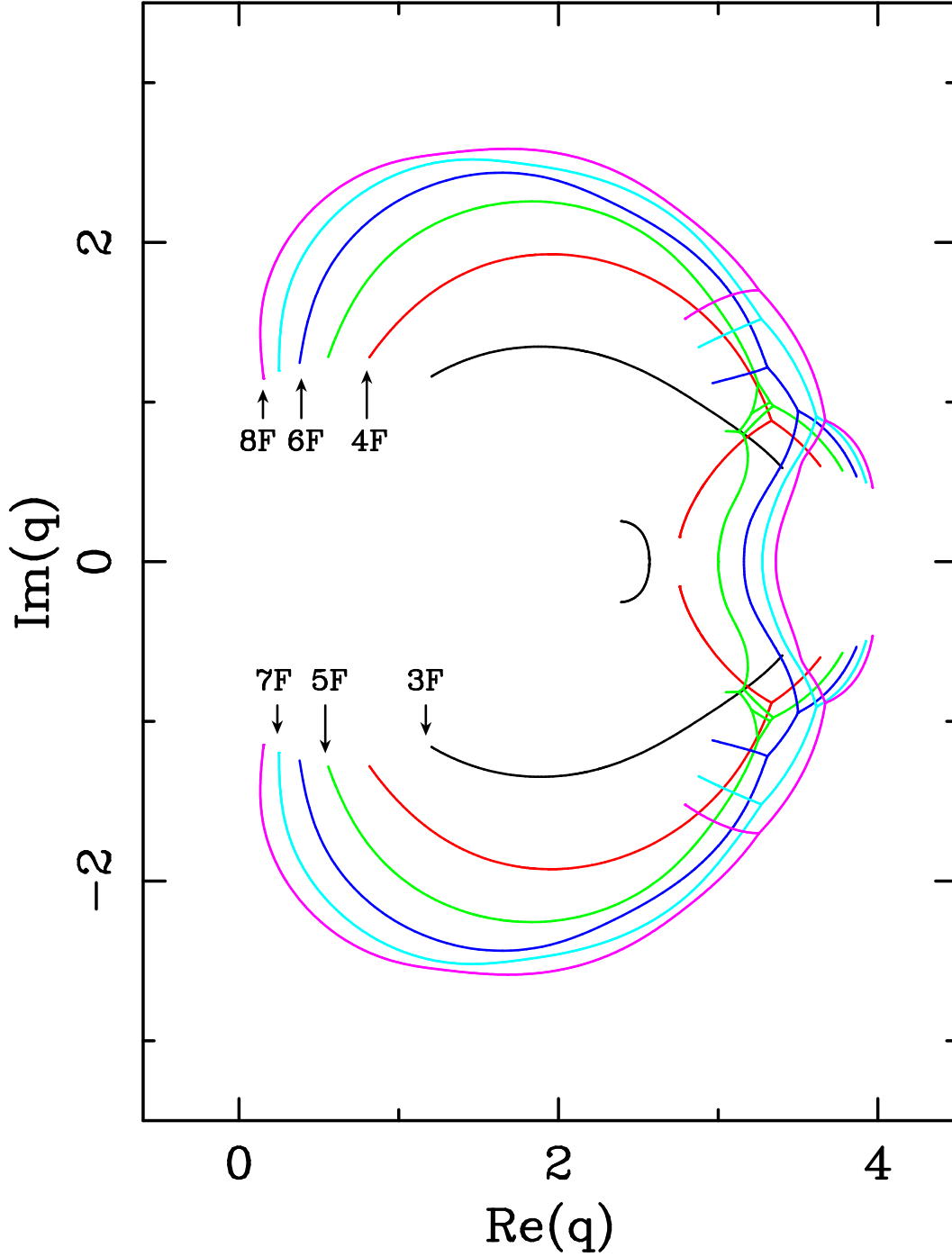


Figure 27: Limiting curves for the triangular-lattice strips $L_F \times \infty_F$ with $3 \le L \le 8$.

# Limiting Curves Tri Lattice
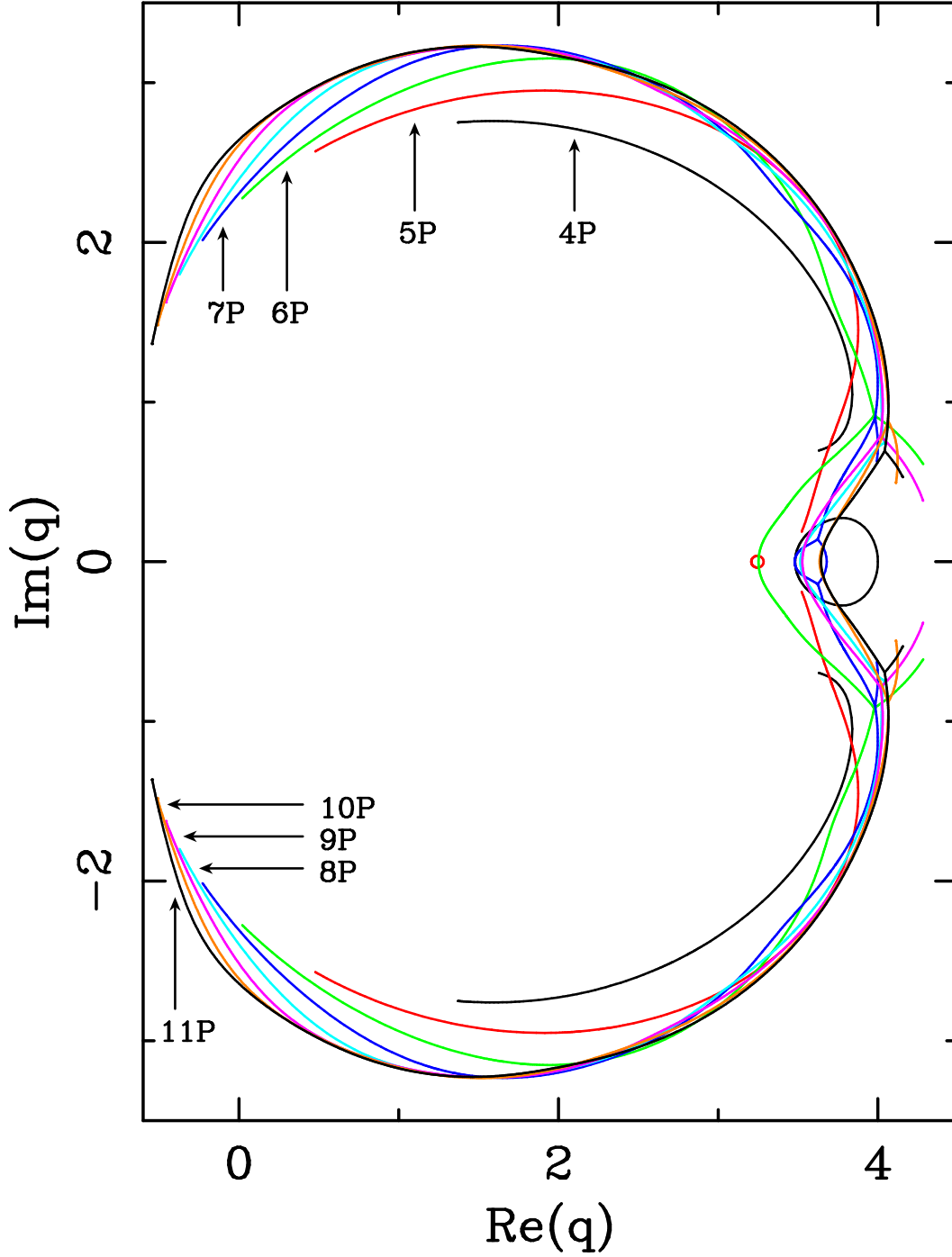


Figure 28: Limiting curves for the triangular-lattice strips $L_P \times \infty_F$ with $4 \leq L \leq 11$.
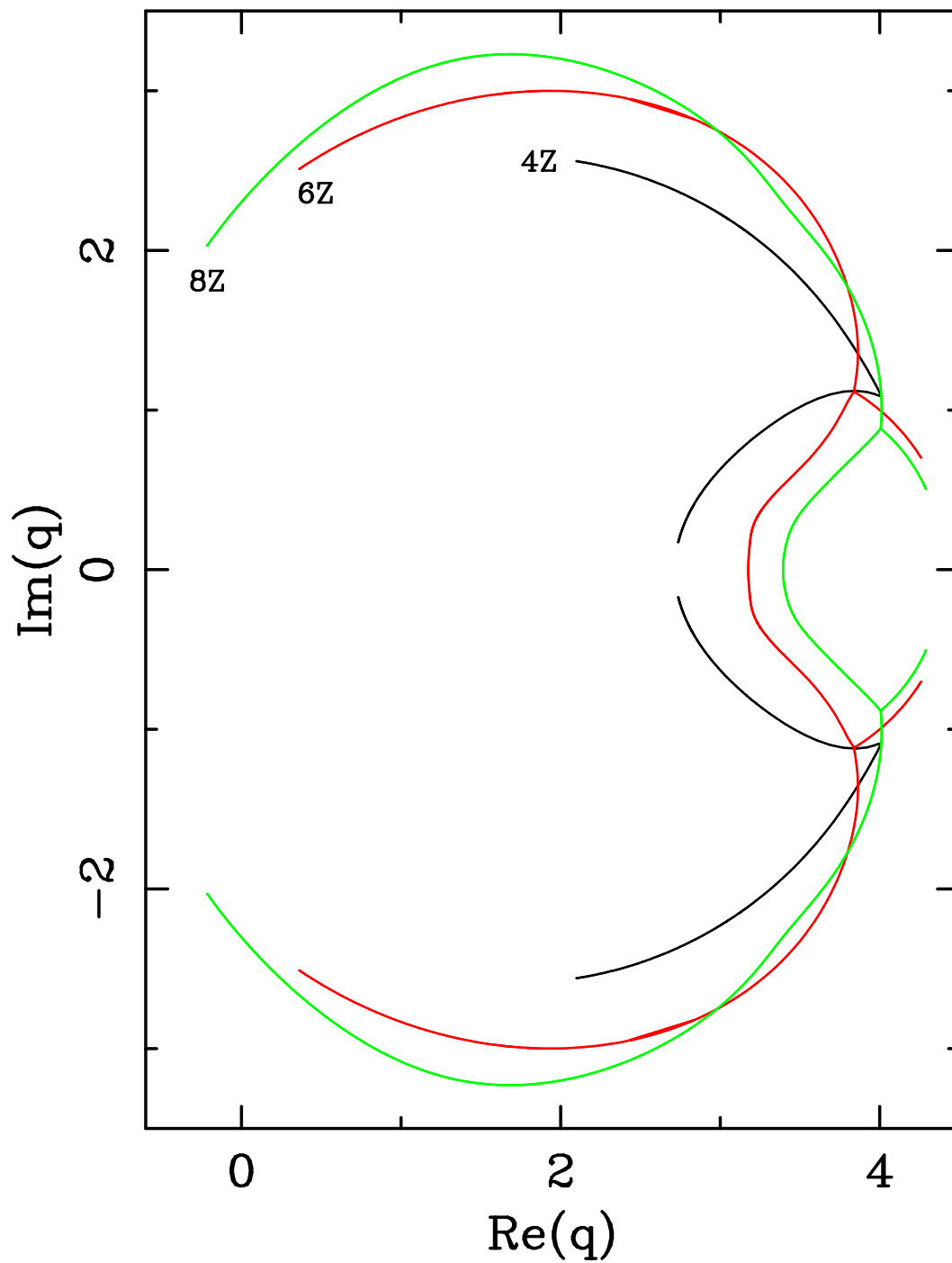
Figure 29: Limiting curves for the triangular-lattice strips $L_Z \times \infty_F$ with $L = 4, 6, 8$.
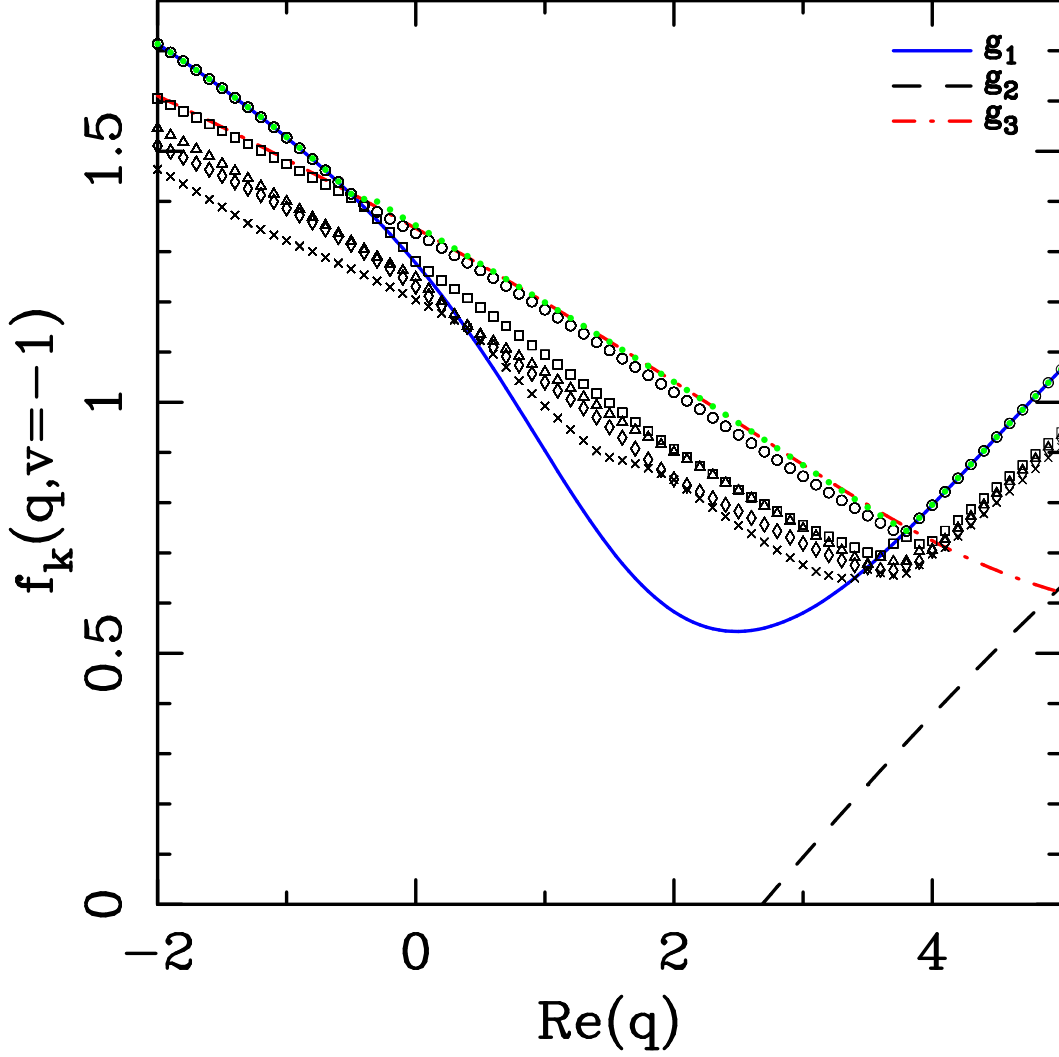
Figure 30: Comparison of Baxter's eigenvalues (6.2) with the most dominant eigenvalues of the transfer matrix for $\text{Im}\, q = 2$. Curves show the logarithm of Baxter's eigenvalues $\log |g_i|$: the solid curve corresponds to $g_1$, the dashed curve to $g_2$, and the dot-dashed curve to $g_3$. Points show the free energy $f_k = (1/L) \log |\lambda_k|$ associated to the five largest eigenvalues (in modulus) of the transfer matrix for a triangular-lattice strip of width $L = 12_{\text{P}}$. The index $k$ is coded as follows: $k = 1$ (the dominant eigenvalue, $\circ$), 2 ($\square$), 3 ($\triangle$), 4 ($\diamond$), and 5 ($\times$). The solid green dots represent the extrapolation of the dominant eigenvalue to $L = \infty$.
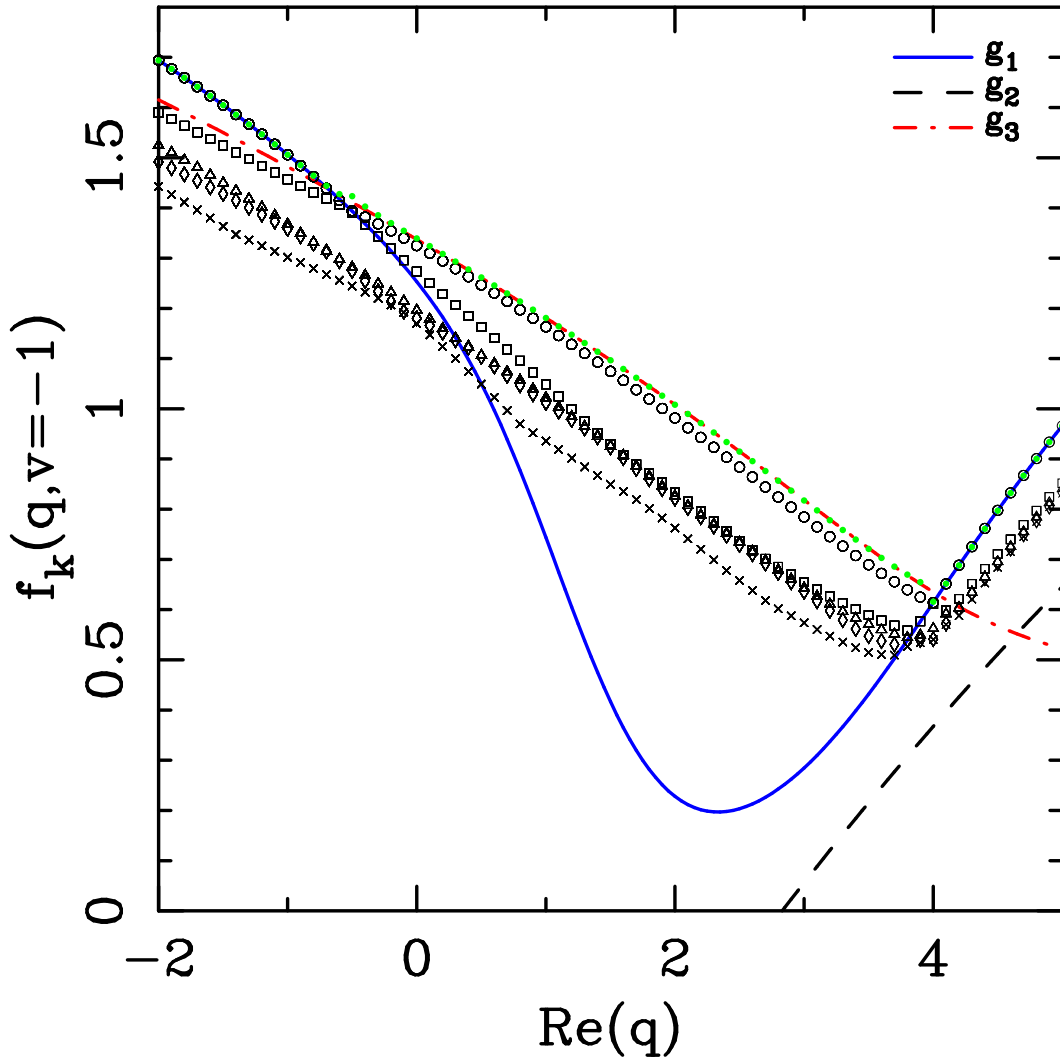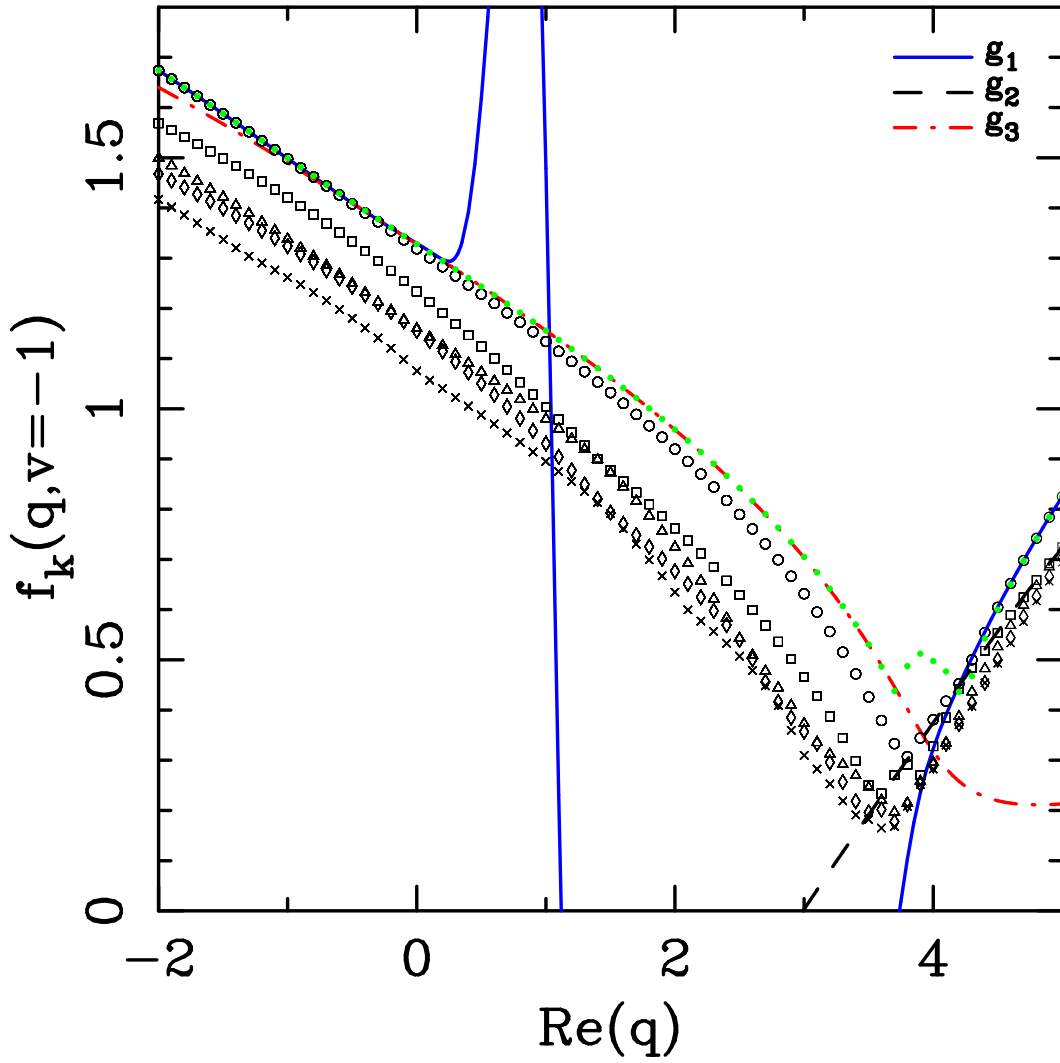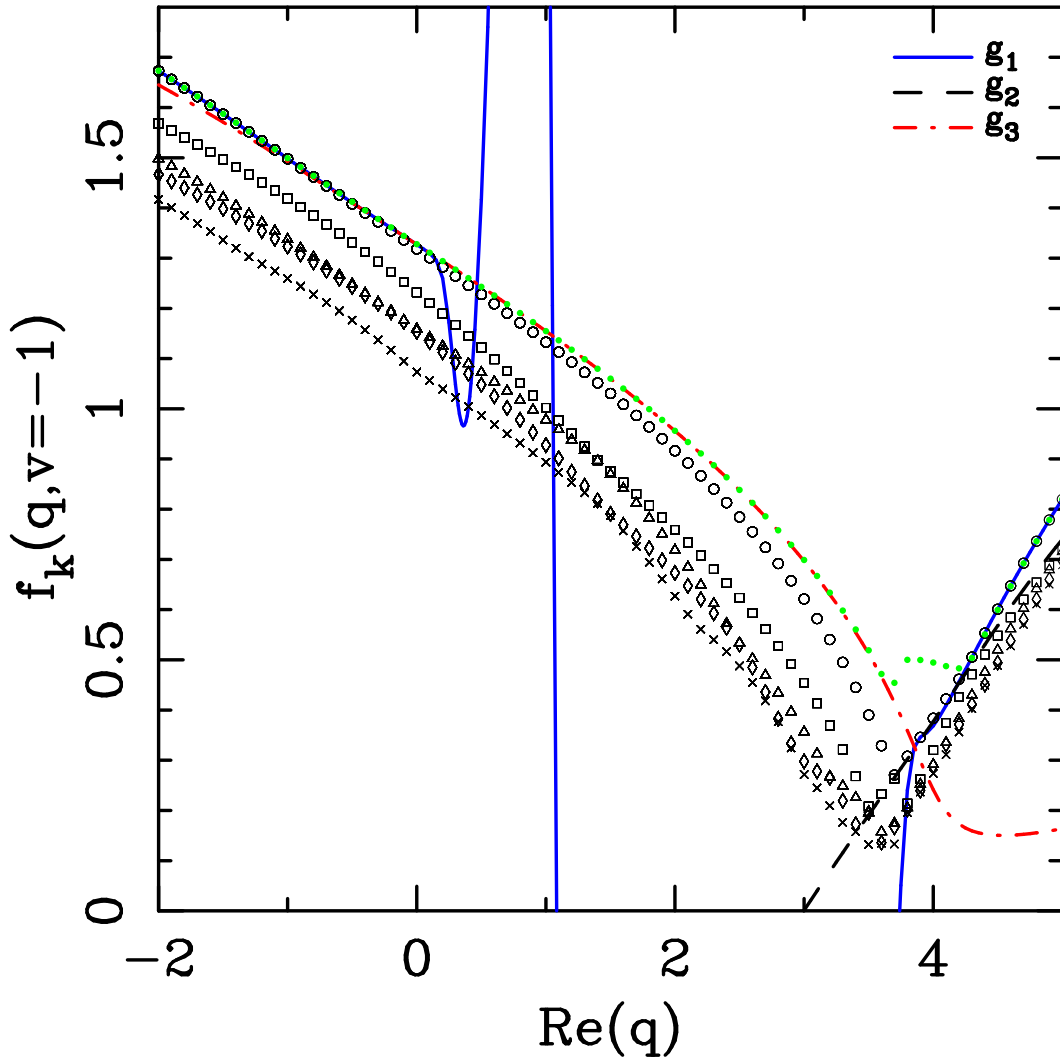
Figure 31: Comparison of Baxter's eigenvalues (6.2) with the most dominant eigenvalues of the transfer matrix for $\mathrm{Im}\, q = 1.5$. The notation is as in Figure 30.
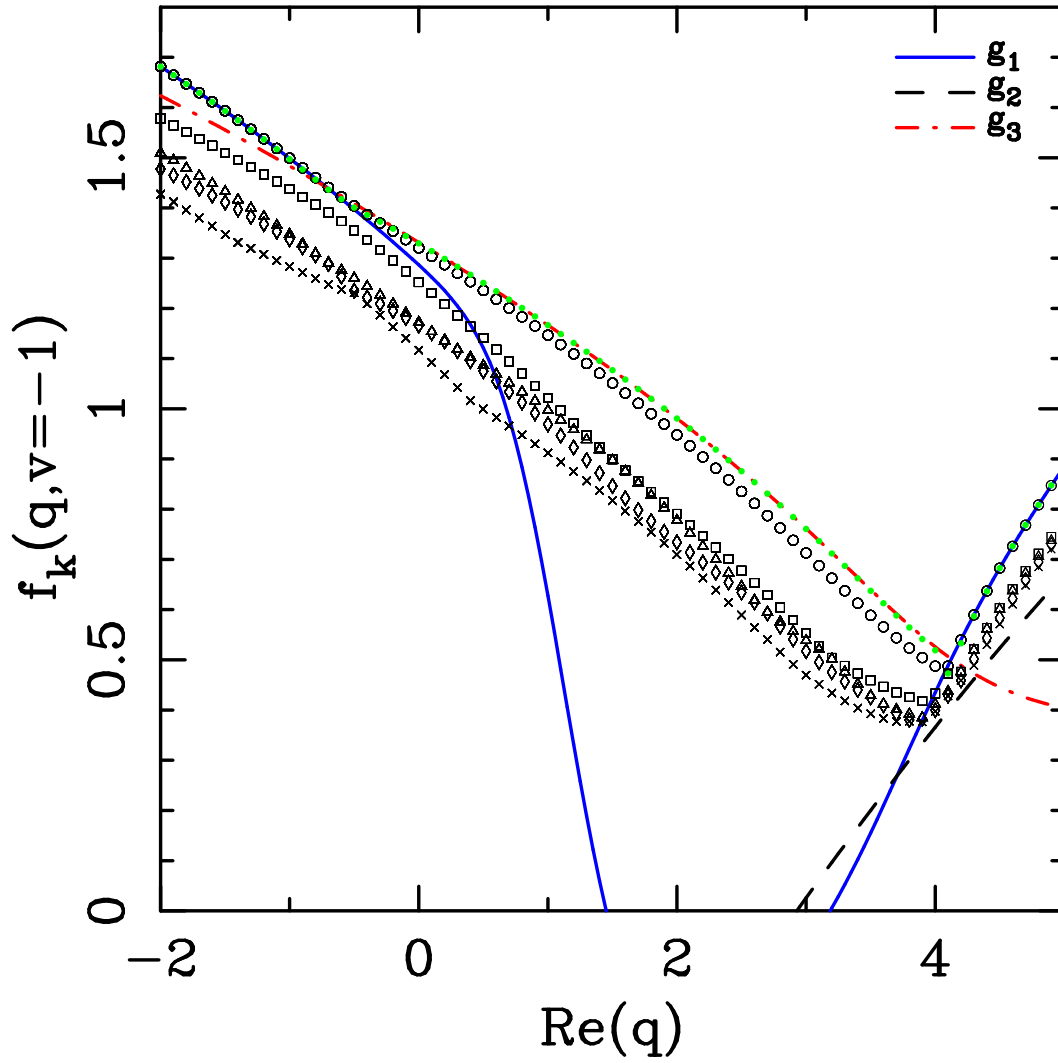
Figure 32: Comparison of Baxter's eigenvalues (6.2) with the most dominant eigenvalues of the transfer matrix for $\operatorname{Im} q = 1$. The notation is as in Figure 30.
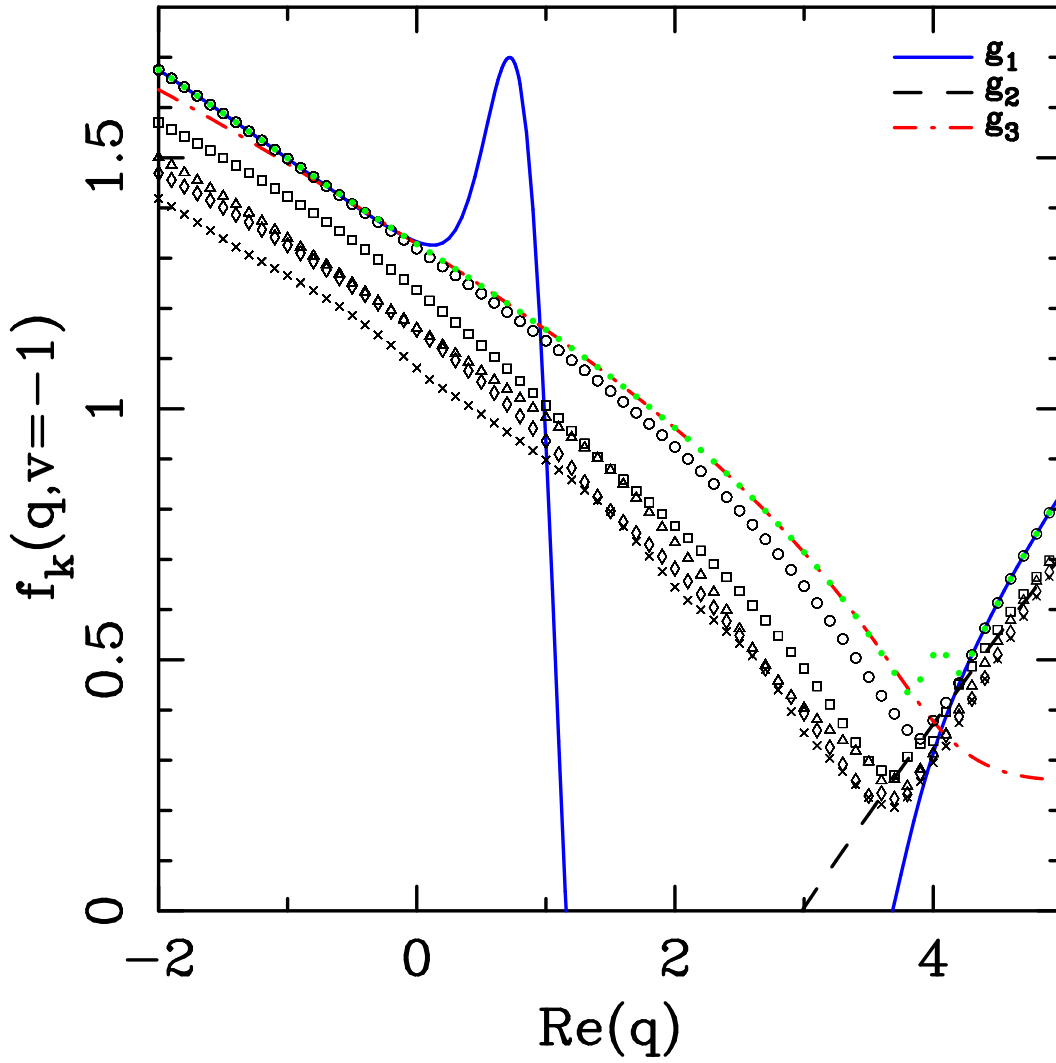
Figure 33: Comparison of Baxter's eigenvalues (6.2) with the most dominant eigenvalues of the transfer matrix for $\mathrm{Im}\,q = 0.5$. The notation is as in Figure 30.

Figure 34: Comparison of Baxter's eigenvalues (6.2) with the most dominant eigenvalues of the transfer matrix for $\operatorname{Im} q = 0.35$. The notation is as in Figure 30.
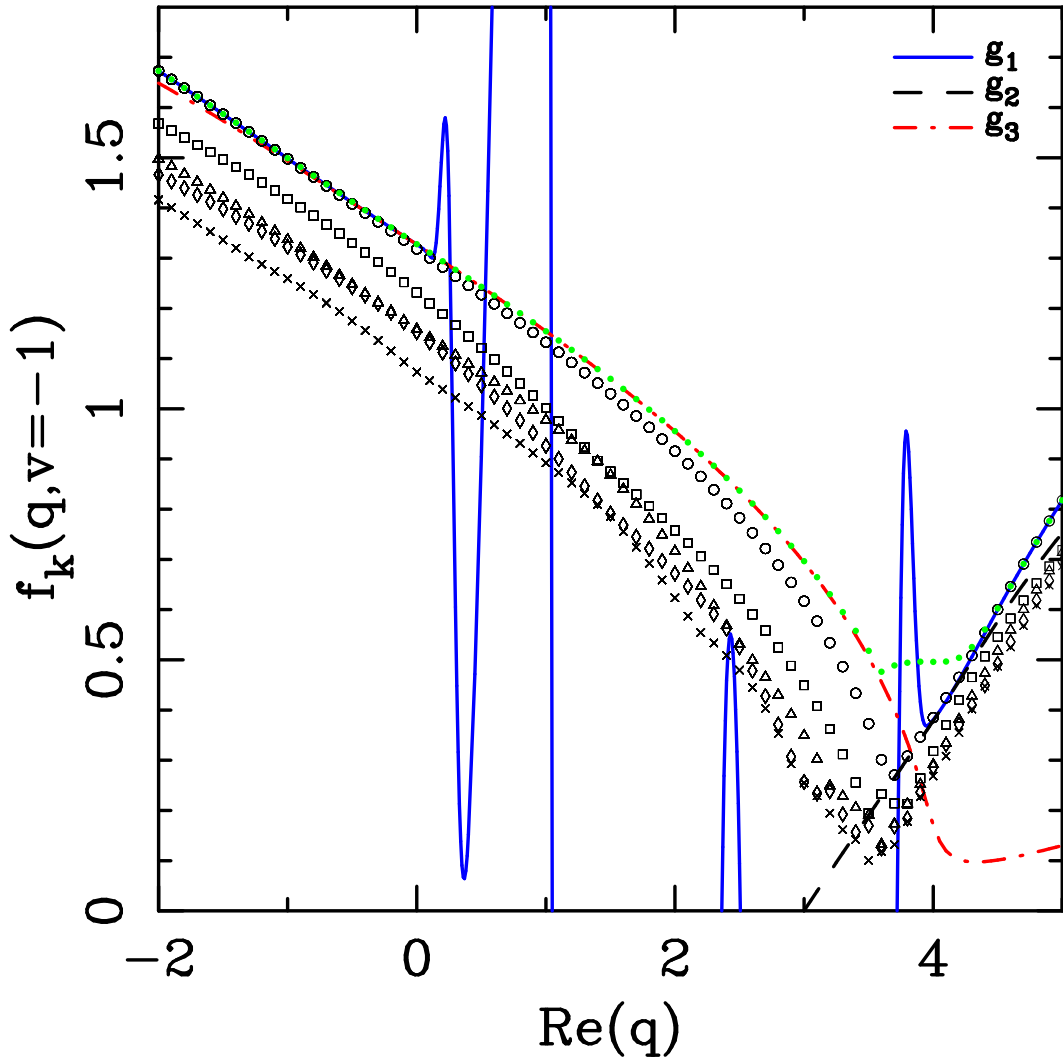
Figure 35: Comparison of Baxter's eigenvalues (6.2) with the most dominant eigenvalues of the transfer matrix for $\operatorname{Im} q = 0.2$. The notation is as in Figure 30.

Figure 36: Comparison of Baxter's eigenvalues (6.2) with the most dominant eigenvalues of the transfer matrix for $\mathrm{Im}\,q = 0.1$. The notation is as in Figure 30.
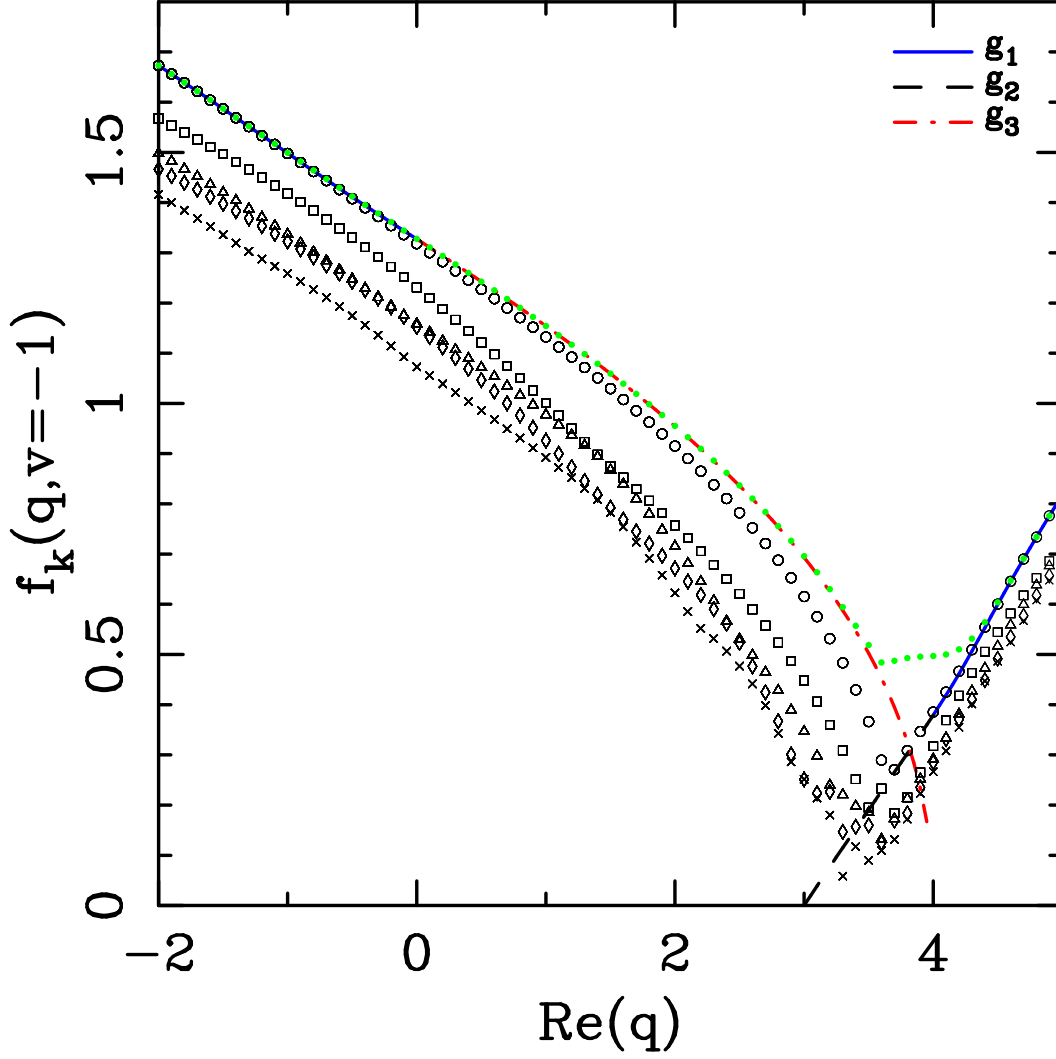
Figure 37: Comparison of Baxter's eigenvalues (6.2) with the most dominant eigenvalues of the transfer matrix for $\mathrm{Im}\, q = 0$. The notation is as in Figure 30. Baxter's eigenvalues $g_2$ [cf. (6.2b)] and $g_3$ [cf. (6.2c)] are depicted only on the interval $0 \le q \le 4$, while $g_1$ [cf. (6.2a)] is shown only outside that interval (see text for details).